



HAL
open science

Implant chargé en nanoparticules pour la libération contrôlée et le ciblage lymphatique de nucléotides et d'analogues nucléotidiques

Giovanna Giacalone

► **To cite this version:**

Giovanna Giacalone. Implant chargé en nanoparticules pour la libération contrôlée et le ciblage lymphatique de nucléotides et d'analogues nucléotidiques. Médecine humaine et pathologie. Université Paris Sud - Paris XI, 2014. Français. NNT : 2014PA114845 . tel-02889750

HAL Id: tel-02889750

<https://theses.hal.science/tel-02889750>

Submitted on 5 Jul 2020

HAL is a multi-disciplinary open access archive for the deposit and dissemination of scientific research documents, whether they are published or not. The documents may come from teaching and research institutions in France or abroad, or from public or private research centers.

L'archive ouverte pluridisciplinaire **HAL**, est destinée au dépôt et à la diffusion de documents scientifiques de niveau recherche, publiés ou non, émanant des établissements d'enseignement et de recherche français ou étrangers, des laboratoires publics ou privés.

UNIVERSITÉ PARIS-SUD

ÉCOLE DOCTORALE :

INNOVATION THÉRAPEUTIQUE : DU FONDAMENTAL À L'APPLIQUÉ

PÔLE : PHARMACOTECHNIE ET PHYSICO-CHIMIE PHARMACEUTIQUE

DISCIPLINE :

Pharmacotechnie et Biopharmacie

ANNÉE 2014-2015

SÉRIE DOCTORAT N° 1298

THÈSE DE DOCTORAT

Date de soutenance 28/11/2014

de

Giovanna GIACALONE

**Implant chargé en nanoparticules pour la libération contrôlée
et le ciblage lymphatique de nucléotides
et d'analogues nucléotidiques**

Composition du jury :

Directeur de thèse :
Co-encadrant de thèse :

Elias FATTAL
Hervé HILLAIREAU

Prof. (Université Paris-Sud)
M. C. U. (Université Paris-Sud)

Rapporteurs :

Giuseppe DE ROSA
Catherine LE VISAGE

M. C. U. (Université de Naples, Italie)
D. R. (Inserm U791)

Examineurs :

Amélie BOCHOT
Thierry DELAIR
Marie-Lise GOUGEON

Prof. (Université Paris-Sud)
Prof. (Université de Lyon 1)
D. R. (Institut Pasteur)

Table des matières

Abréviations	5
Introduction générale.....	8
Travaux antérieurs : Amélioration de la biodisponibilité et de la biodistribution des chimiothérapies anti-VIH	12
Abstract	14
1. Introduction	14
2. Bioavailability improvement: overcoming physiological barriers and extending the efficacy time of drugs	15
2.1 Overcoming physiological barriers	16
2.2 Extending the efficacy time of drugs	21
2.3 Conclusions	28
3. Biodistribution improvement: drug targeting towards virus reservoirs and sanctuaries	28
3.1 Mononuclear phagocyte system (MPS) targeting	28
3.2 Brain and CNS targeting	36
3.3 Conclusions	38
4. Conclusions	38
References	39
Travaux expérimentaux	53
Chapitre 1	54
Formation spontanée de nanovecteurs de nucléotides et d’analogues nucléotidiques pour leur délivrance cellulaire	55
Chapitre 2	74
Stabilisation et délivrance cellulaire de nanoparticules à base de chitosane et de polyphosphates, par ajout de fer ionique	75
Chapitre 3	99
Activité antivirale et ciblage vers les leucocytes et ganglions lymphatiques de la zidovudine triphosphate associée à des nanoparticules de chitosane-fer	100
Chapitre 4	124
Implant à formation <i>in situ</i> de PLGA pour la libération prolongée de nanoparticules de nucléotides	125

Discussion générale	142
Remerciements	158

Abréviations

AIDS	acquired immunodeficiency syndrome
ATP	adenosine 5'-triphosphate
AUC	area under the curve
AZT	3'-Azido-2',3'-dideoxythymidine
AZT-MP	3'-Azido-2',3'-dideoxythymidine-5'-monophosphate
AZT-TP	3'-Azido-2',3'-dideoxythymidine-5'-triphosphate
BBB	blood-brain barrier
BODIPY	boron-dipyrrromethene
CLSM	confocal laser scanning microscopy
CNS	central nervous system
CS	chitosan
CS-Fe	chitosan-iron complex
d4T	stavudine
DC	dendritic cells
ddC	zalcitabine
ddI	didanosine
DLS	dynamic light scattering
DMSO	dimethyl sulfoxide
DNA	deoxyribonucleic acid
EC ₅₀	half maximal effective concentration
FDA	food and drug administration
FT-IR	fourier transform infrared spectroscopy
GALT	gut-associated lymphoid tissue
H ₂ DCFDA	2',7'-dichlorodihydrofluorescein diacetate
HAART	highly active anti retroviral therapy
HEMA	2-hydroxyethyl methacrylate
HIV	human immunodeficiency virus
HPMC	hydroxypropylmethylcellulose
ITC	isothermal titration calorimetry
LDL	low density lipoproteins
MOF	metal organic framework
MPS	mononuclear phagocyte system
MTT	3-(4,5-dimethylthiazol-2-yl)-2,5-diphenyltetrazolium bromide
NMP	N-Methyl-2-pyrrolidone

NP	nanoparticle
NRTI	nucleoside reverse-transcriptase inhibitor
PACA	polyalkylcyanoacrylate
PBL	peripheral blood lymphocytes
PBS	phosphate buffer saline
PCL	poly- ϵ -caprolactone
PCS	photon correlation spectroscopy
PDI	polydispersity index
PEG	polyethylene glycol
PEI	polyethylenimine
PI	protease inhibitor
PLGA	poly(lactic- <i>co</i> -glycolic acid)
PMA	phorbol 12-myristate 13-acetate
PMBC	peripheral blood mononuclear cells
PMEA	adefovir
PMPA	tenofovir
PV	pseudovirus
RLU	relative luminescence unit
siRNA	small interfering RNA
SLN	solid lipid nanoparticles
STED	stimulated emission depletion
TAT	trans-activating transcriptor
TEM	transmission electron microscopy
TPP	tripolyphosphate

Introduction générale

Dans le contexte de la maladie du VIH/SIDA, de nombreux progrès ont été réalisés depuis l'introduction du premier médicament antirétroviral, la zidovudine (AZT). Néanmoins, aucune guérison n'est encore disponible, en raison de la persistance du virus dans les cellules et les compartiments de l'organisme appelés respectivement réservoirs et sanctuaires. Une stratégie de ciblage est donc nécessaire pour diriger les molécules actives vers ces sites spécifiques. En outre, l'observance du patient est critique afin d'éviter tout rebond viral, ce qui représente une contrainte importante pour un traitement à vie. Un système permettant une libération prolongée pourrait donc réduire la fréquence de la prise des médicaments et ainsi d'améliorer la vie du patient.

Une solution à ces deux problèmes pourrait venir de l'utilisation de systèmes de drug delivery. Des nanoparticules pourraient assurer la protection et l'administration ciblée des molécules actives, alors qu'un implant à formation *in situ* pourrait permettre la libération prolongée de ces nanoparticules à partir du site de l'injection.

La première partie du manuscrit dresse un état de l'art de l'amélioration de la biodisponibilité et de la biodistribution des chimiothérapies anti-VIH. En particulier, il est centré dans une première partie sur les stratégies pour cibler les réservoirs et les sanctuaires viraux, et dans une deuxième partie sur les formulations permettant d'obtenir une libération prolongée. Il est écrit sous forme de revue, qui sera soumise pour publication.

La seconde partie est écrite sous la forme d'articles et décrit les travaux expérimentaux, selon le plan suivant :

1. Le premier chapitre porte sur la formulation de nanoparticules pour encapsuler la forme active d'une molécule antirétrovirale, la zidovudine triphosphate (AZT-TP), ainsi que l'adénosine triphosphate (ATP), utilisée en tant que molécule modèle, à l'aide de chitosane (CS). Ces nanoparticules sont formées par interactions ioniques entre les charges positives du chitosane et les charges négatives des groupes triphosphates de l'ATP/AZT-TP. Les nanoparticules sont caractérisées et la délivrance cellulaire de l'ATP et de l'AZT-TP est démontrée sur une lignée cellulaire de macrophages. Ce chapitre a été publié comme article de recherche dans le journal *Biomacromolecules* en 2013.
2. Dans un deuxième temps, la stabilité de ces systèmes a été améliorée afin d'obtenir un meilleur comportement en conditions physiologiques. Cette amélioration de la stabilité a été obtenue par la complexation du fer au chitosane (CS-Fe). Cette stratégie a été appliquée aux nanoparticules de tripolyphosphate (TPP) et d'ATP. Les nanoparticules ont été ensuite

testées sur deux lignées de cellules macrophages, montrant une internalisation améliorée de l'ATP par rapport aux nanoparticules précédentes. Ce chapitre a été publié comme article de recherche dans la revue *Journal of Controlled Release* en 2014.

3. Les nanoparticules stabilisées ont été ensuite formulées aussi avec l'AZT-TP, afin d'étudier leur activité antivirale sur les cellules humaines infectées par le VIH. Auparavant, ces systèmes ont été caractérisés et évalués sur deux lignées cellulaires de macrophages non infectés. Une étude *in vivo* sur la souris examine la distribution dans les ganglions lymphatiques de l'AZT-TP sous forme de nanoparticule par rapport à la molécule libre, après injection sous-cutanée.
4. Enfin, les nanoparticules à base de CS-Fe et ATP ont été dispersées dans une solution de PLGA, dans le but de mettre au point un implant à formation *in situ*. Ce système devrait idéalement permettre, après injection sous-cutanée, une libération prolongée des nanoparticules sur plusieurs jours, pour qu'elles puissent atteindre les ganglions lymphatiques, un sanctuaire important du VIH.

À la fin du manuscrit, une discussion générale reprendra et développera tous les résultats obtenus au cours de cette thèse, et discutera des perspectives d'avenir issues de ce travail.

Cette thèse de doctorat a été réalisée à l'Institut Galien Paris-Sud, sous la supervision du Professeur Elias Fattal et du Docteur Hervé Hillaireau, grâce à un financement du Ministère Français de la Recherche.

Travaux antérieurs

Travaux antérieurs**Amélioration de la biodisponibilité et de la biodistribution
des chimiothérapies anti-VIH****Résumé**

Dans le contexte du traitement du VIH/SIDA, de nombreuses améliorations ont été apportées après l'introduction des trithérapies (HAART). Cependant, elles ne permettent pas encore une guérison complète, en raison de certaines caractéristiques du virus et du traitement. Parmi celles-ci, deux problématiques importantes ont été sélectionnées et feront l'objet de ce chapitre. La première contrainte principale dans le traitement du VIH est la faible biodisponibilité de certaines molécules actives, qui impose des administrations répétées et aboutit donc à une observance contraignante. La seconde problématique repose sur la nécessité de délivrer les molécules actives dans les réservoirs et les sanctuaires viraux, c'est-à-dire des cellules ou des compartiments de l'organisme dans lesquels elles n'arrivent pas à pénétrer ou sont distribuées en concentration insuffisante. Le manque d'activité antivirale dans ces régions permet au virus de rester sous sa forme latente et de reprendre sa réplication à tout moment après l'interruption de la thérapie. Les récentes stratégies de vectorisation qui abordent ces deux limitations seront passées en revue dans ce chapitre.

Introduction

Improving bioavailability and biodistribution of anti-HIV chemotherapy

Abstract

In the context of the treatment of HIV/AIDS, many improvements have been achieved since the introduction of the combination therapy (HAART). Nevertheless, no cure for this disease has been so far possible, because of some particular features of the virus and of the therapies. Among them, two important issues have been selected and will be the subject of this chapter. The first main concern in the HIV treatment is the poor drug bioavailability, resulting in repeated administrations and therefore a demanding compliance. On the other hand, there is a need to target the drugs into the so-called reservoirs and sanctuaries, i.e. cells or body compartments where drugs cannot penetrate or are distributed in sub-active concentrations. The lack of antiviral action in these regions allows the virus to lie latent and start to replicate at any moment after therapy suspension. Recent drug delivery strategies addressing these two limitations will be reviewed in this chapter.

1. Introduction

Many progresses have been achieved in the treatment of the human immunodeficiency virus (HIV) infection and the acquired immune deficiency syndrome (AIDS) since the introduction in 1987 of the first antiretroviral drug zidovudine (azidothymidine, AZT). AZT belongs to the class of nucleoside analog reverse transcriptase inhibitors (NRTIs), which interfere with the viral DNA synthesis by competing with natural nucleosides. Throughout the years, the development of more nucleoside analogues as well as other antiretroviral classes' drugs, along with their association into the so-called highly active anti retroviral therapy (HAART), significantly improved the life expectancy and quality of individuals affected by this disease. Today, a typical drug association for HAART consists in two nucleoside reverse transcriptase inhibitors (NRTI) and one other chosen among protease inhibitors (PI), non-nucleoside reverse transcriptase inhibitors or integrase strand transfer inhibitors [1, 2].

Nevertheless, eradicating the infection is still not possible due to some limitations concerning this treatment [3]; among them, two main aspects will be the focus of this chapter.

One of the most important drawbacks of current HIV therapy drugs is the demanding drug-regimen compliance, due to the poor drug bioavailability [4]. More than a single tablet has to be taken every day by the patient, respecting their daily lifelong schedule, because of the relatively short drug half-life. No suspension of the treatment is allowed, in order to avoid the insurgence of resistances and viral rebound. All these factors make the regimen hard to follow for the patient, and it is one important reason for treatment failure [5]. To face this aspect of the therapy limitations, a sustained drug release system would allow reducing the frequency of dosing. In the last years several strategies have been proposed, which will be summarized in the first section of this chapter.

The second main drawback of current HAART is their poor biodistribution in certain regions of the body. Although patients who are fully compliant with the therapy may reach a near undetectable virus level in the blood, the interruption of the treatment will, most of the times, bring the patient back to his original viremia [6]. This can be explained by the presence in the body of so called viral reservoirs and sanctuaries, i.e. sites hardly accessible to the drugs, where the virus is therefore protected from their action and can hide in its latent form. Reservoirs are cellular sites formed among others by macrophages, CD4⁺ T cells and dendritic cells [7]; virus sanctuaries are anatomical sites including brain, lymphoid tissues, gut-associated lymphoid tissue (GALT), liver, lungs, genital tract [8]. After therapy interruption, the virus present in these sites can re-emerge from its latent phase and replicate, bringing the viral load up to values of untreated patients. In other cases, the narrow therapeutic index of some drugs induces unwanted side effects because of their distribution in healthy parts of the body. Therefore, there is a strong need to target the antiretroviral drugs to the body reservoirs and sanctuaries [9]. The major approach to face this difficulty is the use of nanomedicine, namely encapsulating the active drug into a carrier which can drive it to the reservoir or sanctuary regions. Few reviews have already addressed this issue [10-13], which will be summarized, completed and updated in the second section of this chapter.

A solution about these two topics would bring us a big step closer to a cure for the HIV. The authors want to specify that prevention treatments are not the object of this chapter. For topical prophylaxis sustained delivery aspects, the reader is invited to refer to the work of Kiser *et al.* [14].

2. Bioavailability improvement: overcoming physiological barriers and extending the efficacy time of drugs

In the context of this chapter, bioavailability should be seen as the amount of drug available not only in the blood, but also in the target cells. In the case of HIV treatment, the low drug bioavailability can

be due to poor cell membrane penetration, which reduces the actual drug dose in the blood and/or at the site of interest, and/or to the quick drug elimination from the action site and from the body. This often results in frequent and important doses for the patients, mainly orally but also subcutaneously. Because of the insurgence of compliance problems from HIV-infected patients, new researches have been started in order to improve bioavailability, by promoting the membrane penetration or by extending the action time of HAART drugs. The different drug delivery systems described in this section are summarized in Table 1.

IMPEDIMENTS to BIOAVAILABILITY	DRUGS INVOLVED	STRATEGY PROPOSED
Overcome absorption barrier:		
by decreasing hydrophilicity	Hydrophilic: tenofovir, ddl, ddC, AZT	Prodrugs
by promoting dissolution	Hydrophobic: tipranavir, efavirenz	Micelles
Overcome target cell barrier	Hydrophilic: AZT, ddl, d4T	Prodrugs
	ddC-TP, ddl-TP, AZT-TP, oligonucleotides	NPs
Extend efficacy time	indinavir, d4T, AZT, nevirapine	Extended release tablets
	AZT, AZT-MP	Prodrugs
	Oligonucleotide, AZT, d4T, ddl, ritonavir, lopinavir, efavirenz, lamivudine	Polyester NPs
	atazanavir, ritonavir, efavirenz, rilpivirine, GSK1265744	Nanocrystals
	tenofovir, saquinavir, indinavir	Lipid-based formulations
	darunavir, enfuvirtide	Implants and devices

Table 1. Bioavailability issues of anti-HIV molecules and drug delivery strategies adopted to address them.

2.1 Overcoming biological barriers

2.1.1 Absorption barrier

The limitation of several orally administered drugs is their poor absorption through the gastrointestinal tract, resulting in a low bioavailability. This is the case of several nucleoside and nucleotide analogues, which are hydrophilic molecules. Many attempts have been made to formulate them as prodrugs, in order to decrease their hydrophilicity and promote their passage through the intestinal epithelium. A successful example of a solution to this problem is the marketed drug Tenofovir

disoproxil fumarate (Viread®). Tenofovir, a nucleotide reverse transcriptase inhibitor, is in itself a hydrophilic and charged molecule because of the presence of the phosphonate group, strongly limiting its absorption at the intestinal level [15]. The modification through the disoproxil fumarate ester increased its partition coefficient (log P) from -4.13 to 1.25, thus improving its oral absorption. The transport through intestinal mucosa has been improved from 0.1 to 2.7%, reaching an oral bioavailability of 20% when the molecule was administered as ester form (as compared to 1.9% of free-administered tenofovir). Furthermore, no detectable levels of ester molecules were found in plasma, showing the complete release of the active drug from the prodrug form. More recently, the nucleoside analogues ddi and ddC have been associated to the natural triterpene squalene (Sq), resulting in amphiphilic prodrugs able to self-assemble as nanoparticles in water. After oral administration to rats, ³H-ddi-Sq led to 4-times higher concentrations in the plasma than ³H-ddi administered as a solution [16]. The design of glycerolipidic prodrugs is a complementary approach consisting not only in decreasing the drug hydrophilicity, but also in mimicking the metabolism of long chain triglycerides in the gastrointestinal tract. These triglycerides are metabolized by the pancreatic lipase and colipase into a 2-monoglyceride and two fatty acids which are absorbed by enterocytes; after reesterification into triglycerides and packing into chylomicrons, these metabolites are secreted into the mesenteric lymph. This biomimetic approach was exemplified with didanosine (ddi) [17]. Formulated as liposomes in the presence of DPPC, this glycerolipidic ddi prodrug has been tested *in vitro* for its anti-HIV activity on PMBC, giving similar results to the free drug, meaning the activity was conserved and the enzymatic cleavage to the parent drug was successfully obtained. After oral administration to rats, these liposomes exhibited an enhanced accumulation in organs, particularly the intestine, as compared to the free drug [18]. Prodrugs have also been proposed to promote the gastro-intestinal passage of nucleoside analogues through natural membrane transporters. In particular, amino acids prodrugs have been conceived in order to exploit the transporters in the intestinal epithelial cells, which promote the absorption of amino acids and nucleotides. For example, 5'-O-valyl-AZT was able to cross intestinal barrier 3 times better than the parent drug [19].

Besides hydrophilic drugs, hydrophobic ones can also exhibit a limited bioavailability due to a poor dissolution. This is the case of some protease inhibitors such as Tipranavir [20] or non-nucleoside reverse transcriptase inhibitors such as efavirenz, a highly lipophilic and practically water-insoluble drug with an oral bioavailability of 45%. The formulation of efavirenz with micelles made of poloxamines has been proposed with the aim of improving bioavailability and organoleptic properties, especially for the treatment of pediatric patients. Thanks to its encapsulation into micelles, efavirenz improved its apparent water solubility and therefore its oral bioavailability [21]. These systems have been tested *in vivo* on rats, where they increased the C_{max} up to 88% and the

AUC up to 87%, as compared to efavirenz in suspension or in solution in a medium-chain triglyceride (Miglyol® 812).

2.1.2 Target cell barrier

The pharmacological target of anti-HIV drugs can be located at the surface of the infected cells (e.g. fusion inhibitors) or in the cell cytoplasm (e.g. reverse transcriptase inhibitors). For the latter, the cell membrane can thus act as a barrier, especially for hydrophilic drugs. To face this issue, several prodrugs have been proposed to render the molecule more lipophilic and therefore promote their cellular uptake, similarly to what was shown in the previous section. Examples in this sense come from the esterification of the 5'OH termination of AZT [22]. This part of the molecule is hydrophilic, so the addition of an ester group allows its masking and increases the molecule logP. Once inside the cells, esterases will cleave the bond and release the active form of the drug. Such esters of AZT include steroid esters [23], adamantane conjugates [24] and 5'-O-Aliphatic acids derivatives [25]. Along the same line, the aforementioned ddi-Sq prodrug was tested on HIV-infected cells [16] and found to decrease the median effective dose (ED_{50}) of the drug by 2- to 3-fold towards HIV-1-LAI infected peripheral blood mononuclear cells, and the ED_{90} (effective dose for 90% of the population) by up to 8-fold on ddi-resistant HIV-infected cells, compared to the free molecule. This effect was correlated to a 3- to 4-fold increase of the amount of the intracellular metabolite of ddi when delivered as squalene conjugate, suggesting a higher uptake of ddi-Sq compared to free ddi.

Another limitation of nucleoside analogs is that once they reach the cell cytoplasm, they need to be triphosphorylated by kinases in order to be in their active form. Since these drugs are not the natural substrate of the enzymes, the recognition is not optimal, leading for some of them to dramatically low percentages of drug in the final active triphosphate form [26, 27]. To bypass these metabolic bottlenecks, a solution might come from the administration of the molecule already in its mono- or tri-phosphorylated form. Yet, these hydrophilic and charged forms of the molecule introduce two new pharmacokinetics issues: the instability towards natural phosphatases, and the very low diffusibility through biological membranes.

To make this strategy possible, several prodrugs were proposed to mask the phosphate group of the monophosphate derivative of AZT (AZT-MP), thus increasing lipophilicity and the membrane diffusibility. In this class, phosphodiester such as ether lipids have been proposed [28], even though they still present a negative charge on their molecule so they are not the ideal candidate to cross membranes [22]. Phosphotriesters derivatives of AZT-MP are the most extensively tested and also the ideal form because of their neutral character, even though their release process of AZT-MP

requires a further step. These compounds showed an interesting anti-HIV activity, demonstrating that the cleavage is correctly taking place inside the cell. Few studies though investigated the uptake of the AZT-MP prodrugs compared to AZT-MP. One of them concerns the coupling of AZT-MP to a (pivaloxy)methyl group, which gave rise inside the cells to AZT-MP, AZT-DP and AZT-TP metabolites, whereas no such metabolites have been seen after incubation of free AZT [29]. Phosphoramidate derivatives of AZT-MP have been chosen because this bond is a substrate of aspartate proteinase, which would bind to the complex and release AZT-MP inside the cell [30]. These compounds as well showed significantly higher activity towards HIV compared to free AZT [31].

An interesting approach was developed in order to chemically couple stavudine in its monophosphate form (d4T-MP) to the natural polysaccharide chitosan [32]. This conjugate was subsequently used to form nanoparticles thanks to the interaction with tripolyphosphate (TPP). *In vitro* studies at pH = 1.1 and 7.4 revealed that nanoparticles as well as chitosan-d4T-MP conjugate released the monophosphate derivative rather than the simple d4T (Figure 1), assuring therefore the protection of the phosphate group.

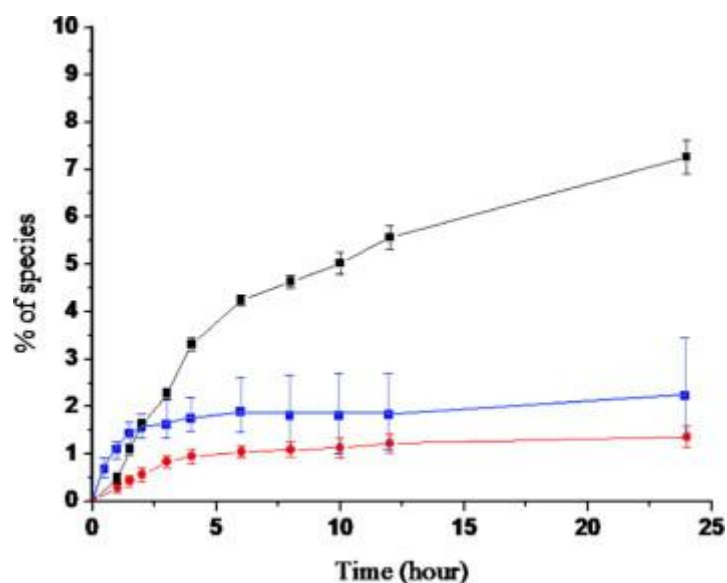


Figure 1. Release of d4T-MP (■) and d4T (●) from chitosan conjugate and d4T-MP from nanoparticles (■) at pH = 7.4 buffer solution. Reproduced from Ref. [32], with kind permission from Elsevier, Bioorganic and medicinal chemistry.

Nanotechnologies have also been proposed as a solution to protect the triphosphate derivatives of nucleoside analogues and facilitate their transport across the cell membrane. The first example comes through the use of liposomes [33]. The triphosphorylated form of ddC, ddC-TP, has been

encapsulated and compared to free ddC-TP and free ddC. No improvement on the *in vitro* efficacy against HIV was observed, and the action of liposome or free ddC-TP was lower than the free ddC. An improvement came with ddi-TP liposomes [34]. The molecule has been encapsulated and a modified mouse monoclonal antibody has been attached to the surface. Uptake by human macrophages has been improved up to 80 times compared to the free ddi-TP.

The triphosphorylated form of zidovudine, AZT-TP, has been encapsulated into aqueous-core poly(isobutylcyanoacrylate) nanocapsules after complexation of AZT-TP to cationic polymers such as chitosan or polyethylenimine (PEI), to prevent the leakage of the drug through the nanocapsule membrane [35, 36]. These nanocapsules increased the cellular delivery of AZT-TP by 10-to 30 fold compared to the free molecule [37]. AZT-TP was also associated to magnetic Fe₃O₄ nanoparticles thanks to ionic interactions [38] by simple incubation. When tested *in vitro* on PBMC, both free AZT-TP and nanoparticles gave similar concentration-dependent virus inhibition results on HIV-infected cells. Moreover, nanoparticles are not toxic towards these cells at any concentration tested.

Although these formulations exhibit high encapsulation efficiencies (80-100%), they still result in a poor drug loading (< 1% w/w), or uncontrolled drug release in the case of liposomes, limiting therefore their applications.

An improvement in terms of drug loading was proposed by Vinogradov *et al.* [39] through the use of nanogels based on cross-linked copolymers of PEI and a modified polyethylene glycol (PEG) or poloxamer P85. This polymeric network was condensed by AZT-TP through charge interactions with the protonated amino groups of PEI, resulting in so-called nanogels loaded with up to 30% w/w AZT-TP. AZT-TP has also been successfully encapsulated into nanoscale mesoporous iron trimesate metal-organic frameworks (nanoMOFs) [40]. When tested on PBMC, these systems were able to deliver 8-times more AZT-TP inside the cells than the free drug, reducing viral replication by up to 4-fold compared to AZT.

Similarly to phosphorylated nucleoside analogues, oligonucleotides are another class of drugs which, in spite of their promising antiviral efficacy, are strongly limited in their passage through cell membranes. Their encapsulation into protamine nanoparticles allowed a significantly enhanced intracellular delivery as compared to the naked oligonucleotide [41]. The cellular uptake, depending on the cell line and the oligonucleotide used, was improved between 4 to 25 times, as compared to the free molecule. Once inside the cells, these systems were able to release the oligonucleotide and to inhibit the HIV transactivation up to 54% for a concentration of 5 μ M, as compared to the free oligonucleotide which inhibited around 20%.

2.2 Extending the efficacy time of drugs

One of the main drawbacks of antiretroviral drugs is their short half-life, especially for NRTIs (half-life of AZT is 1.1 h [42], d4T 0.9-1.2 h [43] and ddC 1.2 h [44]) and PIs (half-life of indinavir is 2 h, ritonavir 3 h [11]). Therefore, many attempts have been carried out in order to extend their action time, by formulating extended release tablets, by creating prodrugs of the molecules, or through the use of nanoparticles and devices.

2.2.1 Extended release tablets

Some clinical trials have investigated the improvement of patient compliance when tablet regimens were switched from twice-daily to once-daily. This has been possible thanks to the formulation of extended release tablets of different antiretroviral drugs.

The first example of an attempt to improve plasma half-life of a drug involved a change in the formulation strategy, which consisted of coating the tablet with a semi-permeable membrane of cellulose acetate [45]. Nevertheless, this technique was not successful in extending the absorption of L-735,524 (which became then indinavir), after *in vivo* experiments on beagle dogs. No further attempts are found concerning the extended release of indinavir. In 2005, prolonged-release capsules of d4T have been proposed, which proved to enhance patient adherence compared to the group who remained on the twice-daily therapy on a 24 week study [46]. Extended release capsules of d4T were then released on the market (Zerit XR, Bristol-Myers Squibb) for once-daily treatment, but its success in the therapy appeared to be limited [47]. Indeed, even though this new formulation allowed overcoming the regimen problems of d4T, it did not significantly reduce the long-term mitochondrial toxicity of this drug which is one of its major adverse effects.

Extended release matrix tablets of AZT have been proposed as well [48]. Thanks to the presence of Eudragit and ethylcellulose in the matrix, these tablets allowed a detectable level of AZT in plasma for up to 12 hours following administration to rabbits, compared to only 4 hours with the conventional form. The tablets were put behind the tongue in order to avoid breaking due to biting. An improvement of this formulation has been developed by Santos *et al.* [49], where a mix of swellable and non-swellable polymers (namely mixing two different viscosity-grade hydroxypropylmethylcellulose (HPMC) with low (RS PO) and high (RL PO) permeability Eudragit) led to the best release profile, reducing significantly the burst release. Once-daily formulation of nevirapine has also been proved to be effective in terms of viral suppression and safety profile in the

same way as the previous twice-daily regimen, on treatment-naïve patients for 48 weeks [50]. This formulation has been marketed under the name of Viramune XR®.

2.2.2 Prodrugs

As described in section 2.1.1, many attempts have been performed to improve AZT pharmacokinetics parameters through formulation as prodrugs. After 2000, few other examples focused on extending the efficacy time using AZT as a model compound. In particular, AZT was coupled to glucose and galactose in order to improve the retention time of the molecule in the blood [51]; after intravenous injection in rats, the AUC values for the ester compounds are lower than those of the parent drug, even though a slight increase is found in the concentration of galactose ester after 4 and 8 hours. Wannachaiyasit *et al.* [52] developed an AZT-dextrin conjugate for parenteral administration. After intravenous administration to rats, this conjugate allowed a prolonged plasma level and an improved mean resident time of AZT up to 30 hours compared to 5 hours with the free molecule. AZT phosphonate derivatives (mimicking AZT-MP) have been investigated as well for purposes of extended release [53]. The new compound AZT 5'-aminocarbonylphosphonate showed interesting results in slowing down the release of AZT after oral administration, along with a decreased toxicity. Recently, the group of De Clercq reported several AZT-PEG conjugates. A first study of 2010 [54] showed a slight improvement in the pharmacokinetics parameters after oral administration of the prodrug to mice, compared to the free drug. The absorption time and the elimination time are extended, reducing the intensity of the C_{max} but shifting the T_{max} . A more comprehensive study comparing different kinds of PEG (from 750 to 10k Da) [55] highlighted the efficacy of this polymer in the shift of T_{max} and in the increase of half-life time, still maintaining their anti-HIV efficacy. A further improvement has been achieved by coupling AZT to 2-hydroxyethyl methacrylate (HEMA) through a succinic spacer [56]. This conjugate was tested *in vitro* in simulated gastric and intestinal fluids and *in vivo* after oral administration to rabbits for its release and compared to the parent drug. The AUC value was significantly improved and the plasma half-life increased from 1 to 8 hours. No further studies are found in the direction of chemically improving AZT pharmacokinetics, and possibly the efforts have been shifted on other drugs.

2.2.3 Polyester particles

Polyester polymers for drug delivery purposes include PLA, poly(lactic-co-glycolic acid) (PLGA) copolymers and poly- ϵ -caprolactone (PCL). Among them, PLGA is a copolymer which is known to degrade in a tunable way upon time; therefore, it has seen a large application in the sustained release domain. In 1998, Lewis *et al.* first introduced the use of PLGA microparticles in order to encapsulate an anti-HIV oligonucleotide [57]. These particles, when formulated like large microspheres (10-20 μm), allowed an *in vitro* sustained release of the antisense nucleic acids for up to 25 days.

PLGA microparticles have been prepared to encapsulate AZT for parenteral administration, in order to extend its half-life. Two different lactic-to-glycolic ratios have been tested *in vitro*, and all formulations exhibited a sustained AZT release for at least 25 days [58]. Nonetheless, these systems presented the inconvenience of having a low encapsulation efficiency (5%). In an effort of improving this feature, PLGA microparticles have been prepared using oil-in-oil solvent evaporation method, reaching excellent values of at least 93% of entrapped AZT [59]. Furthermore, these systems showed a sustained *in vitro* release profile for up to 4 weeks. PLGA microparticles have been developed using a spray-drying technique instead of solvent evaporation, obtaining though AZT encapsulation values from 66 to 86% [60]. These microparticles have been then compared to PLA-PEG microparticles for their release behavior. *In vitro* studies in PBS showed a sustained release for PLGA microparticles up to 125 hours, in comparison with 30 hours for PLA-PEG.

Besides microparticles, nanoparticles have also been investigated. Although their higher specific surface may not be in favor of a sustained drug release, their size is more compatible with a parenteral administration. Basu *et al.* [61] prepared PLGA nanoparticles to encapsulate d4T, chosen because of its particularly short half-life and poor bioavailability. These nanocarriers allow a sustained drug release in PBS over 2 months. The addition of gold nanoparticles in the formulation has been investigated as a tool for the diagnostics, even though the presence of gold reduced both the drug loading and the sustained release. Another formulation based on PLGA nanoparticles was developed to encapsulate ddi [62]. Some parameters were varied like drug/polymer ratio, which ranged between 20 and 300 mg of drug per 250 mg of PLGA; in 2 formulations, DMSO or PEG 400 has been added to increase the drug loading. DMSO or PEG containing formulations achieved a drug loading of 32-34% whereas between 1 and 5% was obtained with the previous nanoparticles. This was due to the amphipathic nature of DMSO which helps in bringing ddi to the polymeric phase, whereas PEG effect might be explained by its viscosity which prevents the diffusion of the drug from the polymeric phase. All the tested formulations released between 35 and 40% of the encapsulated

ddl after 60 days incubation in PBS. PLGA nanoparticles have therefore shown to be a more interesting nanocarrier for ddl than for d4T.

PLGA nanoparticles have been used also for simultaneous encapsulation of 3 drugs [63]. Furthermore, this kind of PLGA nanoparticles has been tested *in vivo* as well. The group of Destache prepared PLGA nanoparticles containing ritonavir, lopinavir and efavirenz for intraperitoneal injection in mice. The corresponding free molecules are detectable in blood and some organs no more than 3 days after injection. On the other side, nanoformulated antiretrovirals are still found in blood and organs up to 28 or 35 days after the administration.

PCL has been chosen as well for sustained release system because of its similar features to PLGA and its safety. Nevertheless, it is quite permeable to lipophilic drugs. For the encapsulation of efavirenz, PCL and a poly(methacrylate) polymer (Eudragit RS 100) have been associated for the formulation of stable nanoparticles, in order to avoid the molecule leakage and therefore a burst release [64]. Pure PCL, pure Eudragit or a mix of the two polymers nanoparticles have been prepared and showed a sustained release for up to one week. Furthermore, the more the Eudragit present in the formulation, the lower the burst release. PCL nanoparticles were tested also to encapsulate Lamivudine [65]. When incubated in media with different pH, these particles also exhibited a sustained release profile (70 to 80% of the drug after 4 days, similarly to the previous group's work).

2.2.4 Nanocrystals

Several anti-HIV drugs have been formulated as nanocrystals, mostly in order to improve their dissolution profile. Nanocrystals are submicron carrier-free drug delivery systems stabilized by surface active agents [66]. The main techniques used for their production are pearl milling [67], precipitation [68] and high-pressure homogenization [69]. This process is particularly adapted to drugs with a low solubility associated with a poor oral bioavailability. It is also suggested that these drugs, formulated as nanoparticles and injected intravenously, will be opsonized and subsequently retained in the Kupffer cells in the liver, providing a sustained release in the reticulo-endothelial system [13].

Atazanavir, ritonavir and efavirenz nanocrystals were prepared by high-pressure homogenization using poloxamer 188 and PEG as excipients in order to avoid aggregation. In first instance, it has been shown that these particles are taken up by human monocyte-derived macrophages and constantly released for up to 20 days. This effect is even increased when these drugs are used in combination [70]. After subcutaneous injection in mice, these formulations consistently exhibited a sustained release profile over a week, in blood and tissues, and maintained an anti-HIV efficacy [71]. Some

toxic effects (variation in platelet and blood lymphocytes counts) have been found but of modest extent. Further pharmacokinetics studies in mice show a sustained release over 7 days between repeated weekly injections, in contrast with level fluctuations in the case of free drug administration (Figure 2) [72]. After subcutaneous administration to monkeys, drug levels are still detectable in plasma after 38 days. Intramuscular injection is found to be better in order to avoid local reactions emerging in the case of subcutaneous injections. The presence of nanoparticles inside hepatic Kupffer cells was confirmed by flow cytometry and confocal microscopy, suggesting a reservoir role of the nanoparticles [72].

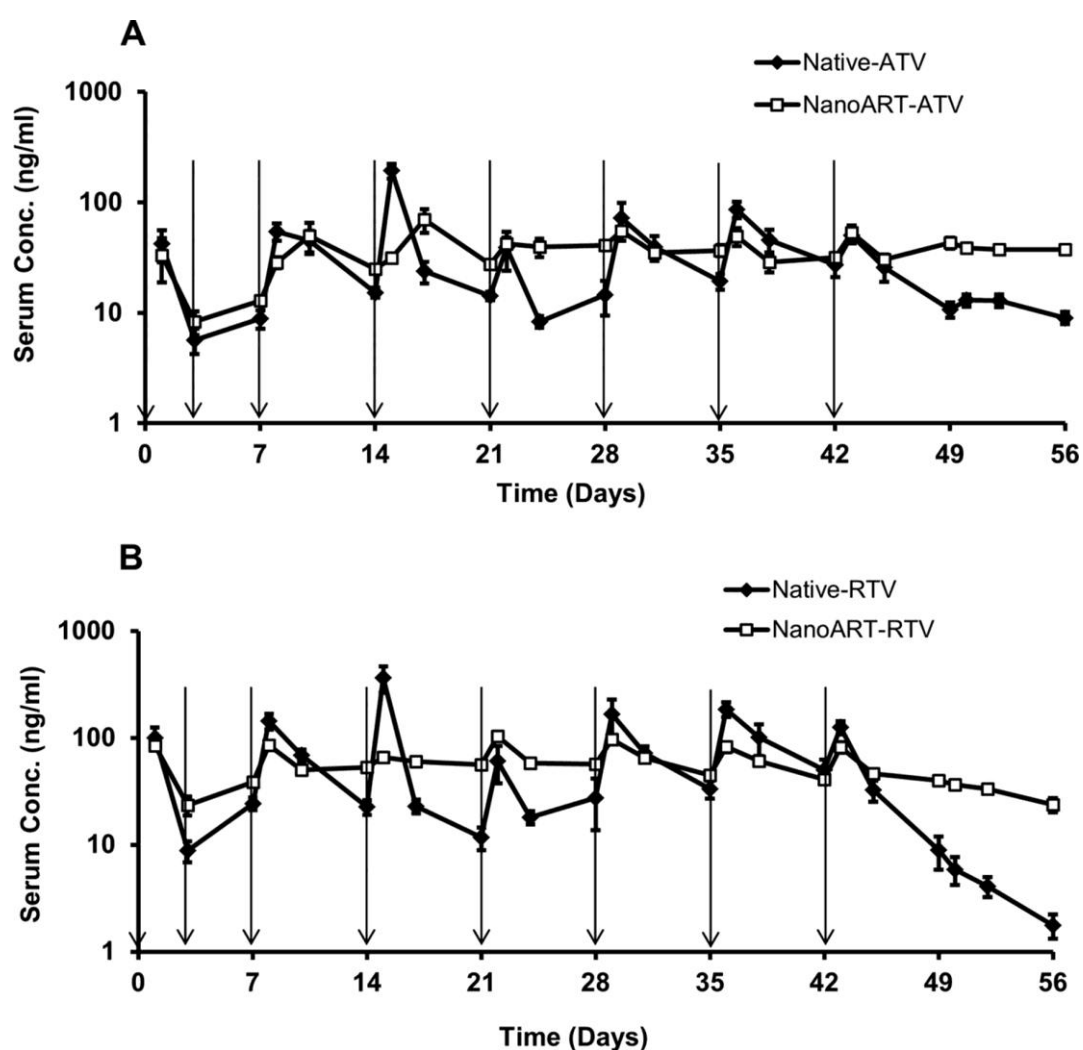


Figure 2. Serum concentrations of atazanavir (ATV) and ritonavir (RTV) nanocrystals after subcutaneous injection in mice as compared to the free drugs. Arrows indicate administration days. Reproduced from Ref. [72], with kind permission from American Society for Microbiology, Antimicrobial agents and chemotherapy.

One of the longest release kinetics from nanoparticles has been obtained by the group of Kesteley, who synthesized a broad series of new protease inhibitor compounds [73]. Among them, the most efficient against HIV were selected for nanosuspension formulation by wet milling using different surfactants (polysorbate 20, poloxamer 338 and Vit-E TPGS) and injected intramuscularly to rats. After an initial burst, the drug level in blood presents a lower but constant profile (1-10 ng/ml) for up to 2 months, without any significant difference among the various formulations.

Two particularly promising nanoparticle formulations of rilpivirine and GSK1265744, an integrase inhibitor similar to dolutegravir, for monthly injectable administration are reviewed by Spreen *et al.* [74]. Both of them have been formulated as nanocrystals because of their low solubility. Rilpivirine nanosuspension has been tested intramuscularly or subcutaneously in a phase I clinical study on healthy volunteers, showing prolonged drug exposure up to 12-26 weeks. Two phase I studies have been run with GSK1265744 injected intramuscularly or subcutaneously, resulting in detectable plasma levels after 24 weeks, regardless of the injection route.

2.2.5 Lipid-based formulations

Few strategies have been investigated to formulate anti-HIV drugs in delivery systems other than polymeric nanoparticles; interesting results are found, which though show altogether less improvement than those brought by the use of polymeric nanoparticles.

Tenofovir has been encapsulated into niosomes, which are nonionic surfactant vesicles, and their release behavior has been studied in different media for 24 hours [75]. 80% of the drug was released in 12 hours, and its totality after 24 hours. *In vivo*, these systems more than doubled the bioavailability of the parent molecule, after oral administration to rats.

The only liposome formulation found for sustained release of anti-HIV drugs introduced an improvement compared to the previous systems. Saquinavir-loaded liposomes have been prepared and compared to PEGylated ones [76]. *In vitro* incubation with PBS triggered the complete release of liposomes after 20 hours, whereas PEGylated ones presented a more sustained release for up to 50 hours. When tested on Jurkat cells, they showed lower cytotoxicity compared to the free molecule.

A lipid-indinavir complex has been prepared to be administered subcutaneously to macaques, where it exhibited important lymphatic tissue distribution and anti-HIV effect [77]. Following this result, a pharmacokinetic model was developed to predict the release of the complexes, finding out that a therapeutic level of indinavir from lipid complex could be expected in lymph nodes up to around 4 days after injection [78]. Despite this interesting prediction, no further studies are found in the literature to demonstrate *in vivo* the sustained release capacity of these complexes.

2.2.6 Implants and devices

Besides the advantages of a possible sustained release, non-oral formulations may also be necessary in some particular cases, e.g. for patients unable to swallow tablets or capsules because of gastrointestinal complications [79].

Baert *et al.* developed an interesting system for the delivery of darunavir, based on an implantable infusion pump (Codman) with a reservoir of 16 mL [80]. After surgery to implant the pump in the flank of dogs, darunavir solubilized in a PEG solution has been delivered to 2 animals with a constant flow of 0.5 mL/day for up to 25 days. Throughout the whole experiment, constant values of about 40 ng/mL of Darunavir were found in the plasma of both animals. In spite of these promising results, the requirement of a surgery may be the major difficulty hindering further development.

Enfuvirtide, because of its peptide nature, is poorly absorbed by the oral route. It therefore needs to be administered twice-daily by subcutaneous injection. Because of the particularly poor patient compliance associated to this regimen, an *in situ* forming implant based on PLGA has been developed [81]. The polymer is solubilized in DMSO and the micronized drug is then added to the solution. After injection in an aqueous medium, the system turns into a solid depot. *In vitro* studies after injection of the system in PBS showed a drug release between 60 and 100% in 2 days depending on the PLGA-to-drug ratio. After subcutaneous injection to rats, drug levels in blood were found rather constant and still of pharmacological interest after 48 hours, thus improving the pharmacokinetic profile of the native drug (Figure 3).

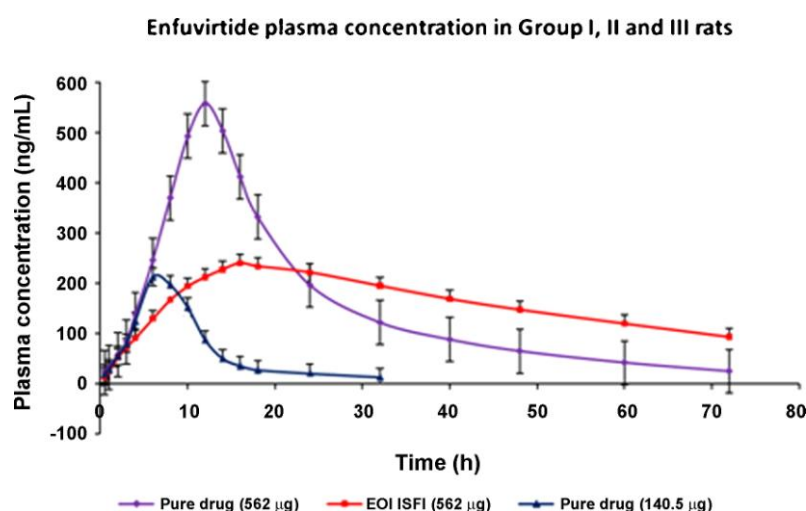


Figure 3. Enfuvirtide plasma concentration as free drug at 2 different doses, compared to PLGA formulated drug after subcutaneous injection to rats. Reproduced from Ref. [81], with kind permission from Elsevier, International Journal of Pharmaceutics.

2.3 Conclusions

The use of prodrugs and the drug encapsulation into micro/nanocarriers has overall allowed a significant improvement in the anti-HIV drugs' bioavailability. Extended release tablets represent the first step in the achievement of patients' life improvement, reducing their 'pill burden'. Some solutions in this sense are already on the market. Other strategies have been proposed as well, for more specific cases and are still under development. PLGA has been widely studied in form of nanoparticles, microparticles or *in vivo* forming implants, revealing its relevance in the context of extending the release of anti-HIV drugs. Systems showing monthly trends of release may be good candidates to be translated into clinical tests.

3. Biodistribution improvement: drug targeting towards virus reservoirs and sanctuaries

Intensive research is currently undertaken to gain better understanding of reservoirs and sanctuaries, in order to target them more efficiently. They are particularly important in the evolution of the disease because they may be responsible for the chronicity and development of resistances. Furthermore, their possible production of new viruses from the latent state prevents therapeutic interruptions, in order to avoid viral rebounds. The different drug delivery systems described in this section are recapped in Table 2.

3.1 Mononuclear phagocyte system (MPS) targeting

Leukocytes are one of the main HIV reservoirs [82] and the first choice as targets, for the following reasons: drug activity inside these cells is particularly poor [83]; an important type of them, the macrophages, are able to phagocyte particles (and potentially drug carriers); thirdly they are an important responsible for the spread of the virus to the brain [84]. For all these reasons, several efforts are reported in the literature about targeting drugs mainly to macrophages and monocytes. Furthermore, when monocytes and macrophages are located in certain regions of the body, they belong to the mononuclear phagocyte system (MPS). This includes lymph nodes, spleen, liver, bone marrow, central nervous system and peritoneal cavity. Therefore, the targeting to these body compartments should also be considered in the strategies against HIV. The studies found about this topic can be distinguished depending on their administration route, mainly parenteral (intravenous or others) and oral, which will be developed in the following sections.

BIODISTRIBUTION CHALLENGES	DRUGS INVOLVED	STRATEGY PROPOSED
MPS targeting:		
by intravenous route	AZT, AZT-MP, d4T-MP, ddl	Prodrugs
	AZT, L-689,502, ddl	Liposomes
	AZT	LDL
	saquinavir, ddC, AZT	PIBCA NPs
	Oligonucleotides	PLGA MPs
	atazanavir, efavirenz, ritonavir, nevirapine	Nanocrystals
	siRNA	Dendrimers
	ddC-TP, adefovir, tenofovir	Erythrocytes
by intraperitoneal or subcutaneous route	indinavir	SLN
	--	PEG NPs
	ddC-TP	Liposomes
	clodronate	Erythrocytes
by oral route	AZT	PHCA NPs
	ddl	Prodrugs
brain and central nervous system (CNS) targeting	ritonavir, AZT-TP	NPs
	abacavir	Prodrugs
	atazanavir, ritonavir, indinavir, efavirenz	Nanocrystals
	efavirenz	Micelles
	saquinavir	Nanoemulsions

Table 2. Biodistribution challenges, drug delivery strategies developed and drugs involved in their formulation.

3.1.1 Intravenous administration

First approaches started in the 1990s in an attempt to target anti-HIV drugs to the leukocytes, mainly macrophages. Molema *et al.* reported in 1990 the targeting of the monophosphate derivative of AZT (AZT-MP) to the T-lymphocytes, through the conjugation of the molecule to neoglycoproteins [85]. *In vitro* studies showed the recognition of the lectin receptor on the surface of HIV-infected cells. This strategy of targeting the lectin receptor has been also reported using galactosylated liposomes encapsulating AZT [86]. These systems have been tested *ex vivo* on rats' alveolar macrophages,

showing an uptake of liposome drug 8 times higher than free AZT. Evaluated *in vivo* on rats, these systems demonstrated almost no toxicity to hematological parameters, compared to toxic effects of free AZT. Galactosylated liposomes extended the blood circulation time of AZT up to 12 hours, compared to 2 hours of the free molecule. The distribution in the main organs (liver, spleen, lymph nodes and lungs) is significantly higher in the case of liposomes than the free AZT [86].

Another strategy to deliver AZT to macrophages has been developed through the use of acetylated low density lipoproteins (LDL) and their interaction with scavenger receptors [87]. Several chemical modifications have been tested on AZT in order to improve its incorporation efficiency in the lipoproteins. Cell studies on macrophages exhibited a 10 times higher uptake of encapsulated drug compared to the free AZT. AZT has also been encapsulated into a so called emulsome, a nanocarrier consisting in a solid lipid core and a surrounding layer of phospholipids. Positively charged emulsomes have also been prepared through the coating with stearylamine [88]. 24 hours after intravenous administration to rats, no free molecule is detected in the liver, whereas 5% of emulsome-formulated and 12% of stearylamine-coated AZT is found in liver cells.

Liposomes loaded with a protease inhibitor (L-689,502) were able to efficiently deliver the drug to HIV-infected monocyte-derived macrophages and reduce *in vitro* viral replication [89]. These systems also inhibited the production of virions in the H9 CD4⁺ T cell line. Such liposomes are expected to enter macrophages preferentially and work as drug reservoirs following intravenous administration. Myeloid dendritic cells have also been selected as target for anti-HIV drug delivery. Gieseler *et al.* prepared liposomes able to target CD209 on the membrane of these cells, which is responsible for the transfer of the virus to other cells, through the coating with specific antibodies (MOPC-21/P3) [90]. No particular drug was encapsulated, but the concept was exemplified by using calcein as a tracer. These liposomes exhibited a superior targeting efficiency compared to those coated with other markers, as demonstrated by flow cytometry and fluorescence microscopy. Similarly, ddi-loaded liposomes have been tested *in vitro* for their accumulation in murine monocyte-macrophage RAW 264.7 cells and human premonocytoid U937 cells, where they showed a lower uptake and antiviral efficacy on macrophages compared to the free molecule. When tested intravenously in rats, these carriers however improved pharmacokinetic parameters of ddi, increasing drug levels in plasma and lowering its clearance by 120 times compared to free ddi. Furthermore, increased drug accumulation in organs of MPS has been found for liposomal formulations [91].

Other targeted liposomes were designed by coating their surface with a non-toxic variant of diphtheria toxin (CRM197), which is an exogenous substrate for heparin-binding epidermal growth factor expressed on leukocytes membranes [92]. These systems have been loaded with horseradish peroxidase and tested *in vitro* on human lymphocytes T (SupT1) for 24 hours, where they show an efficient uptake, reaching almost all the observed cells. After intravenous injection in hamsters,

around 12% of rhodamine can be seen in leukocytes isolated from the blood of animals which received CRM197 coated liposomes. No fluorescence can be detected in cells of animals receiving plain liposomes.

In parallel to liposomes, other nanocarrier strategies have been investigated. The first example reporting the use of polymeric nanoparticles for anti-HIV applications were the polyhexylcyanoacrylate nanoparticles by Bender *et al.* [93]. These particles were prepared by emulsion polymerization in presence of saquinavir or ddC. They showed an increased antiviral efficacy on HIV-infected human cells in the case of saquinavir (up to 10-times higher), while no difference has been seen for ddC-loaded nanoparticles compared to the free molecule. Interestingly, the uptake of PACA nanoparticles has been found more important by HIV-infected monocytes/macrophages, compared to non-infected ones [94]. For *in vivo* purposes, these particles were loaded with AZT and injected intravenously in rats [95]. AZT levels in organs of the MPS were found up to 18 times higher in the case of nanoparticles, compared to the free drug, especially in those surrounded by reticular connective tissue (liver, spleen, lungs, bone marrow and lymph nodes). PLGA microparticles have been designed for the delivery of anti-HIV oligonucleotides to macrophages in culture [96]. Microspheres have been prepared using a double-emulsion solvent evaporation technique, obtaining a size of 1-2 μm . The uptake of the oligonucleotide was improved 10 times compared to the free drug. Yang *et al.* prepared the aforementioned chemical conjugation between chitosan and d4T-MP [32]. When tested on infected human leukocyte T cells, the antiviral activity of the conjugate is lower than parent drug, but the toxicity also decreases, leading to a better selectivity index (CC_{50}/EC_{50}).

Atazanavir, efavirenz and ritonavir nanocrystals (nanoART) have been proposed as well in the context of targeted delivery [70]. These carriers are taken up by human monocyte-derived macrophages through clathrin-coated pits [97]. Furthermore, nanoART are preserved and released intact from the cells, maintaining also their anti-HIV activity. This shows their interest not only as macrophage-targeting systems but also in using macrophages as vehicles to reach HIV sanctuaries. Nevirapine, chosen because of its poor solubility, has been formulated as well as nanocrystals, which have then been modified on their surfaces with albumin, PEG or dextran. These systems have been tested on peritoneal rat-derived macrophages, showing a higher uptake in the case of albumin and dextran compared to bare nanoparticles and to the free drug [98]. The efficacy of albumin and dextran nanocrystals has been confirmed also in *in vivo* studies in rats. After intravenous administration, drug level detection in different organs (brain, lung, liver, kidney, spleen, heart and thymus) was found higher in animals treated with albumin and dextran nanocrystals as compared to bare nanocrystals and free nevirapine.

Negatively charged albumins have been considered as anti-HIV drugs until clinical studies demonstrated their liver toxicity and lack of effect [99]. Before these findings, the biodistribution of succinylated and aconitylated human serum albumins has been studied after intravenous injection in rats [100]. Because of their negative charge, these proteins have better distribution in lymph rather than in blood, thanks to a receptor-mediated transcytotic process.

Nanoscale self-assembled prodrugs have also been investigated. Vesicular self-assemblies of a dual AZT prodrug were prepared and their anti-HIV effect was tested on MT4 cells [101]. *In vitro*, the systems have the same efficacy as the free drug. After intravenous injection in rabbits, significant levels of AZT are found in the liver, spleen and testis located macrophages, even though no comparison is reported with a corresponding dose of free AZT. Another example of dual prodrug is the association between AZT and ddi through a phosphoryl-deoxycholy spacer [102]. This new lipid compound is able to self-assemble into spherical vesicles. *In vitro* studies on MT4 cells demonstrated that the compound is cleaved to its original molecules, since the same EC_{50} as AZT is found. After intravenous administration of vesicles to mice, high levels of AZT have been found in macrophage-rich tissues (spleen, lymph nodes, thymus, liver, lung), confirming the targeting role of vesicles and the ability of the molecule to release intact AZT.

The delivery of siRNA to CD4 T lymphocytes is particularly challenging as these cells are difficult to transfect with non viral carriers. An original strategy to deliver anti-HIV drugs to cells have been recently developed by Perisé-Barrios *et al.*, who prepared siRNA-loaded dendrimers of carbosilane [103]. Dendrimers are synthetic polymers which arrange in a tree-like structure starting from a central core [104]. Two types of siRNA loaded dendrimers have been tested on CD4 T lymphocytes isolated from human PBMC, showing an internalization of 16 or 36% depending on dendrimer formulation. When tested on HIV-infected CD4 T lymphocytes, free siRNA induced a reduction of p24 level of 10%, whereas 25 and 50% reduction were achieved with the two different types of dendrimers encapsulating siRNA. Furthermore, no inflammatory response was induced in macrophages incubated 10 minutes with the dendrimers, and these systems were also able to reduce the phagocytosis of macrophages, in order to avoid their possible future infection with HIV.

An original strategy has been proposed in 1992 consisting of loading erythrocytes with anti-HIV drugs in order to target the immune system. Erythrocytes have been loaded with ddC-TP and then activated with Zinc, in order to induce the recognition by immune system and the uptake by monocytes and macrophages [105]. These drug carriers were able to inhibit *in vitro* the viral replication in infected macrophages for up to 3 weeks, and to reduce the typical signs of the disease in infected mice. This concept of using erythrocytes was further developed by encapsulating the phosphonate PMEA (adefovir) [106]. These systems were also able to inhibit virus replication up to 90% and to carry 500-fold more drug into macrophages compared to free PMEA. This principle has

also been applied for the encapsulation of a double drug, consisting in the coupling between acyclovir and PMPA (tenofovir), treating thus at the same time herpes virus (HSV-1) and HIV [107]. These systems showed their efficacy in protecting human macrophages from both infections. The last study reported about using red blood cells as carriers deals with the encapsulation of a prodrug of PMEA, which consists in two units bound together (bis-PMEA) [108]. Inside red blood cells, the prodrug is converted into its active form. A higher level of drug was found to be retained inside macrophages when the drug was administered as dimers, compared to the parent drug.

3.1.2 Other parenteral routes of administration

In this section, the other parenteral routes of administration taken into account are the subcutaneous and intraperitoneal ones. This latter one is used especially for *in vivo* studies in animals.

Ho's group developed solid lipid nanoparticles (SLN) encapsulating indinavir, able to accumulate in lymphatic tissue. After subcutaneous injection to macaques, they significantly increased the accumulation of indinavir in peripheral and visceral lymph nodes compared to the free molecule [77]. In order to improve the targeting and the selectivity towards HIV-infected cells, indinavir-loaded nanoparticles have been coated with 4 different CD4-binding peptides, among which two have been selected for their efficacy [109]. These systems efficiently bound to CD4 receptors on CEMx174 cells (a hybrid cell line of human B cell line 721.174 and human T cell line CEM) and enhanced anti-HIV activity of indinavir compared to the free molecule.

Novel peptide-backbone PEG nanoparticles have been prepared by coupling the backbone of the peptide N-formyl-methionyl-leucyl-phenylalanine, which is known to target the formyl peptide receptors on macrophages surface, to a heterobifunctional PEG [110]. After intraperitoneal injection of nanoparticles to mice, peritoneal macrophages were collected and the nanocarrier levels were found to increase with the amount of fMLF on their surface (Figure 4). Pharmacokinetics studies following intravenous administration to rats revealed a prolonged plasma concentration as the amount of fMLF increases, and a preferential distribution in lung, kidneys and spleen but not in brain, heart and intestine. Molecular weight of PEG also played a role: the longer the chain the longer the circulation time, thus increasing nanoparticle possibilities of being taken up by macrophages instead of being eliminated.

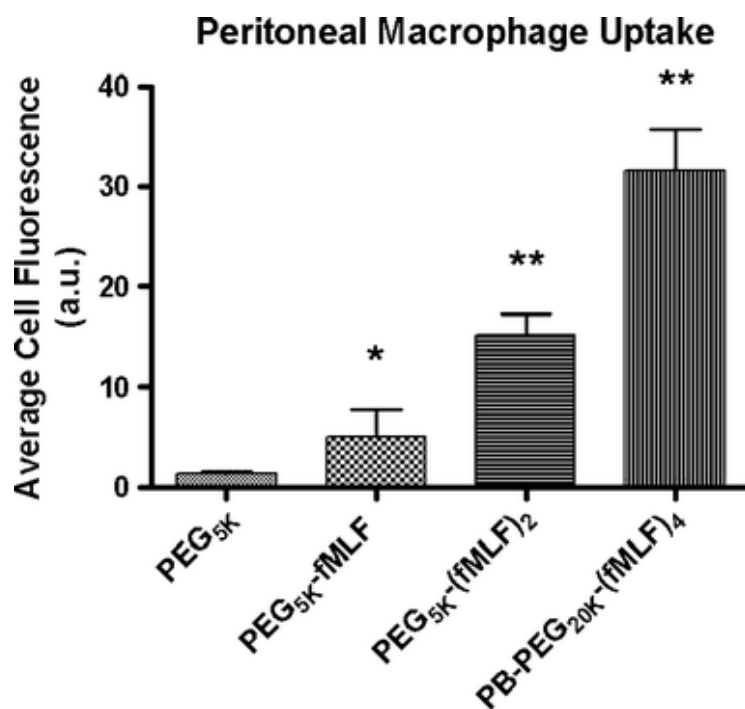


Figure 4. Peritoneal macrophage uptake of PEGylated nanoparticles after intraperitoneal injection to mice as a function of the number of fMLF (N-formyl-methionyl-leucyl-phenylalanine) on the surface and to the length of PEG chain. Reproduced from Ref. [110], with kind permission from Springer, Pharmaceutical Research.

Among the few *in vivo* studies involving the encapsulation of a triphosphate nucleotide analog, ddC-TP-loaded liposomes have been reported by Oussoren *et al.* [111]. These systems were efficient in encapsulating and protecting the drug, maintaining their size and limiting drug leakage. ddC-TP liposomes have been tested by multiple doses of intraperitoneal injection in infected mice (MAIDS), and compared to empty liposomes. ddC-TP liposomes demonstrated to cumulate in spleen and bone marrow, reducing the proviral DNA in the cells of MPS of 32 and 26% respectively.

Recently, the strategy of using red blood cells as drug carriers has been applied to deliver clodronate to infected macrophages, in order to deplete them, on a murine model of AIDS [112]. The effect has been tested after intraperitoneal injection to mice also treated with AZT and ddl, giving similar results in terms of viral reduction but leading to a significant delay in the viral rebound after therapy interruption.

3.1.3 Oral route

Poly(hexylcyanoacrylate) nanoparticles encapsulating AZT have been proposed as well, and orally administered to rats by gavage [113]. The greatest nanoparticle effect has been proved in the liver where the difference of AZT accumulation was of 30% as compared to the free administered drug. Improvements in AZT concentration have been achieved also in spleen, lungs, brain and bone marrow. The mechanism suggested for the high concentration in spleen, liver and lymph nodes is an improved lymphatic uptake. Poly(isohexylcyanoacrylate) nanospheres have been developed by another group to deliver AZT to the gastrointestinal mucosa [114]. After intragastric administration in rats, the AZT level in the intestinal mucosa and the Peyer's patches was found 4 times higher when formulated as nanoparticles, compared to the free molecule. This approach shows to be efficient to cumulate drugs in the GALT and in the gastro-intestinal tract.

Squalene-based ddl nanoparticle prodrugs have also been investigated for delivery by the oral route [16]. After oral administration in rats, ddl-Sq demonstrated to cumulate in several tissues, particularly in liver, spleen and bone marrow, in a higher concentration than free ddl (Figure 5).

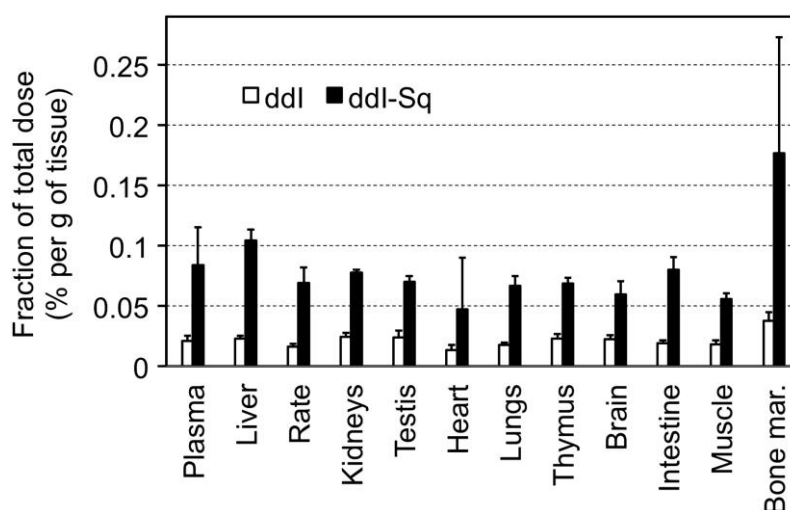


Figure 5. Biodistribution of ddl and ddl-squalene, 24 hours after oral administration to rats. Reproduced from Ref. [16], with kind permission from Elsevier, Biomaterials.

3.2 Brain and central nervous system (CNS) targeting

Brain is an organ protected from possible infections and threats by the presence of the blood-brain barrier (BBB) including the efflux transporters (e.g. P-glycoprotein). Unfortunately, this efficient system also prevents the passage of many drugs. Because of this peculiarity, brain constitutes a virus sanctuary, where the infection can also create neurological disorders. Therefore, there is a great need to target anti-HIV drugs to the brain.

A few excellent reviews have covered the various approaches reported in this field until 2010 [115, 116]. The most studied carriers for this purpose include liposomes, dendrimers, micelles and polymeric nanoparticles. The latter seem very promising in achieving a brain delivery of anti-HIV drugs, especially when they are targeted through the surface-conjugation of peptides. In particular, the TAT (trans-activating transcriptional activator) peptide, which is produced by HIV-infected cells, is able to cross cell membranes of different types of cells, and could therefore be used as targeting moiety [117]. Other strategies involve the use of prodrugs, which increase the lipophilic character of the molecule and allow therefore a better passage through BBB, or the temporary disruption of BBB which can be obtained through hyperosmotic solutions or through low-frequency ultrasound irradiation. In parallel, an effort is required in developing a more adequate model of BBB during HIV-infection, which appears to be modified with functional and structural alterations, for example in terms of membrane proteins [118].

Among the recent findings, Ritonavir-PLA nanoparticles have been formulated to inhibit viral replication in monocyte-derived macrophages [119], particularly those found in the brain. These nanoparticles, prepared by emulsion-evaporation technique, have been conjugated to the TAT peptide in order to cross more easily the BBB. Ritonavir nanoparticles were able to reduce reverse transcriptase activity, even though less efficiently than free ritonavir. No toxicity towards neural cells has been observed. A hybrid form of nanocarrier, halfway between inorganic nanoparticles and liposomes, has been proposed as well to target the brain: AZT-TP is ionically adsorbed onto magnetic iron oxide nanoparticles, after which phosphatidyl choline and cholesterol are added to form liposomes [120]. These composite systems have been tested on an *in vitro* model of BBB, showing their ability to cross the membrane when an external magnetic field was applied, as compared to free AZT-TP. Furthermore, these particles were also taken up by monocytes, which were then able, under a magnetic field, to migrate through BBB 3 times better than non-magnetic monocytes. Therefore, monocytes could be used as drug carriers to deliver AZT-TP containing magnetic nanoparticles to the brain. A prodrug strategy has been proposed by using abacavir [121], consisting in forming a dimer of this molecule through a disulfide bond, which is supposed to be reduced in the cytosolic environment of cells and release the two original molecules. This conjugate demonstrated

to be stable towards esterases within blood and to significantly inhibit P-glycoprotein on 12D7-MDR, a T lymphoblastoid cell line, as compared to monomeric abacavir. Furthermore, once passed through BBB, this prodrug is able to revert to its monomeric form and inhibit viral replication more efficiently than the parent drug. The groups of Kanmogne, Gendelman and Kabanov prepared nanocrystals of atazanavir, ritonavir, indinavir and efavirenz. *In vitro* studies demonstrated that mononuclear phagocytes were able not only to take up these nanocrystals [122], but also to transfer them to human brain microvascular endothelial cells [123]. Moreover, the transfer efficiency is improved when nanoparticles are coated with folate. *In vivo* studies on mice show a 3- to 4-times higher accumulation of folate nanoparticles in brain compared to non-coated nanoparticles, associated with a viral reduction and diminished macrophage activation.

The group of Sosnik recently reported the delivery of efavirenz to the brain by intranasal administration of drug-loaded poloxamer micelles [124]. When tested *in vivo* on rats, micelles resulted in a 4 fold increase in brain accumulation and 5 fold relative exposure index (which is the ratio between the area under the curve in the CNS and plasma), as compared to the intravenous injection of the same micelles (Figure 6). The transport mechanism suggested involves the nanoparticle internalization by the terminals of the olfactory and trigeminal nerve systems.

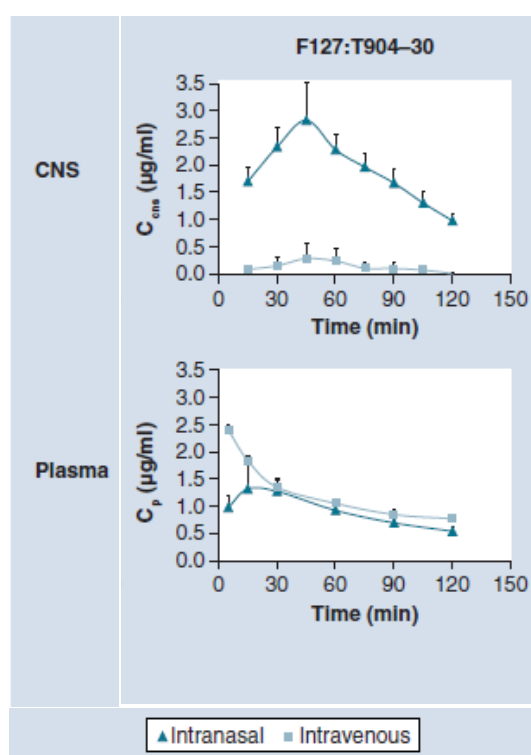


Figure 6. CNS and plasma distribution of micelle-encapsulated efavirenz after intranasal or intravenous administration in rats. Reproduced from Ref. [124], with kind permission from Future Medicine Ltd, Nanomedicine.

Another approach involving the intranasal route has been proposed to encapsulate Saquinavir mesylate into nanoemulsions prepared with a mixture of glycerides (Capmul MCM), Tween and PEG [125]. *Ex vivo* permeation studies have been run on a sheep nasal mucosa, demonstrating a passage of 77% of nanoparticles compared to 27% of the free drug. Biodistribution studies were carried out on rats, revealing higher drug concentration in brain after intranasal administration of nanoparticles, as compared to the same amount of intravenously administered free drug. A peak was reached after 1 hour, with a brain accumulation 62 times higher than with the free drug.

Another strategy to target the brain consists in decorating the surface of poly(butylcyanoacrylate) nanoparticles with PEG [126] or polysorbate 80 [127]. Further studies to understand the mechanism revealed that they enter the blood brain barrier thanks to the absorption of apolipoprotein E on their surface and the consequent interaction with lipid receptor [128-130]. No studies are found with encapsulation of an anti-HIV drug, but this seems a promising way to deliver antiretroviral to the brain sanctuary.

3.3 Conclusions

Several researches have been developed in order to target the viral reservoirs and sanctuaries. Despite all these promising results, translation into clinical trials remains challenging. Among the possible reasons, there could be the difficulty in scaling-up the production on laboratory amounts [131]. Furthermore, the peculiarity of drug carriers often renders toxicology data not always satisfactory or pertinent. The same concern can be applied to excipients in the case of repeated injections (chronic treatment). Another limitation of nanocarriers is their drug loading, often very low because of the presence of the carrier. Nevertheless, this issue has been partially solved by the use of prodrugs. Systems developed for intravenous administration are not always realistic; if they do not provide a sustained release, a daily intravenous injection for an HIV-infected patient is most likely not conceivable. Addressing these problems should be the way to promote their translation into clinical applications.

4. Conclusions

From the beginning of 1990s, several strategies have been investigated in order to improve HIV chemotherapy, mainly involving drug delivery systems. At first, efforts have been concentrated on

the targeted delivery towards virus reservoirs and sanctuaries; more recently, the patient compliance issue also took a relevant place in the HIV-related research topics. Even if drug delivery strategies did not provide a cure yet, sustained release studies seem promising in bringing soon an improvement in therapy regimens. Additionally, simultaneous intake of multiple drugs appears to be a necessary feature of HIV treatment. Therefore, drug delivery systems should be tested in combination with conventional HAART or minimum other two drugs, which has started to be applied in the research of the last few years. Finally, concerning the reservoirs and sanctuaries targeting, concrete applications seem to be more distant, because of the complexity of the systems and of human physiology. Further studies and characterizations need to be achieved before a possible clinical translation.

References

- [1] Department of Health and Human, S.; Available at <http://aidsinfo.nih.gov/ContentFiles/AdultandAdolescentGL.pdf>, **2013**.
- [2] Ministère des affaires sociales et de la Santé, Conseil national du Sida, Agence nationale de recherches sur le sida et les hépatites virales; Available at <http://www.sante.gouv.fr/rapport-2013-sur-la-prise-en-charge-medicale-des-personnes-vivant-avec-le-vih.html#>, **2013**.
- [3] Kumari, G.; Singh, R. K., Anti-HIV Drug Development: Structural Features and Limitations of Present Day Drugs and Future Challenges in the Successful HIV/AIDS Treatment, *Curr. Pharm. Design*, **2013**, *19*, 1767-1783.
- [4] Krentz, H. B.; Cosman, I.; Lee, K.; Ming, J. M.; Gill, M. J., Pill burden in HIV infection: 20 years of experience, *Antivir. Ther.*, **2012**, *17*, 833-840.
- [5] Mocroft, A.; Youle, M.; Moore, A.; Sabin, C. A.; Madge, S.; Lepri, A. C.; Tyrer, M.; Chaloner, C.; Wilson, D.; Loveday, C.; Johnson, M. A.; Phillips, A. N., Reasons for modification and discontinuation of antiretrovirals: results from a single treatment centre, *Aids*, **2001**, *15*, 185-194.
- [6] Deeks, S. G.; Autran, B.; Berkhout, B.; Benkirane, M.; Cairns, S.; Chomont, N.; Chun, T.; Churchill, M.; Di Mascio, M.; Katlama, C.; Lefeuvre, A.; Landay, A.; Lederman, M.; Lewin, S.; Maldarelli, F.; Margolis, D.; Markowitz, M.; Martinez-Picado, J.; Mullins, J.; Mellors, J.; Moreno, S.; O'Doherty, U.; Palmer, S.; Penicaud, M.; Peterlin, M.; Poli, G.; Routy, J.-P.; Rouzioux, C.; Silvestri, G.; Stevenson, M.; Telenti, A.; Van Lint, C.; Verdin, E.; Woolfrey, A.; Zaia, J.; Barré-Sinoussi, F., for The International AIDS Society Scientific Working Group on HIV Cure, Towards an HIV cure: a global scientific strategy, *Nat Rev Immunol*, **2012**, *12*, 607-614.

- [7] Coleman, C. M.; Wu, L., HIV interactions with monocytes and dendritic cells: viral latency and reservoirs, *Retrovirology*, **2009**, *6*.
- [8] North, T. W.; Higgins, J.; Deere, J. D.; Hayes, T. L.; Villalobos, A.; Adamson, L.; Shacklett, B. L.; Schinazi, R. F.; Luciw, P. A., Viral sanctuaries during highly active antiretroviral therapy in a nonhuman primate model for AIDS, *J Virol*, **2010**, *84*, 2913-22.
- [9] Cory, T. J.; Schacker, T. W.; Stevenson, M.; Fletcher, C. V., Overcoming pharmacologic sanctuaries, *Curr. Opin. HIV AIDS*, **2013**, *8*, 190-195.
- [10] Ojewole, E.; Mackraj, I.; Naidoo, P.; Govender, T., Exploring the use of novel drug delivery systems for antiretroviral drugs, *Eur. J. Pharm. Biopharm.*, **2008**, *70*, 697-710.
- [11] das Neves, J.; Amiji, M. M.; Bahia, M. F.; Sarmiento, B., Nanotechnology-based systems for the treatment and prevention of HIV/AIDS, *Adv. Drug Deliv. Rev.*, **2010**, *62*, 458-477.
- [12] Gupta, U.; Jain, N. K., Non-polymeric nano-carriers in HIV/AIDS drug delivery and targeting, *Adv Drug Deliv Rev*, **2010**, *62*, 478-90.
- [13] Parboosing, R.; Maguire, G. E.; Govender, P.; Kruger, H. G., Nanotechnology and the treatment of HIV infection, *Viruses*, **2012**, *4*, 488-520.
- [14] Kiser, P. F.; Johnson, T. J.; Clark, J. T., State of the Art in Intravaginal Ring Technology for Topical Prophylaxis of HIV Infection, *Aids Rev.*, **2012**, *14*, 62-77.
- [15] Naesens, L.; Bischofberger, N.; Augustijns, P.; Annaert, P.; van den Mooter, G.; Arimilli, M. N.; Kim, C. U.; De Clercq, E., Antiretroviral efficacy and pharmacokinetics of oral bis(isopropylloxycarbonyloxymethyl) 9-(2-phosphonylmethoxypropyl)adenine in mice, *Antimicrob. Agents Chemother.*, **1998**, *42*, 1568-1573.
- [16] Hillaireau, H.; Dereuddre-Bosquet, N.; Skanji, R.; Bekkara-Aounallah, F.; Caron, J.; Lepetre, S.; Argote, S.; Bauduin, L.; Yousfi, R.; Rogez-Kreuz, C.; Desmaele, D.; Rousseau, B.; Gref, R.; Andrieux, K.; Clayette, P.; Couvreur, P., Anti-HIV efficacy and biodistribution of nucleoside reverse transcriptase inhibitors delivered as squalenoylated prodrug nanoassemblies, *Biomaterials*, **2013**, *34*, 4831-4838.
- [17] Lalanne, M.; Khoury, H.; Deroussent, A.; Bosquet, N.; Benech, H.; Clayette, P.; Couvreur, P.; Vassal, G.; Paci, A.; Andrieux, K., Metabolism evaluation of biomimetic prodrugs by in vitro models and mass spectrometry, *Int. J. Pharm.*, **2009**, *379*, 235-243.
- [18] Skanji, R.; Andrieux, K.; Lalanne, M.; Caron, J.; Bourgaux, C.; Degrouard, J.; Brisset, F.; Gueutin, C.; Chacun, H.; Dereuddre-Bosquet, N.; Paci, A.; Vassal, G.; Bauduin, L.; Garcia-Argote, S.; Rousseau, B.; Clayette, P.; Desmaele, D.; Couvreur, P., A new nanomedicine based on didanosine glycerolipidic prodrug enhances the long term accumulation of drug in a HIV sanctuary, *Int. J. Pharm.*, **2011**, *414*, 285-297.

- [19] Han, H. K.; de Vrueth, R. L. A.; Rhie, J. K.; Covitz, K. M. Y.; Smith, P. L.; Lee, C. P.; Oh, D. M.; Sadee, W.; Amidon, G. L., 5'-amino acid esters of antiviral nucleosides, acyclovir, and AZT are absorbed by the intestinal PEPT1 peptide transporter, *Pharm. Res.*, **1998**, *15*, 1154-1159.
- [20] Croom, K. F.; Keam, S. J., Tipranavir - A ritonavir-boosted protease inhibitor, *Drugs*, **2005**, *65*, 1669-1677.
- [21] Chiappetta, D. A.; Hocht, C.; Taira, C.; Sosnik, A., Efavirenz-loaded polymeric micelles for pediatric anti-HIV pharmacotherapy with significantly higher oral bioavailability, *Nanomedicine*, **2010**, *5*, 11-23.
- [22] Parang, K.; Wiebe, L. I.; Knaus, E. E., Novel approaches for designing 5'-O-ester prodrugs of 3'-azido-2',3'-dideoxythymidine (AZT), *Curr. Med. Chem.*, **2000**, *7*, 995-1039.
- [23] Sharma, A. P.; Ollapally, A. P.; Lee, H. J., Synthesis and Anti-Hiv Activity of Prodrugs of Azidothymidine, *Antivir. Chem. Chemother.*, **1993**, *4*, 93-96.
- [24] Tsuzuki, N.; Hama, T.; Kawada, M.; Hasui, A.; Konishi, R.; Shiwa, S.; Ochi, Y.; Futaki, S.; Kitagawa, K., Adamantane as a Brain-Directed Drug Carrier for Poorly Absorbed Drug .2. Azt Derivatives Conjugated with the 1-Adamantane Moiety, *J. Pharm. Sci.*, **1994**, *83*, 481-484.
- [25] Kawaguchi, T.; Ishikawa, K.; Seki, T.; Juni, K., Ester Prodrugs of Zidovudine, *J. Pharm. Sci.*, **1990**, *79*, 531-533.
- [26] Balzarini, J.; Herdewijn, P.; Declercq, E., Differential Patterns of Intracellular Metabolism of 2',3'-Didehydro-2',3'-Dideoxythymidine and 3'-Azido-2',3'-Dideoxythymidine, 2 Potent Anti-Human Immunodeficiency Virus Compounds, *J. Biol. Chem.*, **1989**, *264*, 6127-6133.
- [27] Bourdais, J.; Biondi, R.; Sarfati, S.; Guerreiro, C.; Lascu, I.; Janin, J.; Veron, M., Cellular phosphorylation of Anti-HIV nucleosides - Role of nucleoside diphosphate kinase, *J. Biol. Chem.*, **1996**, *271*, 7887-7890.
- [28] Tsotinis, A.; Calogeropoulou, T.; Koufaki, M.; Souli, C.; Balzarini, J.; DeClercq, E.; Makriyannis, A., Synthesis and antiretroviral evaluation of new alkoxy and aryloxy phosphate derivatives of 3'-azido-3'-deoxythymidine, *J. Med. Chem.*, **1996**, *39*, 3418-3422.
- [29] Pompon, A.; Lefebvre, I.; Imbach, J. L.; Kahn, S.; Farquhar, D., Decomposition Pathways of the Mono-(Pivaloyl-Oxymethyl) and Bis(Pivaloyl-Oxymethyl) Esters of Azidothymidine 5'-Monophosphate in Cell Extract and in Tissue-Culture Medium - an Application of the Online Isrp-Cleaning Hplc Technique, *Antivir. Chem. Chemother.*, **1994**, *5*, 91-98.
- [30] McGuigan, C.; Devine, K. G.; Oconnor, T. J.; Kinchington, D., Synthesis and Anti-Hiv Activity of Some Haloalkyl Phosphoramidate Derivatives of 3'-Azido-3'-Deoxythymidine (Azt) - Potent Activity of the Trichloroethyl Methoxyalaninyl Compound, *Antiviral Res.*, **1991**, *15*, 255-263.

- [31] Curley, D.; McGuigan, C.; Devine, K. G.; Oconnor, T. J.; Jeffries, D. J.; Kinchington, D., Synthesis and Anti-Hiv Evaluation of Some Phosphoramidate Derivatives of Azt - Studies on the Effect of Chain Elongation on Biological-Activity, *Antiviral Res.*, **1990**, *14*, 345-356.
- [32] Yang, L.; Chen, L. Q.; Zeng, R.; Li, C.; Qiao, R. Z.; Hu, L. M.; Li, Z. L., Synthesis, nanosizing and in vitro drug release of a novel anti-HIV polymeric prodrug: Chitosan-O-isopropyl-5'-O-d4T monophosphate conjugate, *Bioorg. Med. Chem.*, **2010**, *18*, 117-123.
- [33] Szebeni, J.; Wahl, S. M.; Betageri, G. V.; Wahl, L. M.; Gartner, S.; Popovic, M.; Parker, R. J.; Black, C. D. V.; Weinstein, J. N., Inhibition of Hiv-1 in Monocyte Macrophage Cultures by 2',3'-Dideoxycytidine-5'-Triphosphate, Free and in Liposomes, *Aids Res. Hum. Retrovir.*, **1990**, *6*, 691-702.
- [34] Betageri, G. V.; Jenkins, S. A.; Ravis, W. R., Drug-Delivery Using Antibody-Liposome Conjugates, *Drug Dev. Ind. Pharm.*, **1993**, *19*, 2109-2116.
- [35] Hillaireau, H.; Le Doan, T.; Besnard, M.; Chacun, H.; Janin, J.; Couvreur, P., Encapsulation of antiviral nucleotide analogues azidothymidine-triphosphate and cidofovir in poly(isobutylcyanoacrylate) nanocapsules, *Int. J. Pharm.*, **2006**, *324*, 37-42.
- [36] Hillaireau, H.; Le Doan, T.; Chacun, H.; Janin, J.; Couvreur, P., Encapsulation of mono- and oligo-nucleotides into aqueous-core nanocapsules in presence of various water-soluble polymers, *Int. J. Pharm.*, **2007**, *331*, 148-152.
- [37] Hillaireau, H.; Le Doan, T.; Appel, M.; Couvreur, P., Hybrid polymer nanocapsules enhance in vitro delivery of azidothymidine-triphosphate to macrophages, *J. Control. Release*, **2006**, *116*, 346-352.
- [38] Saiyed, Z. M.; Gandhi, N. H.; Nair, M. P. N., AZT 5'-triphosphate nanoformulation suppresses human immunodeficiency virus type 1 replication in peripheral blood mononuclear cells, *J. Neurovirol.*, **2009**, *15*, 343-347.
- [39] Vinogradov, S. V.; Kohli, E.; Zeman, A. D., Cross-linked polymeric nanogel formulations of 5'-triphosphates of nucleoside analogues: Role of the cellular membrane in drug release, *Mol. Pharm.*, **2005**, *2*, 449-461.
- [40] Agostoni, V.; Chalati, T.; Horcajada, P.; Willaime, H.; Anand, R.; Semiramoth, N.; Baati, T.; Hall, S.; Maurin, G.; Chacun, H.; Bouchemal, K.; Martineau, C.; Taulelle, F.; Couvreur, P.; Rogez-Kreuz, C.; Clayette, P.; Monti, S.; Serre, C.; Gref, R., Towards an Improved anti-HIV Activity of NRTI via Metal-Organic Frameworks Nanoparticles, *Adv. Healthc. Mater.*, **2013**, *2*, 1630-1637.
- [41] Dinauer, N.; Lochmann, D.; Demirhan, I.; Bouazzaoui, A.; Zimmer, A.; Chandra, A.; Kreuter, J.; von Briesen, H., Intracellular tracking of protamine/antisense oligonucleotide nanoparticles and their inhibitory effect on HIV-1 transactivation, *J. Control. Release*, **2004**, *96*, 497-507.

- [42] Blum, M. R.; Liao, S. H. T.; Good, S. S.; Demiranda, P., Pharmacokinetics and Bioavailability of Zidovudine in Humans, *Am. J. Med.*, **1988**, *85*, 189-194.
- [43] Lea, A. P.; Faulds, D., Stavudine - A review of its pharmacodynamic and pharmacokinetic properties and clinical potential in HIV infection, *Drugs*, **1996**, *51*, 846-864.
- [44] Klecker, R. W.; Collins, J. M.; Yarchoan, R. C.; Thomas, R.; McAtee, N.; Broder, S.; Myers, C. E., Pharmacokinetics of 2',3'-Dideoxycytidine in Patients with Aids and Related Disorders, *J. Clin. Pharmacol.*, **1988**, *28*, 837-842.
- [45] Kwei, G. Y.; Novak, L. B.; Hettrick, L. A.; Reiss, E. R.; Ostovic, D.; Loper, A. E.; Lui, C. Y.; Higgins, R. J.; Chen, I. W.; Lin, J. H., Regiospecific Intestinal-Absorption of the Hiv Protease Inhibitor L-735,524 in Beagle Dogs, *Pharm. Res.*, **1995**, *12*, 884-888.
- [46] Portsmouth, S. D.; Osorio, J.; McCormick, K.; Gazzard, B. G.; Moyle, G. J., Better maintained adherence on switching from twice-daily to once-daily therapy for HIV: a 24-week randomized trial of treatment simplification using stavudine prolonged-release capsules, *HIV Med.*, **2005**, *6*, 185-190.
- [47] Mateo, M. G.; Gutierrez, M. D. M.; Vidal, F.; Domingo, P., Stavudine extended release (once-daily, Bristol-Myers Squibb) for the treatment of HIV/AIDS, *Expert Opin. Pharmacother.*, **2013**, *14*, 1055-1064.
- [48] Kuksal, A.; Tiwary, A. K.; Jain, N. K.; Jain, S., Formulation and in vitro, in vivo evaluation of extended-release matrix tablet of zidovudine: Influence of combination of hydrophilic and hydrophobic matrix formers, *Aaps Pharmscitech*, **2006**, *7*.
- [49] Santos, J. V.; Pina, M. E. T.; Marques, M. P. M.; de Carvalho, L., New sustained release of Zidovudine Matrix tablets - cytotoxicity toward Caco-2 cells, *Drug Dev. Ind. Pharm.*, **2013**, *39*, 1154-1166.
- [50] Gathe, J.; Andrade-Villanueva, J.; Santiago, S.; Horban, A.; Nelson, M.; Cahn, P.; Bogner, J.; Spencer, D.; Podzamczar, D.; Yong, C. L.; Nguyen, T.; Zhang, W.; Drulak, M.; Quinson, A. M., Efficacy and safety of nevirapine extended-release once daily versus nevirapine immediate-release twice-daily in treatment-naive HIV-1-infected patients, *Antivir. Ther.*, **2011**, *16*, 759-769.
- [51] Bonina, F.; Puglia, C.; Rimoli, M. G.; Avallone, L.; Abignente, E.; Boatto, G.; Nieddu, M.; Meli, R.; Amorena, M.; de Caprariis, P., Synthesis and in vitro chemical and enzymatic stability of glycosyl 3'-azido-3'-deoxythymidine derivatives as potential anti-HIV agents, *Eur. J. Pharm. Sci.*, **2002**, *16*, 167-174.
- [52] Wannachaiyasit, S.; Chanvorachote, P.; Nimmannit, U., A Novel Anti-HIV Dextrin-Zidovudine Conjugate Improving the Pharmacokinetics of Zidovudine in Rats, *Aaps Pharmscitech*, **2008**, *9*, 840-850.

- [53] Khandazhinskaya, A.; Matyugina, E.; Shirokova, E., Anti-HIV therapy with AZT prodrugs: AZT phosphonate derivatives, current state and prospects, *Expert Opin. Drug Metab. Toxicol.*, **2010**, *6*, 701-714.
- [54] Li, W. J.; Chang, Y.; Zhan, P.; Zhang, N.; Liu, X. Y.; Pannecouque, C.; De Clercq, E., Synthesis, In Vitro and In Vivo Release Kinetics, and Anti-HIV Activity of A Sustained-Release Prodrug (mPEG-AZT) of 3'-Azido-2'-deoxythymidine (AZT, Zidovudine), *Chemmedchem*, **2010**, *5*, 1893-1898.
- [55] Li, W. J.; Wu, J. D.; Zhan, P.; Chang, Y.; Pannecouque, C.; De Clercq, E.; Liu, X. Y., Synthesis, drug release and anti-HIV activity of a series of PEGylated zidovudine conjugates, *Int. J. Biol. Macromol.*, **2012**, *50*, 974-980.
- [56] Neeraj, A.; Chandrasekar, M. J. N.; Sara, U. V. S.; Rohini, A., Poly(HEMA-Zidovudine) conjugate: A macromolecular pro-drug for improvement in the biopharmaceutical properties of the drug, *Drug Deliv.*, **2011**, *18*, 272-280.
- [57] Lewis, K. J.; Irwin, W. J.; Akhtar, S., Development of a sustained-release biodegradable polymer delivery system for site-specific delivery of oligonucleotides: Characterization of P(LA-GA) copolymer microspheres in vitro, *J. Drug Target.*, **1998**, *5*, 291-302.
- [58] Mandal, T. K.; LopezAnaya, A.; Onyebueke, E.; Shekleton, M., Preparation of biodegradable microcapsules containing zidovudine (AZT) using solvent evaporation technique, *J. Microencapsul.*, **1996**, *13*, 257-267.
- [59] Khang, G.; Lee, J. H.; Lee, J. W.; Cho, J. C.; Lee, H. B., Preparation and characterization of poly(lactide-co-glycolide) microspheres for the sustained release of AZT, *Korea Polym. J.*, **2000**, *8*, 80-88.
- [60] Mundargi, R. C.; Rangaswamy, V.; Aminabhavi, T. M., Spray Drying Technique to Produce Controlled Release Formulations of Zidovudine-an Anti-HIV Drug, *J. Appl. Polym. Sci.*, **2011**, *122*, 2244-2251.
- [61] Basu, S.; Mukherjee, B.; Chowdhury, S. R.; Paul, P.; Choudhury, R.; Kumar, A.; Mondal, L.; Hossain, C. M.; Maji, R., Colloidal gold-loaded, biodegradable, polymer-based stavudine nanoparticle uptake by macrophages: an in vitro study, *Int. J. Nanomed.*, **2012**, *7*, 6049-6061.
- [62] Pattnaik, G.; Sinha, B.; Mukherjee, B.; Ghosh, S.; Basak, S.; Mondal, S.; Bera, T., Submicron-size biodegradable polymer-based didanosine particles for treating HIV at early stage: an in vitro study, *J. Microencapsul.*, **2012**, *29*, 666-676.
- [63] Destache, C. J.; Belgum, T.; Goede, M.; Shibata, A.; Belshan, M. A., Antiretroviral release from poly(dl-lactide-co-glycolide) nanoparticles in mice, *J. Antimicrob. Chemother.*, **2010**, *65*, 2183-2187.

- [64] Seremeta, K. P.; Chiappetta, D. A.; Sosnik, A., Poly(epsilon-caprolactone), Eudragit (R) RS 100 and poly(epsilon-caprolactone)/Eudragit (R) RS 100 blend submicron particles for the sustained release of the antiretroviral efavirenz, *Colloid Surf. B-Biointerfaces*, **2013**, *102*, 441-449.
- [65] Tshweu, L.; Katata, L.; Kalombo, L.; Swai, H., Nanoencapsulation of water-soluble drug, lamivudine, using a double emulsion spray-drying technique for improving HIV treatment, *J. Nanopart. Res.*, **2013**, *15*.
- [66] Gao, L.; Zhang, D.; Chen, M., Drug nanocrystals for the formulation of poorly soluble drugs and its application as a potential drug delivery system, *J. Nanopart. Res.*, **2008**, *10*, 845-862.
- [67] Liversidge, G., Cundy, K.C., Bishop, J., et al, **1992**, **8 Sept**.
- [68] Gassmann, P.; List, M.; Schweitzer, A.; Sucker, H., Hydrosols - Alternatives for the Parenteral Application of Poorly Water-Soluble Drugs, *Eur. J. Pharm. Biopharm.*, **1994**, *40*, 64-72.
- [69] Krause, K. P.; Muller, R. H., Production and characterisation of highly concentrated nanosuspensions by high pressure homogenisation, *Int. J. Pharm.*, **2001**, *214*, 21-24.
- [70] Nowacek, A. S.; McMillan, J.; Miller, R.; Anderson, A.; Rabinow, B.; Gendelman, H. E., Nanoformulated Antiretroviral Drug Combinations Extend Drug Release and Antiretroviral Responses in HIV-1-Infected Macrophages: Implications for NeuroAIDS Therapeutics, *J. Neuroimmune Pharm.*, **2010**, *5*, 592-601.
- [71] Roy, U.; McMillan, J.; Alnouti, Y.; Gautam, N.; Smith, N.; Balkundi, S.; Dash, P.; Gorantla, S.; Martinez-Skinner, A.; Meza, J.; Kanmogne, G.; Swindells, S.; Cohen, S. M.; Mosley, R. L.; Poluektova, L.; Gendelman, H. E., Pharmacodynamic and Antiretroviral Activities of Combination Nanoformulated Antiretrovirals in HIV-1-Infected Human Peripheral Blood Lymphocyte-Reconstituted Mice, *J. Infect. Dis.*, **2012**, *206*, 1577-1588.
- [72] Gautam, N.; Roy, U.; Balkundi, S.; Puligujja, P.; Guo, D. W.; Smith, N.; Liu, X. M.; Lamberty, B.; Morse, B.; Fox, H. S.; McMillan, J.; Gendelman, H. E.; Alnouti, Y., Preclinical Pharmacokinetics and Tissue Distribution of Long-Acting Nanoformulated Antiretroviral Therapy, *Antimicrob. Agents Chemother.*, **2013**, *57*, 3110-3120.
- [73] Kesteleyn, B.; Amssoms, K.; Schepens, W.; Hache, G.; Verschueren, W.; Van De Vreken, W.; Rombauts, K.; Meurs, G.; Sterkens, P.; Stoops, B.; Baert, L.; Austin, N.; Wegner, J.; Masungi, C.; Dierynck, I.; Lundgren, S.; Jonsson, D.; Parkes, K.; Kalayanov, G.; Wallberg, H.; Rosenquist, A.; Samuelsson, B.; Van Emelen, K.; Thuring, J. W., Design and synthesis of HIV-1 protease inhibitors for a long-acting injectable drug application, *Bioorg. Med. Chem. Lett.*, **2013**, *23*, 310-317.
- [74] Spreen, W. R.; Margolis, D. A.; Pottage, J. C., Long-acting injectable antiretrovirals for HIV treatment and prevention, *Curr. Opin. HIV AIDS*, **2013**, *8*, 565-571.

- [75] Kamboj, S.; Saini, V.; Bala, S., Formulation and Characterization of Drug Loaded Nonionic Surfactant Vesicles (Niosomes) for Oral Bioavailability Enhancement, *Sci. World J.*, **2014**.
- [76] Ramana, L. N.; Sharma, S.; Sethuraman, S.; Ranga, U.; Krishnan, U. M., Investigation on the stability of saquinavir loaded liposomes: Implication on stealth, release characteristics and cytotoxicity, *Int. J. Pharm.*, **2012**, *431*, 120-129.
- [77] Kinman, L.; Brodie, S. J.; Tsai, C. C.; Bui, T.; Larsen, K.; Schmidt, A.; Anderson, D.; Morton, W. R.; Hu, S. L.; Ho, R. J. Y., Lipid-drug association enhanced HIV-1 protease inhibitor indinavir localization in lymphoid tissues and viral load reduction: A proof of concept study in HIV-2(287)-infected macaques, *Aids*, **2003**, *34*, 387-397.
- [78] Snedecor, S. J.; Sullivan, S. M.; Ho, R. J. Y., Feasibility of weekly HIV drug delivery to enhance drug localization in lymphoid tissues based on pharmacokinetic models of lipid-associated indinavir, *Pharm. Res.*, **2006**, *23*, 1750-1755.
- [79] Swindells, S.; Flexner, C.; Fletcher, C. V.; Jacobson, J. M., The Critical Need for Alternative Antiretroviral Formulations, and Obstacles to Their Development, *J. Infect. Dis.*, **2011**, *204*, 669-674.
- [80] Baert, L.; Schueller, L.; Tardy, Y.; Macbride, D.; van't Klooster, G.; Borghys, H.; Clessens, E.; Van den Mooter, G.; Van Gysegheem, E.; Van Remoortere, P.; Wigerinck, P.; Rosier, J., Development of an implantable infusion pump for sustained anti-HIV drug administration, *Int. J. Pharm.*, **2008**, *355*, 38-44.
- [81] Kapoor, D. N.; Katare, O. P.; Dhawan, S., In situ forming implant for controlled delivery of an anti-HIV fusion inhibitor, *Int. J. Pharm.*, **2012**, *426*, 132-143.
- [82] Blankson, J. N.; Persaud, D.; Siliciano, R. F., The challenge of viral reservoirs in HIV-1 infection, *Annu. Rev. Med.*, **2002**, *53*, 557-593.
- [83] Pomerantz, R. J., Reservoirs, sanctuaries, and residual disease: The hiding spots of HIV-1, *HIV Clin. Trials*, **2003**, *4*, 137-143.
- [84] Crowe, S. M., Macrophages and residual HIV infection, *Curr. Opin. HIV AIDS*, **2006**, *1*, 129-133.
- [85] Molema, G.; Jansen, R. W.; Pauwels, R.; Declercq, E.; Meijer, D. K. F., Targeting of Antiviral Drugs to Lymphocytes-T4 - Anti-Hiv Activity of Neoglycoprotein Aztmp Conjugates Invitro, *Biochem. Pharmacol.*, **1990**, *40*, 2603-2610.
- [86] Garg, M.; Jain, N. K., Reduced hematopoietic toxicity, enhanced cellular uptake and altered pharmacokinetics of azidothymidine loaded galactosylated liposomes, *J. Drug Target.*, **2006**, *14*, 1-11.
- [87] Hu, J. H.; Liu, H.; Wang, L. L., Enhanced delivery of AZT to macrophages via acetylated LDL, *J. Control. Release*, **2000**, *69*, 327-335.

- [88] Vyas, S. P.; Subhedar, R.; Jain, S., Development and characterization of emulsomes for sustained and targeted delivery of an antiviral agent to liver, *J. Pharm. Pharmacol.*, **2006**, *58*, 321-326.
- [89] Pretzer, E.; Flasher, D.; Düzgünes, N., Inhibition of human immunodeficiency virus type-1 replication in macrophages and H9 cells by free or liposome-encapsulated L-689,502, an inhibitor of the viral protease, *Antiviral Res.*, **1997**, *34*, 1-15.
- [90] Gieseler, R. K.; Marquitan, G.; Hahn, M. J.; Perdon, L. A.; Driessen, W. H. P.; Sullivan, S. M.; Scolaro, M. J., DC-SIGN-specific liposomal targeting and selective intracellular compound delivery to human myeloid dendritic cells: Implications for HIV disease, *Scand. J. Immunol.*, **2004**, *59*, 415-424.
- [91] Desormeaux, A.; Harvie, P.; Perron, S.; Makabipanzu, B.; Beauchamp, D.; Tremblay, M.; Poulin, L.; Bergeron, M. G., Antiviral Efficacy, Intracellular Uptake and Pharmacokinetics of Free and Liposome-Encapsulated 2',3'-Dideoxyinosine, *Aids*, **1994**, *8*, 1545-1553.
- [92] Schenk, G. J.; Haasnoot, P. C. J.; Centlivre, M.; Legrand, N.; Rip, J.; de Boer, A. G.; Berkhout, B., Efficient CRM197-mediated drug targeting to monocytes, *J. Control. Release*, **2012**, *158*, 139-147.
- [93] Bender, A. R.; vonBriesen, H.; Kreuter, J.; Duncan, I. B.; RubsamenWaigmann, H., Efficiency of nanoparticles as a carrier system for antiviral agents in human immunodeficiency virus-infected human monocytes/macrophages in vitro, *Antimicrob. Agents Chemother.*, **1996**, *40*, 1467-1471.
- [94] Schafer, V.; Vonbriesen, H.; Andreesen, R.; Steffan, A. M.; Royer, C.; Troster, S.; Kreuter, J.; Rubsamenwaigmann, H., Phagocytosis of Nanoparticles by Human-Immunodeficiency-Virus (Hiv)-Infected Macrophages - a Possibility for Antiviral Drug Targeting, *Pharm. Res.*, **1992**, *9*, 541-546.
- [95] Lobenberg, R.; Araujo, L.; von Briesen, H.; Rodgers, E.; Kreuter, J., Body distribution of azidothymidine bound to hexyl-cyanoacrylate nanoparticles after i.v. injection to rats, *J. Control. Release*, **1998**, *50*, 21-30.
- [96] Akhtar, S.; Lewis, K. J., Antisense oligonucleotide delivery to cultured macrophages is improved by incorporation into sustained-release biodegradable polymer microspheres, *Int. J. Pharm.*, **1997**, *151*, 57-67.
- [97] Kadiu, I.; Nowacek, A.; McMillan, J.; Gendelman, H. E., Macrophage endocytic trafficking of antiretroviral nanoparticles, *Nanomedicine*, **2011**, *6*, 975-994.
- [98] Shegokar, R.; Singh, K. K., Surface modified nevirapine nanosuspensions for viral reservoir targeting: In vitro and in vivo evaluation, *Int. J. Pharm.*, **2011**, *421*, 341-352.

- [99] Vermeulen, J. N.; Meijer, D. K. F.; Over, J.; Lange, J. M. A.; Proost, J. H.; Bakker, H. I.; Beljaars, L.; Wit, F.; Prins, J. M., A Phase I/IIa study with succinylated human serum albumin (Suc-HSA), a candidate HIV-1 fusion inhibitor, *Antivir. Ther.*, **2007**, *12*, 273-278.
- [100] Swart, P. J.; Beljaars, L.; Kuipers, M. E.; Smit, C.; Nieuwenhuis, P.; Meijer, D. K. F., Homing of negatively charged albumins to the lymphatic system - General implications for drug targeting to peripheral tissues and viral reservoirs, *Biochem. Pharmacol.*, **1999**, *58*, 1425-1435.
- [101] Jin, Y. G.; Qi, N. N.; Tong, L.; Chen, D. W., Self-assembled drug delivery systems. Part 5: Self-assemblies of a bolaamphiphilic prodrug containing dual zidovudine, *Int. J. Pharm.*, **2010**, *386*, 268-274.
- [102] Jin, Y. G.; Xin, R.; Tong, L.; Du, L. N.; Li, M., Combination Anti-HIV Therapy with the Self-Assemblies of an Asymmetric Bolaamphiphilic Zidovudine/Didanosine Prodrug, *Mol. Pharm.*, **2011**, *8*, 867-876.
- [103] Perisé-Barrios, A. J.; Jiménez, J. L.; Domínguez-Soto, A.; de la Mata, F. J.; Corbí, A. L.; Gomez, R.; Muñoz-Fernandez, M. A., Carbosilane dendrimers as gene delivery agents for the treatment of HIV infection, *JControl Release*, **2014**, *184*, 51-57.
- [104] Lee, C. C.; MacKay, J. A.; Frechet, J. M. J.; Szoka, F. C., Designing dendrimers for biological applications, *Nat. Biotechnol.*, **2005**, *23*, 1517-1526.
- [105] Magnani, M.; Rossi, L.; Brandi, G.; Schiavano, G. F.; Montroni, M.; Piedimonte, G., Targeting Antiretroviral Nucleoside Analogs in Phosphorylated Form to Macrophages - Invitro and Invivo Studies, *Proc. Natl. Acad. Sci. U. S. A.*, **1992**, *89*, 6477-6481.
- [106] Perno, C. F.; Santoro, N.; Balestra, E.; Aquaro, S.; Cenci, A.; Lazzarino, G.; DiPierro, D.; Tavazzi, B.; Balzarini, J.; Garaci, E.; Grimaldi, S.; Calio, R., Red blood cells mediated delivery of 9-(2-phosphonylmethoxyethyl)adenine to primary macrophages: Efficiency, metabolism and activity against human immunodeficiency virus or herpes simplex virus, *Antiviral Res.*, **1997**, *33*, 153-164.
- [107] Franchetti, P.; Abu Sheikha, G.; Cappellacci, L.; Marchetti, S.; Grifantini, M.; Balestra, E.; Perno, C. F.; Benatti, U.; Brandi, G.; Rossi, L.; Magnani, M., A new acyclic heterodinucleotide active against human immunodeficiency virus and herpes simplex virus, *Antiviral Res.*, **2000**, *47*, 149-158.
- [108] Rossi, L.; Serafini, S.; Cappellacci, L.; Balestra, E.; Brandi, G.; Schiavano, G. F.; Franchetti, P.; Grifantini, M.; Perno, C. F.; Magnani, M., Erythrocyte-mediated delivery of a new homodinucleotide active against human immunodeficiency virus and herpes simplex virus, *J. Antimicrob. Chemother.*, **2001**, *47*, 819-827.

- [109] Endsley, A. N.; Ho, R. J. Y., Design and Characterization of Novel Peptide-Coated Lipid Nanoparticles for Targeting Anti-HIV Drug to CD4 Expressing Cells, *Aaps J.*, **2012**, *14*, 225-235.
- [110] Wan, L.; Pooyan, S.; Hu, P.; Leibowitz, M. J.; Stein, S.; Sinko, P. J., Peritoneal macrophage uptake, pharmacokinetics and biodistribution of macrophage-targeted PEG-fMLF (N-formyl-methionyl-leucyl-phenylalanine) nanocarriers for improving HIV drug delivery, *Pharm. Res.*, **2007**, *24*, 2110-2119.
- [111] Oussoren, C.; Magnani, M.; Fraternali, A.; Casabianca, A.; Chiarantini, L.; Ingebrigsten, R.; Underberg, W. J. M.; Storm, G., Liposomes as carriers of the antiretroviral agent dideoxycytidine-5'-triphosphate, *Int J Pharm*, **1999**, *180*, 261-270.
- [112] Serafini, S.; Fraternali, A.; Rossi, L.; Casabianca, A.; Antonelli, A.; Paoletti, M. F.; Orlandi, C.; Pierige, F.; Sfara, C.; Schiavano, G. F.; Magnani, M., Effect of macrophage depletion on viral DNA rebound following antiretroviral therapy in a murine model of AIDS (MAIDS), *Antiviral Res.*, **2009**, *81*, 93-102.
- [113] Lobenberg, R.; Araujo, L.; Kreuter, J., Body distribution of azidothymidine bound to nanoparticles after oral administration, *Eur. J. Pharm. Biopharm.*, **1997**, *44*, 127-132.
- [114] Dembri, A.; Montisci, M. J.; Gantier, J. C.; Chacun, H.; Ponchel, G., Targeting of 3'-azido 2'-deoxythymidine (AZT)-loaded poly(isohexylcyanoacrylate) nanospheres to the gastrointestinal mucosa and associated lymphoid tissues, *Pharm. Res.*, **2001**, *18*, 467-473.
- [115] Rao, K. S.; Ghorpade, A.; Labhasetwar, V., Targeting anti-HIV drugs to the CNS, *Expert Opin. Drug Deliv.*, **2009**, *6*, 771-784.
- [116] Wong, H. L.; Chattopadhyay, N.; Wu, X. Y.; Bendayan, R., Nanotechnology applications for improved delivery of antiretroviral drugs to the brain, *Adv. Drug Deliv. Rev.*, **2010**, *62*, 503-517.
- [117] Rao, K. S.; Labhasetwar, V., Trans-Activating Transcriptional Activator (TAT) Peptide-Mediated Brain Drug Delivery, *J. Biomed. Nanotechnol.*, **2006**, *2*, 173-185.
- [118] Toborek, M.; Lee, Y. W.; Flora, G.; Pu, H.; Andras, I. E.; Wylegala, E.; Hennig, B.; Nath, A., Mechanisms of the blood-brain barrier disruption in HIV-1 infection, *Cell. Mol. Neurobiol.*, **2005**, *25*, 181-199.
- [119] Borgmann, K.; Rao, K. S.; Labhasetwar, V.; Ghorpade, A., Efficacy of Tat-Conjugated Ritonavir-Loaded Nanoparticles in Reducing HIV-1 Replication in Monocyte-Derived Macrophages and Cytocompatibility with Macrophages and Human Neurons, *Aids Res. Hum. Retrovir.*, **2011**, *27*, 853-862.
- [120] Saiyed, Z. M.; Gandhi, N. H.; Nair, M. P. N., Magnetic nanoformulation of azidothymidine 5'-triphosphate for targeted delivery across the blood-brain barrier, *Int. J. Nanomed.*, **2010**, *5*, 157-166.

- [121] Namanja, H. A.; Emmert, D.; Davis, D. A.; Campos, C.; Miller, D. S.; Hrycyna, C. A.; Chmielewski, J., Toward Eradicating HIV Reservoirs in the Brain: Inhibiting P-Glycoprotein at the Blood-Brain Barrier with Prodrug Abacavir Dimers, *J. Am. Chem. Soc.*, **2012**, *134*, 2976-2980.
- [122] Nowacek, A. S.; Balkundi, S.; McMillan, J.; Roy, U.; Martinez-Skinner, A.; Mosley, R. L.; Kanmogne, G.; Kabanov, A. V.; Bronich, T.; Gendelman, H. E., Analyses of nanoformulated antiretroviral drug charge, size, shape and content for uptake, drug release and antiviral activities in human monocyte-derived macrophages, *J. Control. Release*, **2011**, *150*, 204-211.
- [123] Kanmogne, G. D.; Singh, S.; Roy, U.; Liu, X. M.; McMillan, J.; Gorantla, S.; Balkundi, S.; Smith, N.; Alnouti, Y.; Gautam, N.; Zhou, Y.; Poluektova, L.; Kabanov, A.; Bronich, T.; Gendelman, H. E., Mononuclear phagocyte intercellular crosstalk facilitates transmission of cell-targeted nanoformulated antiretroviral drugs to human brain endothelial cells, *Int. J. Nanomed.*, **2012**, *7*, 2373-2388.
- [124] Chiappetta, D. A.; Hocht, C.; Opezzo, J. A. W.; Sosnik, A., Intranasal administration of antiretroviral-loaded micelles for anatomical targeting to the brain in HIV, *Nanomedicine*, **2013**, *8*, 223-237.
- [125] Mahajan, H. S.; Mahajan, M. S.; Nerkar, P. P.; Agrawal, A., Nanoemulsion-based intranasal drug delivery system of saquinavir mesylate for brain targeting, *Drug Deliv.*, **2014**, *21*, 148-154.
- [126] Calvo, P.; Gouritin, B.; Chacun, H.; Desmaele, D.; D'Angelo, J.; Noel, J. P.; Georgin, D.; Fattal, E.; Andreux, J. P.; Couvreur, P., Long-circulating PEGylated polycyanoacrylate nanoparticles as new drug carrier for brain delivery, *Pharm. Res.*, **2001**, *18*, 1157-1166.
- [127] Kreuter, J.; Alyautdin, R. N.; Kharkevich, D. A.; Ivanov, A. A., Passage of Peptides through the Blood-Brain-Barrier with Colloidal Polymer Particles (Nanoparticles), *Brain Res.*, **1995**, *674*, 171-174.
- [128] Kim, H. R.; Andrieux, K.; Gil, S.; Taverna, M.; Chacun, H.; Desmaele, D.; Taran, F.; Georgin, D.; Couvreur, P., Translocation of poly(ethylene glycol-co-hexadecyl)cyanoacrylate nanoparticles into rat brain endothelial cells: Role of apolipoproteins in receptor-mediated endocytosis, *Biomacromolecules*, **2007**, *8*, 793-799.
- [129] Kim, H. R.; Gil, S.; Andrieux, K.; Nicolas, V.; Appel, M.; Chacun, H.; Desmaele, D.; Taran, F.; Georgin, D.; Couvreur, P., Low-density lipoprotein receptor-mediated endocytosis of PEGylated nanoparticles in rat brain endothelial cells, *Cell. Mol. Life Sci.*, **2007**, *64*, 356-364.
- [130] Zensi, A.; Begley, D.; Pontikis, C.; Legros, C.; Mihoreanu, L.; Wagner, S.; Buchel, C.; von Briesen, H.; Kreuter, J., Albumin nanoparticles targeted with Apo E enter the CNS by transcytosis and are delivered to neurones, *J. Control. Release*, **2009**, *137*, 78-86.

- [131] Ocheke, N. A.; Olorunfemi, P. O.; Ngwuluka, N. C., Nanotechnology and Drug Delivery Part 2: Nanostructures for Drug Delivery, *Trop. J. Pharm. Res.*, **2009**, *8*, 275-287.

Travaux expérimentaux

Chapitre 1

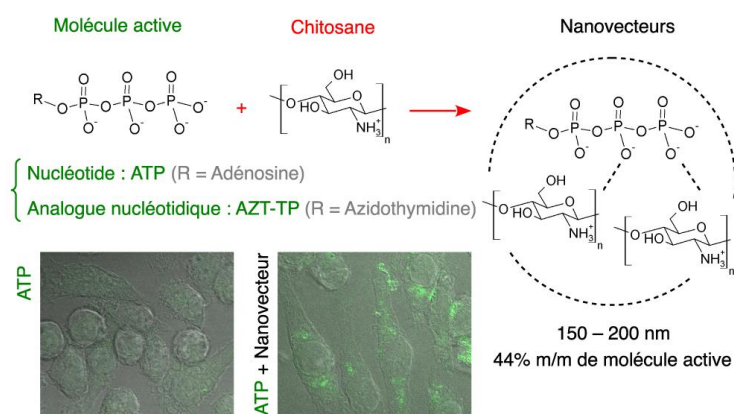
**Formation spontanée de nanovecteurs de nucléotides et d'analogues
nucléotidiques pour leur délivrance cellulaire**

Chapitre 1

Formation spontanée de nanovecteurs de nucléotides et d'analogues nucléotidiques pour leur délivrance cellulaire¹

Résumé

Les analogues nucléotidiques tels que l'azidothymidine triphosphate (AZT-TP) possèdent d'importantes activités pharmacologiques pour le traitement des infections par le VIH. Cependant leur utilisation clinique est limitée à cause de leur caractère hydrophile, qui restreint fortement leur diffusion dans les cellules cibles. Quelques nanovecteurs ont été proposés pour relever le défi de délivrer l'AZT-TP aux cellules, mais le rendement d'encapsulation et la complexité de la préparation restent des barrières importantes à leur développement. Dans ce chapitre, nous proposons une méthode de préparation directe et générale de nanovecteurs d'analogues nucléotidiques, basée sur un polymère naturel, le chitosane (CS). Nous montrons qu'un analogue nucléotidique comme l'AZT-TP, mais également un nucléotide naturel comme l'ATP (utilisé ici comme « molécule modèle »), peuvent induire la « gélification ionotropique » du CS, ce qui mène à la formation de nanoparticules CS/ATP et CS/AZT-TP, avec un rendement d'encapsulation et un taux de charge élevés, jusqu'à respectivement 75% et 45% m/m. De tels nanovecteurs libèrent l'ATP et l'AZT-TP dans des milieux physiologiques et permettent une délivrance intracellulaire de ces molécules à des macrophages *in vitro*.

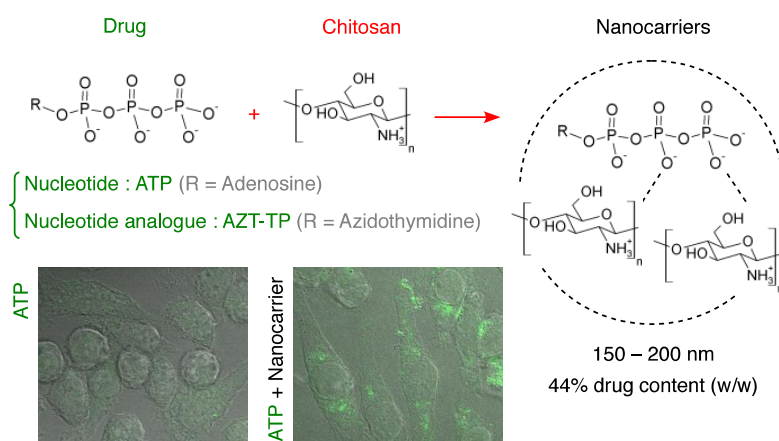


¹ Chapitre publié sous forme d'article dans *Biomacromolecules*, Volume 14, 2013, 737-742.
Auteurs : Giovanna Giacalone, Amélie Bochot, Elias Fattal, Hervé Hillaireau.

Drug-induced nanocarrier assembly as a strategy for the cellular delivery of nucleotides and nucleotide analogues¹

Abstract

Nucleotide analogues like azidothymidine triphosphate (AZT-TP) display important pharmacological activities for the treatment of HIV infections. Their clinical use is however limited mostly due to their hydrophilicity which highly restricts their diffusion into the target cells. Few nanocarriers have been proposed to address the challenge of AZT-TP cellular delivery, but the loading efficiency, preparation complexity and efficient cellular delivery remain important barriers to their development. In this chapter, we propose a straightforward and general design of nucleotide analogues nanocarriers based on the natural polysaccharide chitosan (CS). We show that the drug AZT-TP, but also a natural nucleotide such as ATP (here used as model molecule) can induce ionotropic gelation of CS, leading to CS/ATP and CS/AZT-TP nanoparticles with high drug entrapment efficiency and loading rate—up to 75% and 45% w/w respectively. Such nanocarriers release ATP and AZT-TP in physiological media and allow an efficient *in vitro* cellular delivery of these molecules to macrophages cells.



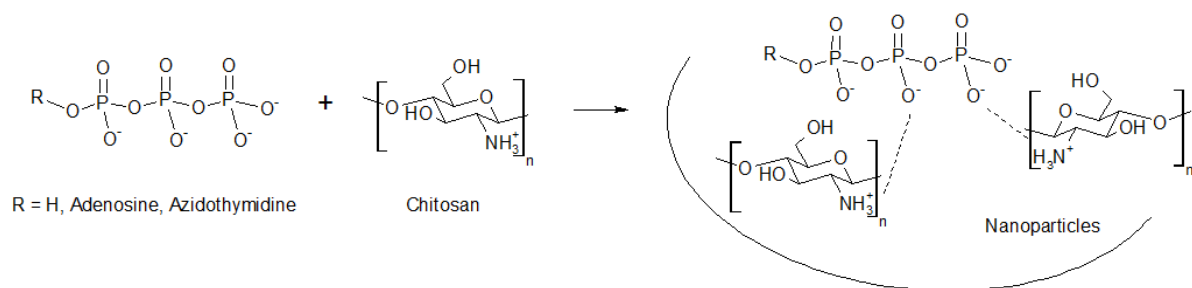
¹ Chapter published as an article in *Biomacromolecules*, Volume 14, **2013**, 737-742. Authors: Giovanna Giacalone, Amélie Bochot, Elias Fattal, Hervé Hillaireau.

1. Introduction

Natural nucleotides and nucleotide analogues display important pharmacological activities. The well-known nucleotide adenosine triphosphate (ATP), the most important and ubiquitous source of energy of cells, can be used for the treatment of cardiac, hepatic and brain ischemia [1]. 3'-OH-modified nucleotide analogues such as azidothymidine triphosphate (AZT-TP) can display anticancer and/or antiviral activity by interfering with cancer-cell or viral nucleic acid synthesis, respectively [2]. The clinical use of these molecules is however limited due to the presence of a triphosphate group, which is (i) prone to hydrolysis *in vivo* and degradation by ectoenzymes, and (ii) responsible for the high hydrophilicity of the molecules, thereby strongly limiting their uptake by targeted cells and access to their intracellular pharmacological targets.

To overcome these limitations and enable the administration of nucleotides and nucleotide analogues, several nanocarriers have been investigated [3]: liposomes [4], aqueous-core polymeric nanocapsules [5], poloxamer-polyethyleneimine copolymer nanoparticles [6], metal organic frameworks [7]. Various technological locks remain however to translate these nucleotide- and nucleotide analogue-based nanosystems to the clinics, such as drug entrapment efficiency, drug loading, material biocompatibility – and mostly, synthesis complexity.

In this study, we investigate a new, versatile and straightforward design of nucleotide and nucleotide-analogue nanocarriers. Chitosan (CS), a biocompatible and biodegradable polysaccharide [8], has been shown to form nanoparticles through complexation with the tripolyphosphate (TPP) polyanion, a process coined “ionotropic gelation” [9]. Such nanoparticles have been further loaded with various drugs and macromolecules, which has led to many developments in drug delivery [10]. In contrast with such approaches consisting in loading preformed nanoparticles, we have investigated the potential of nucleotides and nucleotide analogues to induce ionotropic gelation of CS, in order to formulate highly-loaded nanocarriers (Scheme 1).



Scheme 1. Small, triphosphate group-containing molecules like the nucleotide ATP (R = adenosine) or the nucleotide analogue AZT-TP (R = azidothymidine [AZT]) have been investigated for their potential to form colloidal suspensions of nanoparticles in the presence of chitosan (CS), similarly to what is known for TPP (R = H).

2. Materials and methods

2.1. Materials

Nanoparticles were prepared using low viscosity CS (95% deacetylated, Fluka) TPP or ATP purchased from Sigma (France), or AZT-TP purchased from Trilink Biotechnologies (San Diego, USA). In the following, PBS refers to PBS without CaCl_2 and MgCl_2 from Dulbecco (Lonza), and water to MilliQ[®] purified water (Millipore, France). $[\gamma\text{-}^{33}\text{P}]\text{-ATP}$, $[\text{methyl-}^3\text{H}]\text{-AZT-TP}$, the scintillation liquid Ultima Gold and the strong base Solvable (used here to solubilize the pellets after centrifugation) were from Perkin Elmer (France), $[\text{8-}^{14}\text{C}]\text{-ATP}$ from Moravek, and BODIPY[®]-FL ATP (fluorescently-labeled ATP) from Invitrogen (France). Most reagents used were purchased from Sigma; all solvents were of analytical grade.

2.2. Preparation of nanoparticles

Stock solutions of low viscosity CS were obtained by dissolving the CS powder at a final concentration between 1 and 5 mg/mL in a 1.75% v/v acetic acid aqueous solution, stirring overnight and filtrating through 0.22 μm filter. A 10 mg/mL TPP stock solution, a 15 mg/mL ATP stock solution and a 13.8 mg/mL AZT-TP stock solution were obtained (these concentrations have been chosen in order to keep the same molarity for all the solutions, i.e. 27.2 mM).

For the study of the nanoparticle formation domains, increasing amounts of TPP and ATP solutions, from 0.02 to 0.25 mL, were added dropwise to 3 mL of a CS solution in a 7 mL vial under magnetic stirring. For AZT-TP nanoparticles, increasing amounts of AZT-TP solution from 0.02 to 0.08 mL were added dropwise to 1 mL of a 1 mg/mL CS solution. Evaluation of samples was achieved visually: solution, stable colloidal suspension, sedimenting aggregates. Selected nanoparticle formulations were prepared using 1 mg/mL CS and various N/P ratios: 4.5; 2.3; 1.5; 1.3.

Nanoparticle suspensions were purified as 1 mL aliquots in centrifuge tubes, each of them topped by 250 μ L of 25% trehalose solution. Centrifugation was performed at $6000 \times g$ for one hour at 4 °C. At the end of purification, 1.15 mL of supernatant was withdrawn and pellets were placed on hold for one hour. Afterwards, nanoparticles were re-suspended by shaking or vortexing for few seconds. Nanoparticle concentration was adjusted by adding 0.9 mL of water. This method allowed a complete redispersion of the pellet, contrary to ultracentrifugation. The efficiency of nanoparticle recovery in these conditions was quantified by comparison with ultracentrifugation using radioactivity measurements.

For radioactivity studies, CS/ATP nanoparticles were formed from a 15 mg/mL ATP solution containing [γ - 33 P]-ATP or [8 - 14 C]-ATP as a tracer, by diluting a commercial 10 mCi/mL (25 mM) solution with the appropriate amount of unlabelled ATP solution. CS/AZT-TP nanoparticles were formed from a 13.8 mg/mL AZT-TP solution containing [methyl- 3 H]-AZT-TP as a tracer, by diluting a commercial 1 mCi/mL solution with the appropriate amount of unlabelled AZT-TP solution.

For fluorescence studies, nanoparticles were formed from a 15 mg/mL ATP solution prepared using BODIPY[®]-FL ATP as a tracer (0.5%).

2.3. Nanoparticle characterization

The mean size of nanoparticles was determined by dynamic light scattering (DLS) using a NANO ZS (Malvern Instrument, UK), with a 173° scattering angle at a temperature of 25°C. Unless otherwise noted, the measurement position and attenuator values were automatically selected. The zeta potential of nanoparticles was determined on the same equipment after 1/20 dilution of the sample in a 1 mM NaCl solution.

2.4. Determination of nanoparticle composition

For ATP and AZT-TP association efficiency, nanoparticles with N/P = 4.5, 2.3, 1.5 and 1.3 were prepared as described above using 1 mg/mL CS and isotopic dilutions of [γ - ^{33}P]-ATP or [methyl- ^3H]-AZT-TP (1 μCi). The purification step was replaced by a step of separation of free ATP or AZT-TP from nanoparticles by ultracentrifugation, and radioactivity associated both to the pellets and the supernatants was measured as follows. After centrifugation of 1 mL of the nanoparticle suspension ($28,000 \times g$, 1 h), the supernatant was withdrawn for counting, whereas the pellet was dissolved by addition of 0.5 mL Solvable followed by 2 h stirring at 50°C. Samples were prepared adding a scintillation liquid (Ultima Gold) and counted after one hour using a Beckman Coulter (LS 6500 Multi-Purpose Scintillation Counter) instrument. The association efficiency was calculated as the ratio of the pellet radioactivity to the total (pellet + supernatant) radioactivity.

The chitosan content of nanoparticles was determined following the protocol from Muzzarelli *et al.* [11]. The concentration of free chitosan in the supernatant was measured with UV-spectroscopy at $\lambda = 575$ nm after complexation with the dye; the amount of chitosan associated to nanoparticles was calculated by subtraction of free CS to the total amount of CS used for the preparation.

After determination of the association efficiency of the drug (ATP or AZT-TP) and chitosan to nanoparticles, the drug loading was calculated as the ratio of the nanoparticle-associated drug weight to the nanoparticle (drug + chitosan) weight.

2.5. In vitro release studies

Particle degradation was followed by DLS over 24 h. CS/ATP nanoparticles (N/P = 1.3) were prepared at 1 mg/mL in water (0.9 mL) in a DLS cuvette. DLS measurements were performed immediately after a single addition of 100 μL 10 \times PBS and repeated over 24 h using fixed measurement position (4.65 mm) and attenuation value (6). Data are represented as the size distribution by intensity corrected by the average light intensity (count rate).

ATP and AZT-TP release was followed over 24 h by separation from intact nanoparticles using ultracentrifugation. Radioactive CS/ATP nanoparticles and CS/AZT-TP nanoparticles (N/P = 1.3, 1 $\mu\text{Ci}/\text{mL}$) were prepared as described above. After purification, pellets were recovered in PBS or 5% glucose. Samples of nanoparticles (1 mL) were incubated at 37 °C under stirring for 0 to 24 hours. At scheduled time intervals, samples were centrifuged ($28,000 \times g$, 1 h), the supernatant was withdrawn and the pellet was dissolved in 1 mL Solvable. The radioactivity associated to the supernatant and to

the Solvable pellet solution was counted. The drug release was calculated as the ratio of the supernatant radioactivity to the total (pellet + supernatant) radioactivity.

2.6. Cell culture and viability assessment

J774A.1 mouse macrophages (from ECACC No. 91051511) were grown in RPMI 1640 (BE 12-702 F, Lonza) supplemented with 10% (v/v) heat-inactivated fetal bovine serum (Lonza), penicillin (100 UI/mL) and streptomycin (100 µg/mL). Cells were maintained in a humidified incubator with 95% air/5% CO₂ at 37° C.

The cytotoxicity of nanoparticles (with TPP, ATP and AZT-TP) towards J774A.1 cells was determined using MTT assays. Cells were scraped from flasks and pooled together, counted with Neubauer chamber and brought to needed concentration, so to seed them in a 96-well plate in a density of 10,000 cells/well. They were pre-incubated for 24 hours. Nanoparticles were prepared and purified, diluted at different concentrations in cell medium then incubated with the cells for 2 h. After this time, supernatant was withdrawn and a solution of MTT in medium was added. After 2 h, supernatant was removed and DMSO was added to dissolve the MTT crystals. Plates were stirred for some minutes and absorbance measurements were run at $\lambda = 570$ nm, using a Labsystems Multiskan MS plate reader.

2.7. Evaluation of nanoparticle association to cells

Nanoparticles containing radioactive [8-¹⁴C]-ATP or [methyl-³H]-AZT-TP were prepared as described above then diluted 1:10 in cell culture medium (in order to maintain a viability above 80% as determined by MTT test), so to have 70 nCi/well. A control solution of ATP or AZT-TP at the same radioactivity concentration was prepared and diluted to the same ratio.

Cells were scraped from the culture flasks, counted and seeded in 6-well plates, having 100,000 cells and 2 mL medium per well. After 24 h incubation, the medium was withdrawn and 2 mL of the samples were added. The ATP (or AZT-TP) nanoparticle suspension and the ATP (or AZT-TP) solution were added to the cells at equivalent ATP (or AZT-TP) concentration and incubated from 0.5-2 h, after which the uptake was stopped by removing the cell culture medium. The cells were washed twice with PBS to remove unbound compounds. It was checked that radioactivity in the last washing supernatant was less than 3% of the initial radioactivity. The cells were then mixed with 1 mL of a 1%

Triton X-100 solution. The radioactivity of the supernatant medium, the washing supernatants and the cell lysate were counted. The uptake kinetics of nanoparticle ATP or AZT-TP was studied as described above, for various incubation times (30 min, 1 h, 2 h), and compared to that of free ATP or AZT-TP.

2.8. Intracellular distribution

J774 cells were seeded on coverslips previously placed in 24-well plates, having 25,000 cells and 0.5 mL medium per well, and pre-incubated for 24 hours. Preparation of nanoparticles was realized using fluorescent ATP as described above, and a free fluorescent ATP solution was prepared as control, in order to have the same fluorescence concentration. Nanoparticles and the control solution were diluted 1:10 in cell culture medium and incubated with the cells for 1-2 hours. After scheduled time, supernatant was removed and cells were washed with PBS. A 4% formaldehyde solution was added for ten minutes, then withdrawn and replaced with NH_4Cl at 50 mM for other ten minutes. Cells were then rinsed three times with PBS, then the coverslips with the cells were extracted from the well and mounted upside down on a microscope slide previously prepared with a drop of VECTASHIELD[®] Mounting Medium. Cells were then imaged using a confocal laser scanning microscope LSM 510 META (Zeiss, Oberkochen, Germany) using a Plan-Apochromat 63x objective lens (numerical aperture 1.40, oil immersion), a 1 mW helium neon laser (excitation wavelength 488 nm) and a long pass emission filter 505nm. The pinhole was set at 1.0 Airy unit (0.8 μm optical slice thickness). 12 bit numerical images were acquired with LSM 510 software version 3.2.

3. Results and discussion

3.1. Obtaining nanoparticles from CS and ATP or AZT-TP

When the tested triphosphate molecules are added to a chitosan solution under the conditions described in the material and methods section, the same general pattern is observed: (i) at low phosphate ([P]) concentrations, the system remains limpid; (ii) for increasing [P] concentrations, the system exhibits an increasingly milky aspect with a marked Tyndall effect, still remaining perfectly homogeneous; (iii) above a critical [P] concentration, visible aggregates are formed, rapidly sedimenting and leaving a clear supernatant. As depicted in Figure 1, it is noteworthy that stable

colloidal suspensions are obtained for N/P ratios between around 1 and 5, regardless of the triphosphate molecules tested (TPP, ATP, AZT-TP).

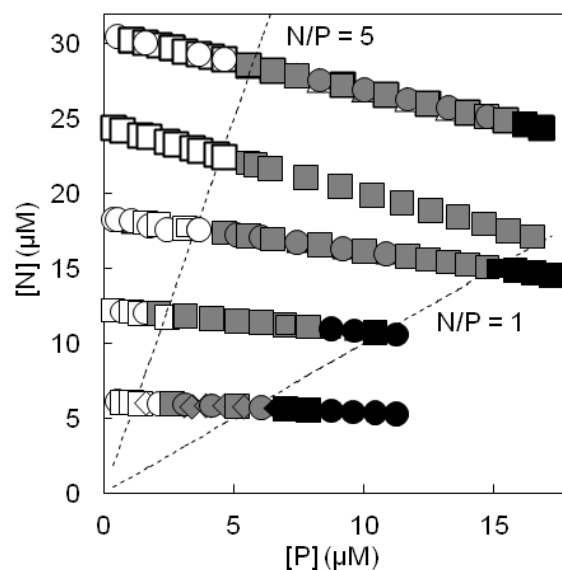


Figure 1. Identification of domains of formation of stable colloidal suspensions (grey), between solution-like (white) and sedimenting suspensions (black), as a function of the concentration in chitosan (expressed as [N]) and triphosphate group-containing molecules (TPP (o), ATP (\square), AZT-TP (\diamond), expressed as [P]).

While the obtention of colloidal suspensions from the complexation of CS to TPP (coined “ionotropic gelation”) [9] has been well established and lead to many developments of such “chitosan nanoparticles” [10], we show here that this strategy can be generalized to triphosphate group-containing molecules such as the nucleotide ATP and the nucleotide analogue AZT-TP. The formation domains of these nanoparticle suspensions are similar when the complexing molecules are expressed as their molar phosphate content, confirming that the presence of triphosphate group is the driving force of the particle formation, regardless of the pending moiety. This constitutes an original and versatile strategy to design nucleotide and nucleotide analogues nanocarriers, where the drug itself induces the nanocarrier assembly.

3.2. Characterization of CS/ATP and CS/AZT-TP nanoparticles

The size, polydispersity and zeta potential of the particles obtained were studied at fixed chitosan concentration and increasing triphosphate molecule concentrations (i.e., decreasing N/P ratios as

represented in Figure 2). The size of the particles formed is found to regularly decrease down to around 180 nm with decreasing N/P ratios until a critical value is reached, below which macroscopic aggregates are formed and instantly sediment (Figure 2 a, b). The zeta potential decreases from above +40 mV down to +10 or +20 mV (Figure 2 c). The critical N/P ratio ranges from 1 (for ATP and AZT-TP) to 1.4 (TPP), corresponding to a charge ratio of very close to 1 in all cases, based on the pK_a values of the relevant phosphate groups (Table 1).

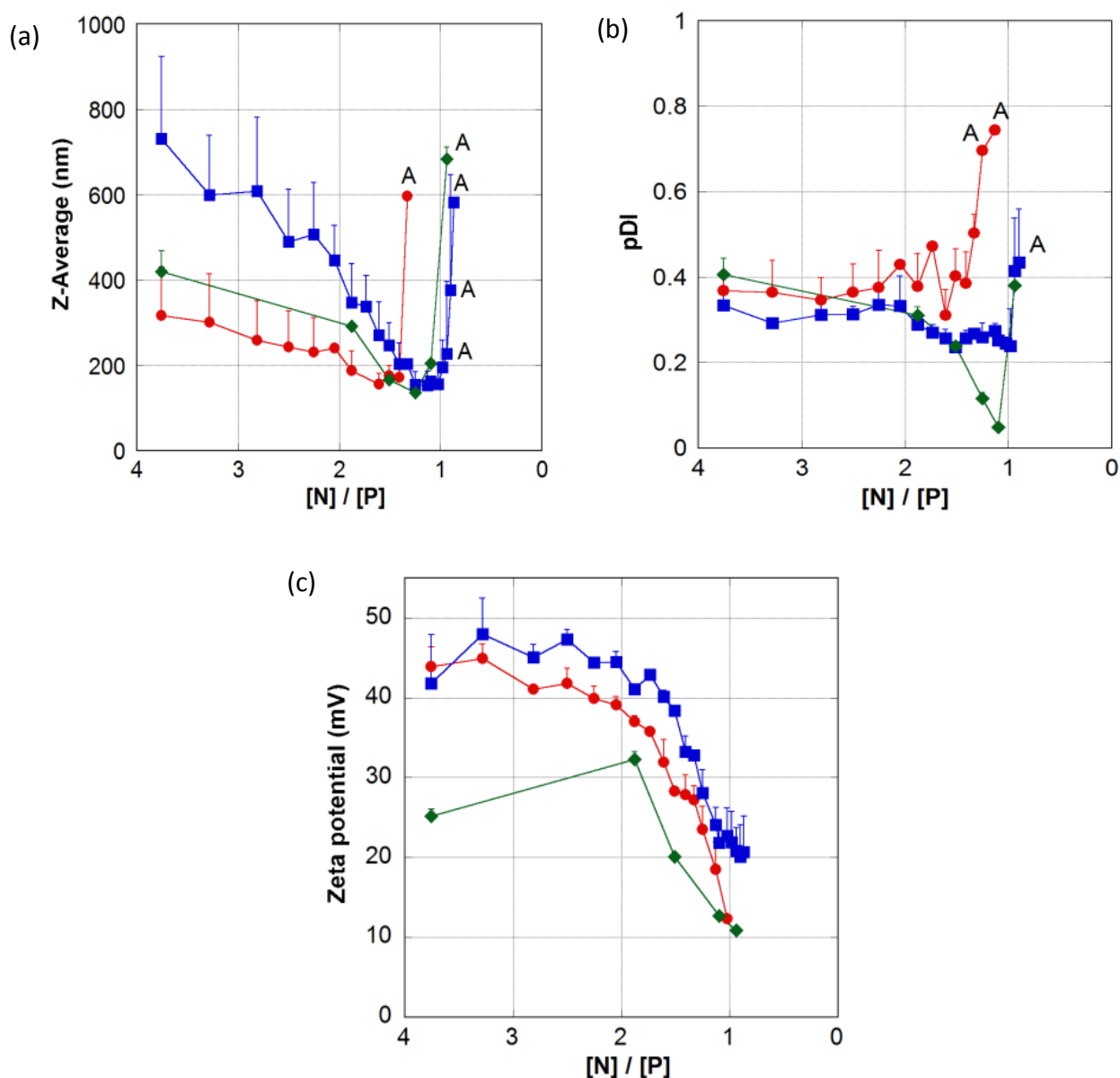


Figure 2. (a) Mean size, (b) polydispersity and (c) zeta potential of CS/TPP (○), CS/ATP (□) and CS/AZT-TP (◇) nanoparticles as a function of the N/P ratio. Appearance of macroscopic aggregates is indicated by “A”.

Table 1. Nanoparticle characteristics at critical N/P ratios.

Triphosphate molecule	TPP	ATP	AZT-TP
Critical N/P	1.41	1.02	1.09
Corresponding +/- charge ratio	0.99	1.03	0.97
Size (nm)	172 ± 25	156 ± 53	204 ± 4
Polydispersity	0.385 ± 0.086	0.245 ± 0.016	0.049 ± 0.006
Zeta potential (mV)	+27.9 ± 2.5	+22.7 ± 3.5	+12.7 ± 0.3

3.3. Encapsulation of ATP and AZT-TP

The fraction of CS and ATP or AZT-TP constitutive of the nanoparticles present in the colloidal suspension was quantified after separation of the particles from the dispersing phase using ultracentrifugation. The association of both ATP and AZT-TP is found to increase with decreasing N/P ratios, reaching around 70% at N/P = 1.3 (Figure 3). The association of CS increases along the same line up to 75% at the same ratio. This ratio (close to the critical ratio, still leaving a safety margin) was therefore selected for further investigations.

As a result, the CS/ATP and CS/AZT-TP nanoparticles prepared at N/P = 1.3 can be seen as ATP and AZT-TP nanocarriers exhibiting a drug payload of up to 44% w/w (Table 2). This is an very efficient loading compared to the few types of nanocarriers developed so far for the delivery of nucleotide analogues – typically up to 30% for liposomes [12, 13] or poloxamer-polyethyleneimine nanogels [12-15] and below 1% for polyalkylcyanoacrylate aqueous-core nanocapsules [5, 16]. CS/ATP and CS/AZT-TP nanoparticles at an N/P ratio of 1.3 were therefore selected for further *in vitro* evaluation.

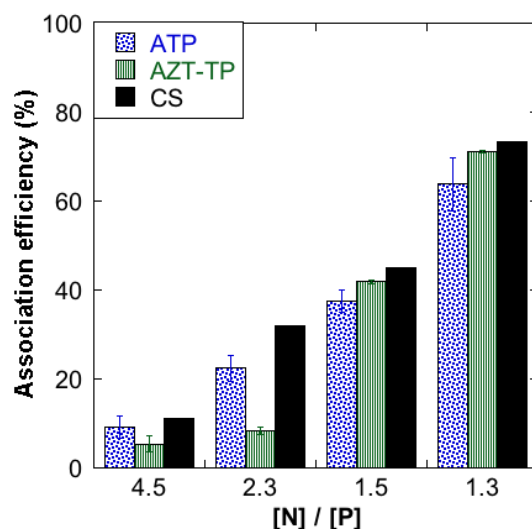


Figure 3. Determination of the association efficiency of ATP and AZT-TP to nanoparticles (ATP/CS, AZT-TP/CS, respectively) and of CS to CS/ATP nanoparticles, as a function of the N/P ratio.

Table 2. Composition of selected CS/ATP and CS/AZT-TP formulations after purification.

N/P Ratio	4.5	2.3	1.5	1.3
ATP loading (w/w)	17.3%	9.50%	38.5%	43.9%
<i>Effective N/P after purification</i>	5.5	3.2	1.8	1.4
AZT-TP loading (w/w)	9.17%	8.04%	37.8%	43.7%
<i>Effective N/P after purification</i>	9.3	8.5	1.6	1.3

3.4. *In vitro* release of ATP and AZT-TP

The *in vitro* release of the drug from nanocarriers is expected to occur through particle degradation in model physiological media. The particle integrity was therefore evaluated by following the relative intensity of scattered light by DLS during incubation of CS/ATP nanoparticles in PBS. The nanoparticle mean size was found to remain constant around 200 nm while the scattered light intensity decreased progressively over 24 h (Figure 4a), suggesting a particle dissociation without aggregation nor

swelling but rather through disentanglement of CS chains from the particles and subsequent dissolution.

The *in vitro* release of ATP and AZT-TP from CS/ATP and CS/AZT-TP nanoparticles respectively was also evaluated by prolonged ultracentrifugation of the suspensions after incubation in model isotonic media at 37°C. The release was found to occur much more rapidly in PBS (burst release in less than 1 h) than in the isotonic, non-ionic glucose medium (50% after 24 h) (Figure 4b), suggesting a release mechanism through particle dissociation due to competitive interactions with ions from the PBS medium, in accordance with the DLS measurements. The extent of release observed here might however be overestimated due the time needed to achieve significant nanoparticle sedimentation and the mechanical stress caused by centrifugation force.

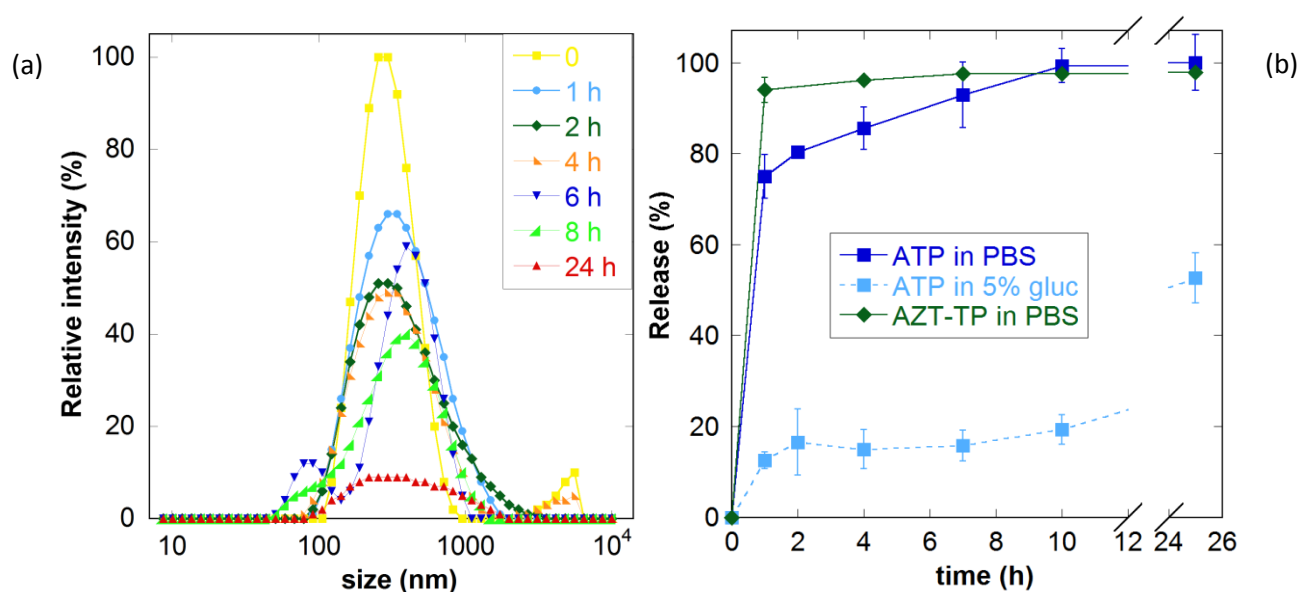


Figure 4. (a) Degradation of CS/ATP nanoparticles (N/P = 1.3) during incubation in PBS as evaluated by relative intensity of DLS. (b) Release of ATP and AZT-TP from CS/ATP and CS/AZT-TP nanoparticles as evaluated by ultracentrifugation after incubation in PBS or 5% glucose.

3.5. ATP and AZT-TP cellular delivery by nanoparticles

Nanoparticles were evaluated on macrophages, an important target cell population of anti-HIV nucleoside analogues. Because they represent a major reservoir of the HIV infection, addressing HIV infection in macrophages is considered as crucial to achieve successful long-term treatments of HIV-infected patients [17]. The effect of CS/ATP and CS/AZT-TP nanoparticle exposure to J774 mouse

macrophages on the cell viability was evaluated through the mitochondrial activity and compared to the effect of conventional CS/TPP nanoparticles. All formulations exhibit a mild cytotoxicity, the viability being around or above 80% for nanoparticle concentrations up to 0.5 mg/mL (Figure 5).

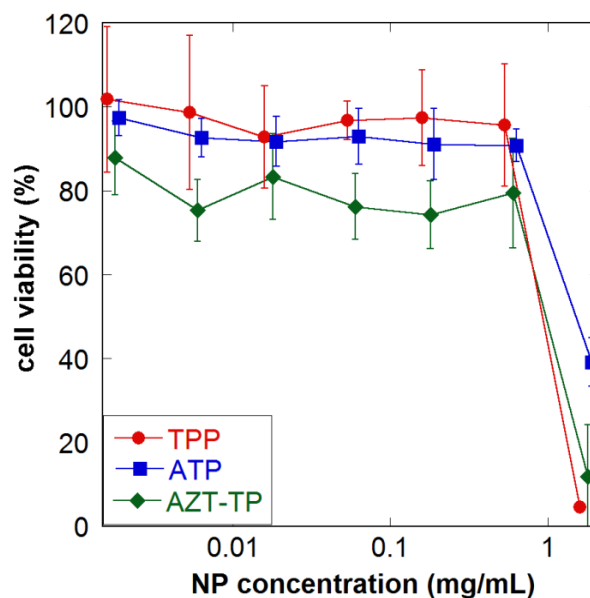


Figure 5. J774 cell viability as a function of CS/ATP and CS/AZT-TP nanoparticle (N/P = 1.3) concentration as determined by MTT test.

The cell uptake of $[8-^{14}\text{C}]\text{-ATP}$ and $[^3\text{H}]\text{-AZT-TP}$ was quantified as the cell-associated radioactivity after extensive washing of the cell layer. The uptake was found to be up to 2-fold higher for AZT-TP and up to 4-fold higher for ATP when the molecules were delivered as nanoparticles compared to the free molecules (Figure 6). This shows the important potential of the CS/ATP and CS/AZT-TP nanoparticles for the cellular delivery of such molecules, their cell-associated levels being orders of magnitude higher than those previously described using other nanocarriers [5], and even higher than the levels measured in peripheral blood mononuclear cells of AZT-treated patients [18].

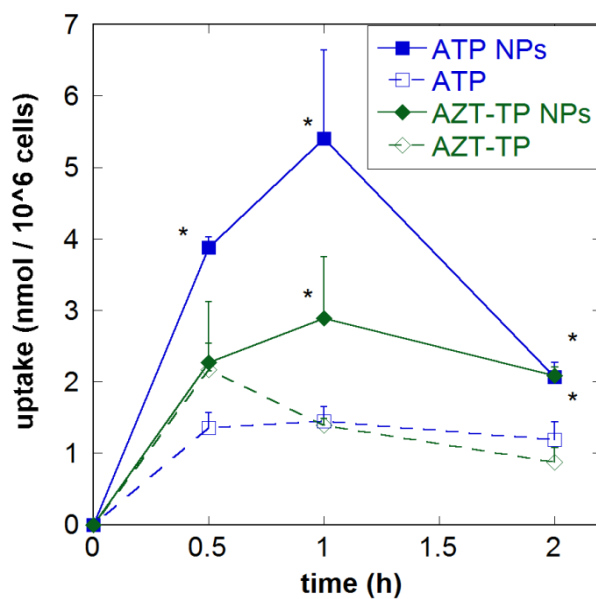


Figure 6. ATP and AZT-TP uptake by J774 cells upon exposure to free molecules (dotted lines) or corresponding nanoparticles (NPs, plain lines), as quantified by radioactivity measurements (*, $p < 0.05$ for nanoparticles vs. free molecule).

The intracellular distribution of the delivered triphosphate molecules was further investigated using fluorescent ATP and confocal laser microscopy. The results confirmed the higher uptake of ATP delivered as CS/ATP nanoparticles and the perinuclear fluorescence observed in median optical slices showed that the molecule was delivered in the cell cytoplasm rather than merely bound to the cell membrane (Figure 7).

This shows the ability of such nanoparticles to deliver nucleotides and nucleotide analogues down to the cell cytoplasm, which is the desired location for the delivery of ATP as well as antiviral nucleotide analogues (the viral reverse transcriptase is active in the cytoplasm of the host cell).

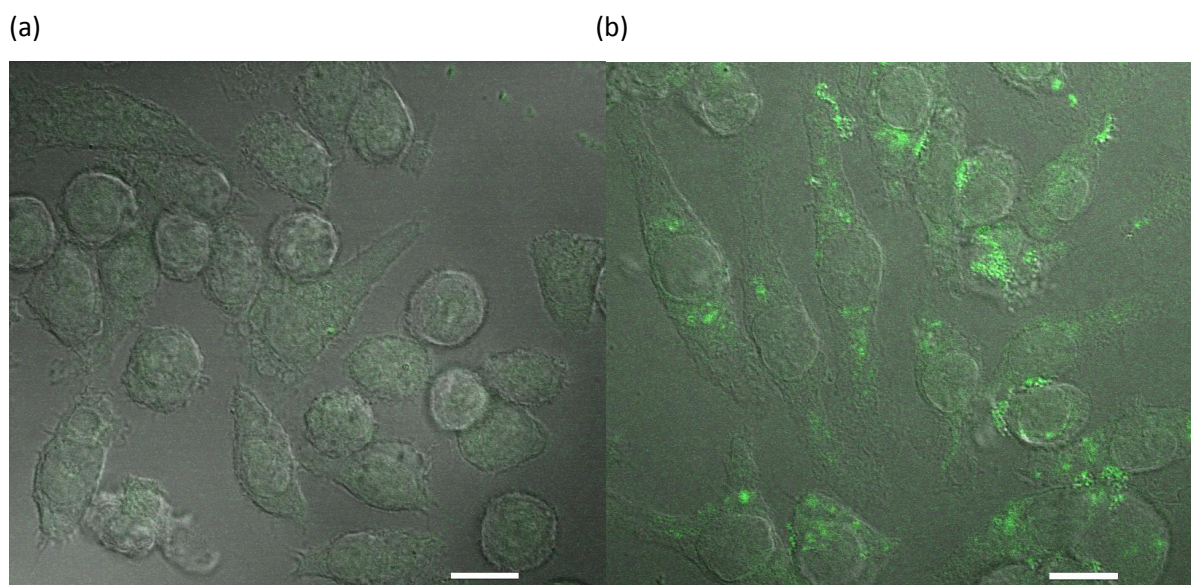


Figure 7. Intracellular distribution of fluorescent ATP in J774 cells upon exposure to (a) the free molecule or (b) the corresponding CS/ATP nanoparticles (N/P = 1.3), as observed by confocal laser microscopy (bar = 20 µm). Images are obtained by merging the DIC observation and the fluorescence of the 0.8 µm thick midpoint optical slice.

4. Conclusions

An original, versatile and straightforward method is proposed to design nanocarriers for nucleotides and nucleotide analogues based on CS. Unlike most nanosystems used for this purpose like polymeric nanocapsules or liposomes, which are limited by the drug loading achievable, the nanocarrier assembly described here is driven by the drug itself, allowing loading rates as high as 44%. Because this drastically lowers the amount of excipients needed in the formulation, this limits the toxicity concerns for potential clinical applications. The described process is moreover easily scalable. When tested *in vitro*, such nanosystems show a limited cytotoxicity indeed and allow an efficient intracellular delivery of nucleotide. Further *in vivo* studies are now worth being investigated to confirm the potential of these CS/nucleotide and CS/nucleotide-analogue nanosystems.

Acknowledgements

The authors wish to thank H el ene Chacun (Institut Galien Paris-Sud) for her guidance and assistance in radioactivity experiments and Val erie Nicolas (IFR IPSIT, Universit e Paris-Sud) for the confocal laser microscopy observations.

References

- [1] Chaudry, I. H., Use of Atp Following Shock and Ischemia, *Ann.NY Acad.Sci.*, **1990**, *603*, 130-141.
- [2] Van Rompay, A. R.; Johansson, M.; Karlsson, A., Substrate specificity and phosphorylation of antiviral and anticancer nucleoside analogues by human deoxyribonucleoside kinases and ribonucleoside kinases, *Pharmacol. Ther.*, **2003**, *100*, 119-139.
- [3] Hillaireau, H.; Couvreur, P., Nanoencapsulation of antiviral nucleotide analogs, *J. Drug Deliv. Sci. Technol.*, **2009**, *19*, 385-390.
- [4] Korb, V.; Tep, K.; Escriou, V.; Richard, C.; Scherman, D.; Cynober, L.; Chaumeil, J. C.; Dumortier, G., Current data on ATP-containing liposomes and potential prospects to enhance cellular energy status for hepatic applications, *Crit. Rev. Ther. Drug Carr. Syst.*, **2008**, *25*, 305-345.
- [5] Hillaireau, H.; Le Doan, T.; Appel, M.; Couvreur, P., Hybrid polymer nanocapsules enhance in vitro delivery of azidothymidine-triphosphate to macrophages, *J. Control. Release*, **2006**, *116*, 346-352.
- [6] Galmarini, C. M.; Warren, G.; Senanayake, M. T.; Vinogradov, S. V., Efficient overcoming of drug resistance to anticancer nucleoside analogs by nanodelivery of active phosphorylated drugs, *Int. J. Pharm.*, **2010**, *395*, 281-289.
- [7] Horcajada, P.; Chalati, T.; Serre, C.; Gillet, B.; Sebrie, C.; Baati, T.; Eubank, J. F.; Heurtaux, D.; Clayette, P.; Kreuz, C.; Chang, J. S.; Hwang, Y. K.; Marsaud, V.; Bories, P. N.; Cynober, L.; Gil, S.; Ferey, G.; Couvreur, P.; Gref, R., Porous metal-organic-framework nanoscale carriers as a potential platform for drug delivery and imaging, *Nat. Mater.*, **2010**, *9*, 172-178.
- [8] Kean, T.; Thanou, M., Biodegradation, biodistribution and toxicity of chitosan, *Adv. Drug Deliv. Rev.*, **2010**, *62*, 3-11.
- [9] Calvo, P.; RemunanLopez, C.; VilaJato, J. L.; Alonso, M. J., Novel hydrophilic chitosan-polyethylene oxide nanoparticles as protein carriers, *Journal of Applied Polymer Science*, **1997**, *63*, 125-132.
- [10] Garcia-Fuentes, M.; Alonso, M. J., Chitosan-based drug nanocarriers: Where do we stand?, *J. Control. Release*, **2012**, *161*, 496-504.
- [11] Muzzarelli, R. A. A., Colorimetric determination of chitosan, *Anal. Biochem.*, **1998**, *260*, 255-257.
- [12] Chaib, S.; Charrueau, C.; Neveux, N.; Nakib, S.; Chaumeil, J. C.; Cynober, L.; De Bandt, J. P., Effect of apoE/ATP-containing liposomes on hepatic energy state, *Liver Int.*, **2003**, *23*, 379-385.

- [13] Neveux, N.; De Bandt, J. P.; Fattal, E.; Hannoun, L.; Poupon, R.; Chaumeil, J. C.; Delattre, J.; Cynober, L. A., Cold preservation injury in rat liver: effect of liposomally-entrapped adenosine triphosphate, *J. Hepatol.*, **2000**, *33*, 68-75.
- [14] Kohli, E.; Han, H. Y.; Zeman, A. D.; Vinogradov, S. V., Formulations of biodegradable Nanogel carriers with 5'-triphosphates of nucleoside analogs that display a reduced cytotoxicity and enhanced drug activity, *J. Control. Release*, **2007**, *121*, 19-27.
- [15] Vinogradov, S. V.; Kohli, E.; Zeman, A. D., Cross-linked polymeric nanogel formulations of 5'-triphosphates of nucleoside analogues: Role of the cellular membrane in drug release, *Mol. Pharm.*, **2005**, *2*, 449-461.
- [16] Hillaireau, H.; Le Doan, T.; Chacun, H.; Janin, J.; Couvreur, P., Encapsulation of mono- and oligo-nucleotides into aqueous-core nanocapsules in presence of various water-soluble polymers, *Int. J. Pharm.*, **2007**, *331*, 148-152.
- [17] Koppensteiner, H.; Brack-Werner, R.; Schindler, M., Macrophages and their relevance in Human Immunodeficiency Virus Type I infection, *Retrovirology*, **2012**, *9*.
- [18] Rodriguez, J. F.; Rodriguez, J. L.; Santana, J.; Garcia, H.; Rosario, O., Simultaneous quantitation of intracellular zidovudine and lamivudine triphosphates in human immunodeficiency virus-infected individuals, *Antimicrob. Agents Chemother.*, **2000**, *44*, 3097-3100.

Chapitre 2

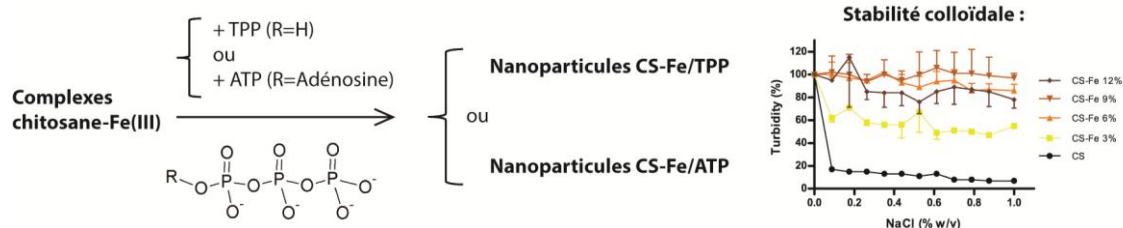
**Stabilisation et délivrance cellulaire de nanoparticules à base de chitosane
et de polyphosphates, par ajout de fer ionique**

Chapitre 2

Stabilisation et délivrance cellulaire de nanoparticules à base de chitosane et de polyphosphates, par ajout de fer ionique¹

Résumé

Les nanoparticules à base de chitosane (CS) et d'ATP ou d'AZT-TP décrites précédemment, malgré leur intérêt pour l'encapsulation et la délivrance intracellulaire de ces molécules, ont tendance à se désagréger rapidement quand elles sont diluées dans des milieux physiologiques. Quelques stratégies pour stabiliser ces systèmes ont été proposées jusqu'à présent, mais elles impliquent typiquement l'ajout d'un agent de recouvrement ou de réticulation chimique. Dans ce chapitre, nous proposons la complexation du CS avec des ions ferriques avant la formation des nanoparticules, afin d'améliorer la stabilité du vecteur, grâce à la capacité du fer(III) à se lier fortement à la fois au CS et aux groupements phosphates. Des nanoparticules ont été obtenues à partir d'une part de complexes de chitosane-fer (CS-Fe), contenant entre 3 et 12% m/m en fer, et d'autre part de polyphosphates, TPP (ion tripolyphosphate) ou ATP. La titration calorimétrique isotherme (ITC) a montré que l'affinité de liaison du TPP ou de l'ATP pour le CS-Fe augmente avec la teneur en fer du complexe CS-Fe. La stabilité colloïdale de ces nanoparticules dans des conditions physiologiques a été évaluée par turbidité et par fluctuation de fluorescence en temps réel, après dilution avec des électrolytes. Les résultats ont montré une stabilité supérieure des nanoparticules à base de CS-Fe par rapport au CS, qui augmente avec la teneur en fer. De plus, des études *in vitro* sur deux lignées cellulaires de macrophages (J774A.1 et THP-1) ont révélé que la capture d'ATP est améliorée de façon cohérente avec le contenu de fer des nanoparticules CS-Fe/ATP, et en corrélation avec leur dissociation réduite dans des milieux biologiques, permettant donc des perspectives intéressantes pour l'utilisation de ces nanoparticules *in vivo*.

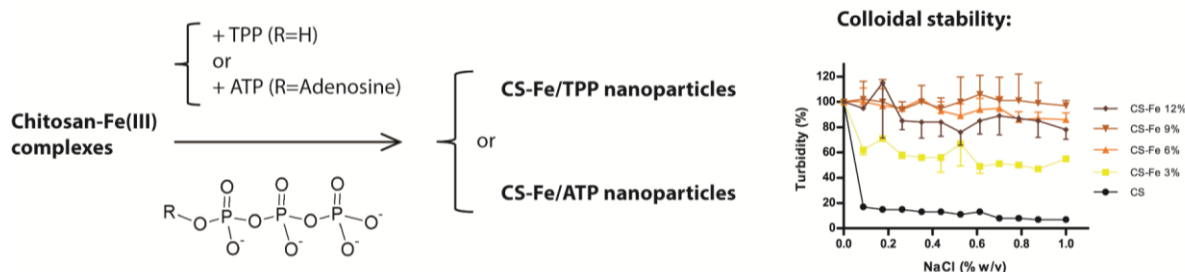


¹ Chapitre publié sous forme d'article dans *Journal of Controlled Release*, Volume 194, 2014, 211-219. Auteurs : Giovanna Giacalone, Hervé Hillaireau, Pauline Capiou, Hélène Chacun, Franceline Reynaud, Elias Fattal.

Stabilization and cellular delivery of chitosan-polyphosphate nanoparticles by incorporation of iron¹

Abstract

The nanoparticles previously described, based on chitosan (CS) and ATP or AZT-TP, despite their interest for the encapsulation and cellular delivery of these molecules, tend to readily disintegrate when diluted in physiological media. Some stabilization strategies have been proposed so far for similar CS-based nanoparticles, but they typically involve the addition of a coating agent or chemical crosslinkers. In this chapter, we propose the complexation of CS with iron ions prior to nanoparticle formation as a strategy to improve the carrier stability, thanks to the ability of iron to strongly bind both chitosan and phosphate groups. Nanoparticles were obtained from either TPP or ATP and chitosan-iron (CS-Fe) complexes containing 3 to 12% w/w iron. Isothermal titration calorimetry showed that the binding affinity of TPP and ATP to CS-Fe increased with the iron content of CS-Fe complexes. The colloidal stability of these nanoparticles in physiological conditions was evaluated by turbidity and by fluorescence fluctuation in real time upon dilution by electrolytes. The results revealed an important stabilization effect of CS-Fe compared to CS, increasing with the iron content. Furthermore, *in vitro* studies on two macrophages cell lines (J774A.1 and THP-1) revealed that ATP uptake is improved consistently with the iron content of CS-Fe/ATP nanoparticles, and correlated to their lower dissociation in biological medium, allowing interesting perspectives for the *in vivo* application of these nanoparticles.



¹ Chapter published as an article in *Journal of Controlled Release*, Volume 194, **2014**, 211-219. Authors: Giovanna Giacalone, Hervé Hillaireau, Pauline Capiou, H el ene Chacun, Franceline Reynaud, Elias Fattal.

1. Introduction

Since their introduction in 1997 by Calvo *et al.* [1], nanoparticles prepared from chitosan (CS) have been widely used, especially in the field of drug delivery. Advantages of these systems include biodegradability and low toxicity of chitosan [2, 3] but also the simple and mild method of nanoparticle preparation, which consists of mixing CS and sodium tripolyphosphate (TPP). This so-called ionotropic gelation technique also gave the name of nanogels to the nanoparticles prepared. First applications were systems for the delivery of proteins [4] or nucleic acids (DNA [5], siRNA [6]). Recently, our group has shown that substituting TPP with triphosphate group-containing active drugs such as adenosine triphosphate (ATP) and azidothymidine triphosphate (AZT-TP) led to highly-loaded nanoparticles [7]. However, despite the main advantage of replacing TPP with drug candidates, the CS-based nanoparticles present a weak point, which is their colloidal stability in physiological media. This issue has been addressed since 2005 by López-León *et al.* [8], reporting their tendency to be unstable when changing pH and ionic strength of the medium, namely aggregating but also disintegrating. Taking into consideration this feature, the use of this kind of nanoparticles has been limited to mucosal delivery purposes.

Our aim is to deliver intracellularly ATP to human macrophages, in order to restore the intracellular pool of this specific nucleoside, since it was shown that ATP depletion is associated to macrophage death in atherosclerotic lesions [9] and increased risk of plaque rupture and acute coronary events or stroke [10]. It is therefore suggested that therapies aimed at restoring energy balance in plaques may constitute a new approach to stabilizing advanced atherosclerotic plaques [18]. However, before we get to the application and because ATP is a highly ionized molecule and poorly stable in biological fluids, it should be delivered by an adequate carrier. Since it has been shown that chitosan nanoparticles are efficiently delivered to atherosclerotic plaques [11], our goal is to design stable chitosan nanoparticles that can deliver efficiently ATP to macrophages. Some strategies have been proposed to improve the stability of these systems, which mainly consist in decorating the nanoparticle surface with additional components, like alginates [12] or hyaluronic acid [13, 14], and the use of chemical crosslinking, often glutaraldehyde. These methods though have the inconvenience of increasing the carrier weight, thus reducing the drug payload, or creating toxicity concerns. Approaches to circumvent the use of toxic cross-linker agents were investigated. Genipin, a naturally occurring molecule, was proposed for the formulation of chitosan microparticles [15], demonstrating less toxicity than glutaraldehyde [16]. In this study, we investigate the stability improvement of CS-based nanoparticles prepared with the ionic cross-linker TPP and the ATP drug, by modifying CS before nanoparticle formation, namely complexing it with ferric ions. The rationale behind this approach is the ability of CS to bind to metal ions including iron, leading to strong

coordination complexes [17, 18], while iron itself can bind to phosphate groups [19, 20], which may create an additional and strong 'bridge' in the nanoparticle formation. In regards to our application, we are aiming to design a stable nanoparticles system with efficient intracellular delivery of ATP.

2. Materials and methods

2.1. Materials

Nanoparticles were prepared using low viscosity CS (95% deacetylated, Fluka) and TPP or ATP purchased from Sigma (France). In the following, PBS refers to PBS without CaCl_2 and MgCl_2 from Dulbecco (Lonza), and water to Milli-Q purified water (Millipore, France).

$[\gamma\text{-}^{33}\text{P}]\text{-ATP}$, the scintillation liquid Ultima Gold and the strong base Solvable were from Perkin Elmer (France); Bodipy-FL ATP (fluorescently-labeled ATP) and H_2DCFDA (2',7'-dichlorodihydrofluorescein diacetate) were from Invitrogen (France).

Complexation of CS with iron was achieved with Iron (III) nitrate nonahydrate, 1,10-Phenanthroline monohydrate and hydroxylamine hydrochloride from Sigma. Other reagents used were purchased from Sigma; all solvents were of analytical grade.

2.2. Preparation of CS-Fe complexes

Several CS-Fe complexes have been prepared in different conditions, among which 4 have been selected as a function of the mass fraction of Fe, expressed as % w/w in the following.

The CS-Fe_{3%} complex was prepared as follows. 1 g of CS was added to 100 mL of a 0.5 M $\text{Fe}(\text{NO}_3)_3$ solution (pH = 1.5) and the complex was allowed to form overnight under mechanical stirring. The complex was then washed from unbound iron through precipitation with acetone, until the filtrate was free from iron, as assessed through the addition of ascorbic acid (which turns brown in presence of iron). The CS-Fe_{6%} complex was prepared similarly using 5 g of chitosan and 500 mL of a 0.1 M iron nitrate solution. The CS-Fe_{9%} complex was achieved in the same conditions as CS-Fe_{6%} but was kept under stirring for 2 days. Eventually, the CS-Fe_{12%} complex was prepared using 100 mL of a 0.1 M iron nitrate solution, adding subsequently 1 g of chitosan and allowed to form overnight. CS-Fe complexes were then dried avoiding the formation of films. All complexes were obtained at least twice in order to validate the method.

2.3. Characterisation of CS-Fe complexes

The fractions of iron, carbon, hydrogen and nitrogen present in the complexes were first determined by elemental analysis. The amount of iron present in the complex was also determined through a colorimetric UV-Vis spectroscopy dosage using phenanthroline [21]. Briefly, the complex between CS and Fe was hydrolyzed through the use of concentrated chloridric and nitric acid on a sand bath at 200 °C. The powder was then recovered with water and let allowed to form a complex with phenanthroline, which was then quantified through absorbance at $\lambda = 510$ nm.

FT-IT spectra of CS and CS-Fe complexes were acquired using a Spectrum Two FT-IR Spectrometer (Perkin Elmer) with a Diamond ATR accessory, between 4000 and 400 cm^{-1} . The spectral resolution was 4 cm^{-1} and 20 scans were averaged. Data were acquired using the software Spectrum Touch and processed with Time Base v.3.1.2.

2.4. Nanoparticle formation and characterization

In all cases 27 mM TPP or ATP solutions (corresponding to a phosphorus concentration [P] = 81 mM) were added dropwise to 3 mL of a 1-5 mg/mL CS-Fe solution (corresponding to a nitrogen concentration [N] = 6.1-30.5 mM) under magnetic stirring at 1000 rpm.

For the study of nanoparticle formation domains, increasing amounts of triphosphate solutions were added to the chitosan solution and the resulting system was visually identified as solution-like, colloidal suspension, or aggregated suspension (presence of sedimenting aggregates/flocculates). The limits of the different regions were drawn on an N/P diagram after at least three repetitions.

For further studies, nanoparticles were purified from free TPP or ATP and CS through centrifugation of 1 mL suspension on a 20 μL glycerol layer at 1500 $\times g$ for 1 h, removal of 0.92 mL supernatant, and redispersion in 1 mL (final volume) of the studied medium.

For radioactivity studies, ATP nanoparticles were formed from an ATP solution prepared using [γ - ^{33}P]-ATP as a tracer, by diluting the commercial 10 mCi/mL (25 mM) with appropriate amounts of unlabeled ATP solution.

For storage purposes, nanoparticles were freeze-dried by adding trehalose as cryoprotectant to a 1 mL suspension at the final 10% w/w concentration. The resulting suspension was frozen with liquid nitrogen and freeze-dried at -55 °C and 0.01 mbar for 24 hours using a Christ Alpha 1-2 LD Plus.

The mean size and polydispersity index of nanoparticles were determined using photon correlation spectroscopy (PCS), with a 173° scattering angle at a temperature of 25°C, and the zeta potential of

nanoparticles was determined after 1/20 sample dilution in 1 mM NaCl solution, using a Zetasizer MAL 500180 (Malvern Instrument, UK).

The morphology of CS/ATP and CS-Fe_{12%}/ATP nanoparticles was studied through transmission electron microscopy (TEM) using a JEOL JEM-1400 microscope. 5 μ L of nanoparticles suspensions were deposited for one minute on copper grids covered with formvar-carbon film. Samples were then stained using 2% uranyl acetate for 30 seconds, and imaged at 80 kV.

2.5. Isothermal titration calorimetry

Isothermal titration calorimetry (ITC) measurements were performed on a Microcal VP-ITC with a cell volume of 1.441 mL at 25° C. For each experiment, a 27 mM TPP or ATP solution was titrated into the cell containing a 1 mg/mL CS or CS-Fe solution (which corresponds to 6.1 mM as CS monomer unit). Volumes of 5 or 10 μ L were injected with spacing times ranging from 600 to 2500 s, while the solution/suspension was stirred at 394 rpm. The heat of dilution was measured for every experiment by titrating TPP or ATP solution into the buffer solution, and these values were then subtracted in order to obtain the actual heat of binding. The fit of the curves was calculated with Origin7 (Chi-square values between 900 and 7000) and values found were used to determine the free Gibbs energy.

2.6. Determination of nanoparticle composition

A 27 mM ATP solution was prepared using [γ -³³P]-ATP as a tracer, by diluting the commercial 10 mCi/mL with appropriate amount of unlabelled ATP solution. Particles were then prepared as described above from CS-Fe complexes containing 0-12% Fe. Nanoparticles were centrifuged at 17000 \times g for one hour in order to separate them from free ATP. The supernatant was withdrawn and both pellets (containing nanoparticles) and supernatants (containing free ATP) were then analyzed to determine their radioactivity content using a Beckman Coulter (LS 6500 Multi-Purpose Scintillation Counter) instrument. The association efficiency was calculated as the ratio of the pellet radioactivity to the total (pellet + supernatant) radioactivity.

2.7. Colloidal stability in physiological media

The colloidal stability of nanoparticle systems was evaluated through the measure of the turbidity of the suspension, namely their absorbance at $\lambda = 590$ nm, using a spectrophotometer. Particles were prepared and purified as described above, then pellets were pooled together and 0.125 mL of nanoparticles was diluted by NaCl solutions at final concentrations ranging from 0.1 to 1% w/v. Turbidity was expressed as a percentage of the turbidity of nanoparticles diluted with water in the same conditions.

The dynamics of nanoparticle dissociation upon dilution with electrolytes was investigated using fluorescence fluctuation spectroscopy using a SPS confocal laser scanning microscope (Leica, Germany). Nanoparticles were prepared using BODIPY-labeled ATP and the fluorescence fluctuation was measured in the small excitation volume (\sim fL) of a confocal microscope. In this experiment, the baseline fluorescence level is due to the ATP in solution (free ATP) while peaks appear when single nanoparticles, bearing a high number of fluorescent ATP molecules, pass through the observation volume. An increase in the baseline level (and the disappearance of peaks) is due to the release of ATP from nanoparticles, thus allowing the monitoring of the nanoparticle dissociation kinetics. Fluctuation measurements were recorded during 30 second intervals at least in triplicate, using the software SymPhoTime (PicoHarp 300, PicoQuant). These measurements were performed 10 min before, during and 30-60 min after addition of NaCl (final concentration 0.9% w/v) to the nanoparticle suspension.

2.8. Cell culture, cell viability and oxidative stress

J774A.1 mouse macrophages (from ECACC, catalogue number 91051511) were grown in RPMI 1640 medium (BE 12-702 F, Lonza) supplemented with 10% (v/v) heat-inactivated fetal bovine serum (Lonza), penicillin (100 UI/mL) and streptomycin (100 μ g/mL). Cells were maintained in a humidified incubator with 95% air/5% CO₂ at 37 °C. Cells were used from passage 3 to 20 after thawing.

THP-1 human acute monocytic leukemia cells (from ATCC, catalogue number TIB-202) were grown in RPMI 1640 (BE 12-702 F, Lonza) supplemented with 10% (v/v) fetal bovine serum (Lonza), penicillin (100 UI/mL) and streptomycin (100 μ g/mL). Cells were maintained in a humidified incubator with 95% air/5% CO₂ at 37 °C. For experiments, monocytes were derived into adherent macrophages by treatment with 10⁻⁸ M phorbol 12-myristate 13-acetate (PMA) for 24 hours, before running the experiment. Cells were used from passage 3 to 12 after thawing.

The cytotoxicity of ATP nanoparticles towards both cell lines was determined using MTT assays [22]. Cells were recovered from flasks and pooled together, counted with a Neubauer chamber and diluted to appropriate concentrations to seed them in 96-well plates at a density of 30,000 cells/well for J774A.1 and 60,000 for THP-1. They were pre-incubated for 24 hours. Nanoparticles were prepared and purified, diluted at different concentrations in cell medium and then incubated with the cells for 24 h. After this time, supernatant was withdrawn and a solution of 0.5 mg/mL MTT in medium was added. After two hours, supernatant was removed and dimethyl sulfoxide was added to dissolve formazan crystals. Plates were stirred for some minutes and absorbance measurements were run at $\lambda = 570$ nm, using a Labsystems Multiskan MS plate reader.

The oxidative stress due to nanoparticle exposure was evaluated on THP-1 macrophages. 600,000 cells per well were seeded in a 12-well plate. After two days, cells were exposed for 5 minutes to 5 μ M H₂DCFDA and allowed to recover for 30 minutes in fresh medium. Nanoparticles or hydrogen peroxide (300 and 750 μ M, used as positive control) were then added on the cells. After 20 or 40 min, supernatant was withdrawn and 1x trypsin was added for 3 minutes. Afterwards cells were recovered and analyzed in flow cytometry immediately after using a BD Accuri C6 flow cytometer, on FL1 channel (530 \pm 30 nm BP).

2.9. Cellular uptake

Nanoparticles containing [γ -³³P]-ATP were prepared as described above then diluted 1:10 in cell culture medium, in order to maintain at least 80% viability as determined by MTT test. A control solution of ATP at the same concentration was prepared and diluted at the same ratio.

For J774A.1, cells were scraped from the culture flasks, counted and seeded in 6-well plates, having 800,000 cells and 2 mL medium per well. After 24 h incubation, the medium was withdrawn and 2 mL of nanoparticles or ATP solution was added to the cells. After 0.5-2 h incubation, the uptake was stopped by removing the cell culture medium. Cells were washed with PBS to remove unbound compounds and then mixed with 1 mL of Solvable to lyse them (2 h, 50 °C). The radioactivity of the supernatant medium, the washing supernatants and the cell lysate were counted. The uptake kinetics of nanoparticle ATP was studied for various incubation times, and compared to that of free ATP.

For THP-1, cells were counted, PMA was added and cells were seeded in 6-well plates having 1,600,000 cells and 2 mL per well and then processed in the same way as J774A.1 cells (2-24 h incubation with ATP formulations).

2.10. Intracellular distribution

J774 and THP-1 cells were seeded on coverslips previously placed in 24-well plates, having respectively 80,000 and 160,000 cells and 0.5 mL medium per well, and pre-incubated for 24 hours. Preparation of nanoparticles was realized using fluorescent ATP as a tracer, and a free fluorescent ATP solution was prepared as a control using the same fluorophore concentration. Nanoparticles and the control solution were diluted 1:10 in cell culture medium and incubated with the cells for 1-2 h. After scheduled times, supernatant was removed and cells were washed with PBS. A 4% formaldehyde solution was added for ten minutes, then withdrawn and replaced with NH_4Cl at 50 mM for other ten minutes. Cells were then rinsed three times with PBS, after which the coverslips with the cells were removed from the well and mounted on a microscope slide previously prepared with a drop of *Vectashield*[®] mounting medium. Cells were then imaged using a confocal laser scanning microscope LSM 510 META (Zeiss, Oberkochen, Germany) using a Plan-Apochromat 63x objective lens (numerical aperture 1.40, oil immersion), a 1 mW helium neon laser ($\lambda_{\text{ex}} = 488 \text{ nm}$) and a long pass emission filter 505 nm. The pinhole was set at 1.0 Airy unit (0.8 μm optical slice thickness). 12 bit numerical images were acquired with LSM 510 software version 3.2.

3. Results and discussion

3.1. Preparation of CS-iron complex

CS is known to form coordination complexes with various metals, thanks to the extra electron pair which is available on nitrogen groups of NH_2 . In the present study, iron was selected due to its ability to complex chitosan [18] as well as phosphate ions [19]. Chitosan-iron (CS-Fe) complexes were first prepared and the conditions optimized in order to control the amount of bounded iron.

CS-Fe complexes containing increasing iron content were obtained from complexation of chitosan with iron (III) nitrate at different concentrations and incubation times. The pH was kept at around 1.5 during the reaction [23] and the purification steps to avoid reprecipitation of iron nitrate but also formation of iron hydroxides (K_{sp} between 10^{-36} and 10^{-39}). This allowed tuning the iron content of the CS-Fe complexes from 3% to 12% as evaluated by a phenanthroline-based assay confirmed by elemental analysis (Supplementary data, Table S1). In the following, 4 CS-Fe complexes have been selected for further investigation, containing 3, 6, 9 and 12% w/w Fe. All the chitosan-iron complexes

were found soluble in acetic acid aqueous solutions in a similar way to the parent CS, at concentrations ranging from 1 to 5 mg/mL.

From the FT-IR spectra (Figure 1) it can be clearly seen that the 4 CS-Fe complexes present a similar spectrum, though different from CS. The two large absorption bands in the region $> 2500\text{ cm}^{-1}$ of the CS spectrum are typically due to $-\text{OH}$ and $-\text{NH}$ stretching. In the CS-Fe complexes, these bands are no longer visible, which is more likely due to the limited movements of these bonds involved in the interaction with iron. Furthermore, the CS band at around 1550 cm^{-1} represents the bending of $-\text{NH}_2$ groups, and this also disappears in the spectra of CS-Fe complexes, confirming the implication of $-\text{NH}$ groups in the binding with iron.

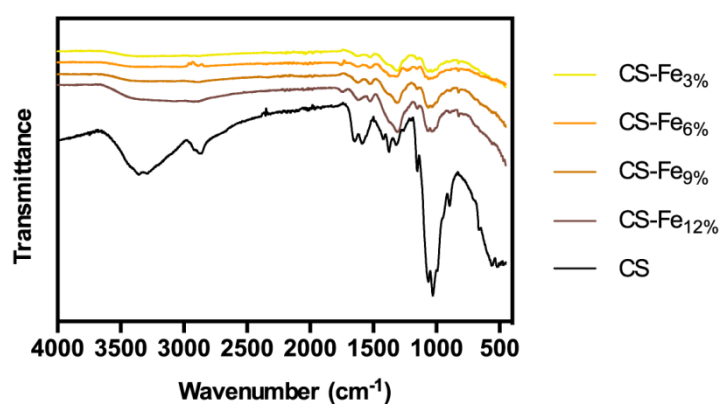


Figure 1. IR spectra of CS and CS-Fe complexes. For each curve, the highest point has to be considered as 100% of transmittance.

These results are consistent with previous hypotheses of iron complexation by CS for which every iron atom binds to 2 chitosan units [17]. Taking into account the average molar weight of a chitosan monomer and an iron atom, this stoichiometry corresponds to a maximum iron content of 17% w/w.

3.2. Formation of nanoparticles from CS-Fe and triphosphate derivatives

CS solutions can form nanoparticles by ionotropic gelation in the presence of TPP [1]. This is also possible using triphosphate group-containing molecules such as ATP or AZT-TP [7] instead of TPP. The formation takes place only under specific ratios expressed as N/P ratios (triphosphate derivative concentrations are expressed as phosphate groups and CS concentration as nitrogen from amine groups, since they are the two chemical groups involved in the binding). Upon addition of triphosphate derivatives to a CS solution (i.e. decreasing N/P), it turns into a milky colloidal

suspension attesting the presence of nanoparticles, until visible aggregation and sedimentation occurs at a so-called 'critical' N/P ratio.

As shown in Figure 2, the addition of TPP as well as ATP to various CS-Fe led to nanoparticle formation in a similar way to CS. Critical N/P ratios obtained are generally higher for TPP than ATP (around 1.4 vs. 1.0 for CS), which can be explained by the number of negative charges of the triphosphate derivatives at the working pH (4 for TPP, 3 for ATP). This behavior is observed for both kinds of chitosan, either with or without iron.

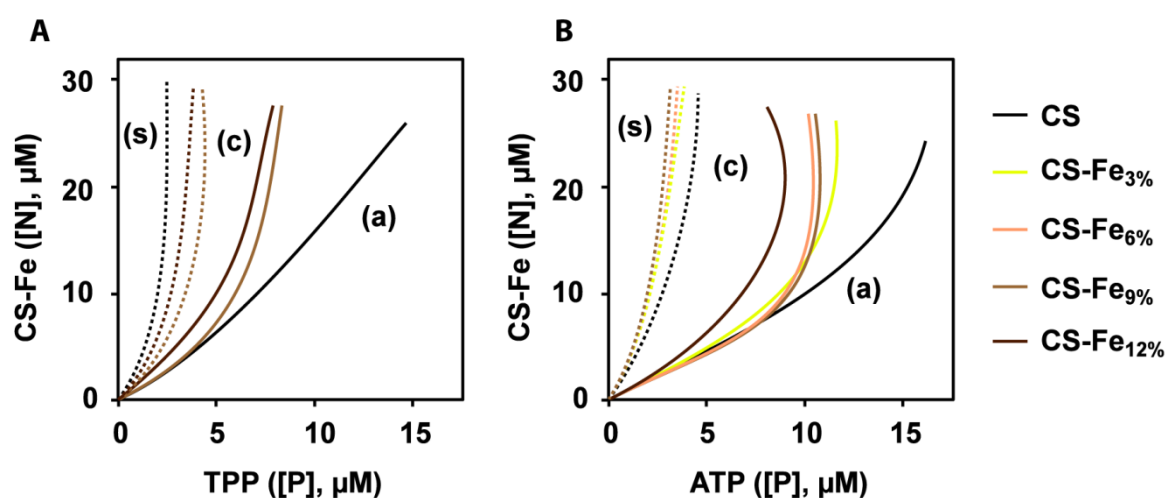


Figure 2. Limits of nanoparticle formation regions upon addition of (A) TPP and (B) ATP solutions to various CS or CS-Fe solutions. Dotted lines, beginning of the nanoparticle formation region; plan lines, beginning of the aggregation region; (s) solution-like system; (c) stable colloidal suspension (nanoparticles); (a) sedimenting aggregates.

When increasing the iron content of CS, a progressive shift of critical N/P ratios towards higher values is observed for both TPP and ATP. This can be explained by the presence of the iron on chitosan amine groups, thus reducing the number of ammonium sites available for ionic phosphate-ammonium bound which contributes to particle formation. However, phosphate groups are also able to interact with the iron, contributing to particle formation and stability.

To further understand the role of iron in the nanoparticle formation, the associated thermodynamic parameters were determined by isothermal titration calorimetry in the same mixing conditions. In all cases, isotherms obtained after subtraction of the heat of dilution revealed endothermic reactions, with a final state consistent with the critical N/P ratios discussed above (Figure 3). For TPP as well as ATP, the use of CS-Fe complexes with an increasing iron content resulted in more spontaneous

reactions (lower Gibbs free energy) with a higher affinity – up to 5-fold (TPP) and 2.5-fold (ATP) for CS-Fe_{12%} compared to CS. Figure 3 B and D show a representative example of a titration curve.

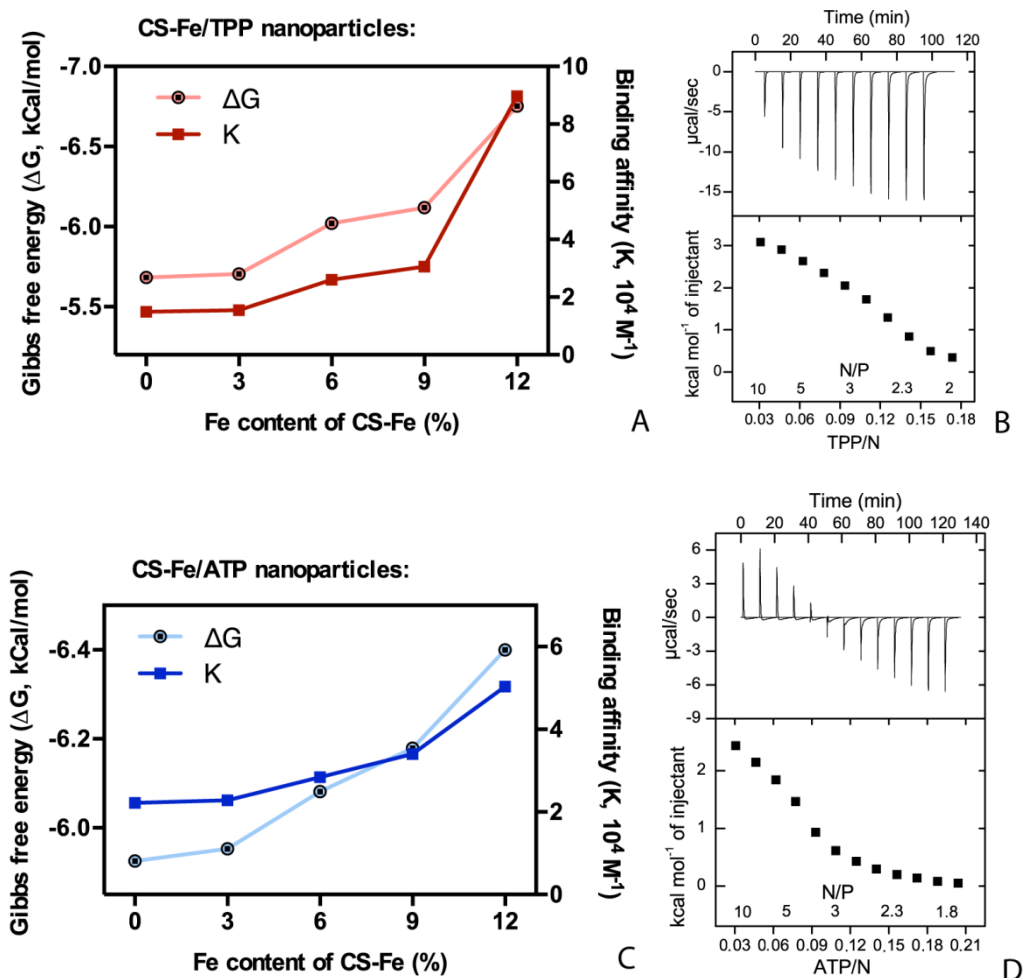


Figure 3. Isothermal titration calorimetry study of the interaction between (A, B) TPP or (C, D) ATP and CS or CS-Fe complexes containing increasing amounts of iron. (A, C) Gibbs free energy (ΔG) and binding constant (K) values as a function of the iron amount of the CS-Fe used for the formation of nanoparticles. (B, D) Typical titration curves showing the heat flow plotted against time (top) where a peak of power can be seen for each injection, and integrated heat plotted against CS-monomer to triphosphate-derivative ratio (also shown as N/P ratio) (bottom).

3.3. Characterization of CS-Fe/TPP and CS-Fe/ATP nanoparticles

Nanoparticles have been characterized as a function of TPP or ATP amounts added to the various CS-Fe complexes. The evolution of nanoparticle size and surface charge as a function of the N/P ratio (Figure S1 and S2) shows the same general pattern compared to CS [7], with a decrease in size and

zeta potential until a critical N/P ratio is reached. The critical N/P ratio is lower for ATP than TPP, which correlates to an additional negative charge on TPP available for complexation with CS. For both ATP and TPP, CS-Fe_{3%} shows a behavior close to CS, while a general trend of a decrease in size with higher iron content of the CS-Fe complexes can be observed, especially for TPP. This may be explained by a denser condensation of nanoparticles in presence of iron and the involvement of iron in the association of triphosphate derivatives to the CS-Fe complexes [24]. In the following, nanoparticles will be used at the critical N/P ratio, which corresponds to the smallest and most homogenous nanoparticle size (Table 1).

	Critical N/P		Size (nm)		Zeta potential (mV)		Association efficiency (%)	
	TPP	ATP	TPP	ATP	TPP	ATP	TPP	ATP
CS (data from ch. 1)	1.41	1.02	172 ± 25	156 ± 53	27.9 ± 2.5	22.7 ± 3.5	--	64 ± 5
CS-Fe _{3%}	2.2 ± 0.2	1 ± 0.2	567 ± 62	202 ± 28	36.8 ± 0.7	24.7 ± 1.1	--	61 ± 5
CS-Fe _{6%}	2.5 ± 0.2	1 ± 0.2	318 ± 8	131 ± 2	29.1 ± 0.8	22.1 ± 0.9	--	70 ± 3
CS-Fe _{9%}	2.5 ± 0.3	1.2 ± 0.1	329 ± 60	148 ± 1	21.8 ± 0.7	25.4 ± 0.2	--	73 ± 2
CS-Fe _{12%}	2.8 ± 0.2	1.2 ± 0.1	309 ± 33	134 ± 2	25 ± 0.5	20.2 ± 0.5	--	81 ± 1

Table 1. Average size and zeta potential of nanoparticles prepared from TPP or ATP and various CS-Fe complexes at the corresponding critical N/P ratio, and ATP association efficiency to CS-Fe/ATP nanoparticles.

Concerning zeta potential, the same trend in all the formulations can be seen. A tendency of shifting the critical N/P towards higher values is observed for CS-Fe_{12%} with TPP.

CS/TPP nanoparticles are useful carriers which can be loaded with several drugs and proteins. Nevertheless, the direct use of triphosphate group-containing drugs such as ATP in place of TPP can bring the advantage of having a carrier already containing the active pharmaceutical ingredient. For this reason, the ATP content of CS-Fe/ATP nanoparticles has been investigated as well. Association efficiency was calculated as the amount of associated ATP divided by total ATP. The association efficiency of ATP was found to increase with the iron content, reaching around 80% for CS-Fe_{12%} (Table 1).

The morphology of nanoparticles was investigated by transmission electron microscopy (TEM). For this purpose, CS-Fe_{12%}/ATP nanoparticles were imaged compared to CS/ATP. TEM images confirmed

the size of ATP-nanoparticles (Figure 4). In the case of iron-containing nanoparticles a stronger signal can be observed, confirming the presence of electron-rich iron atoms in these nanoparticles.

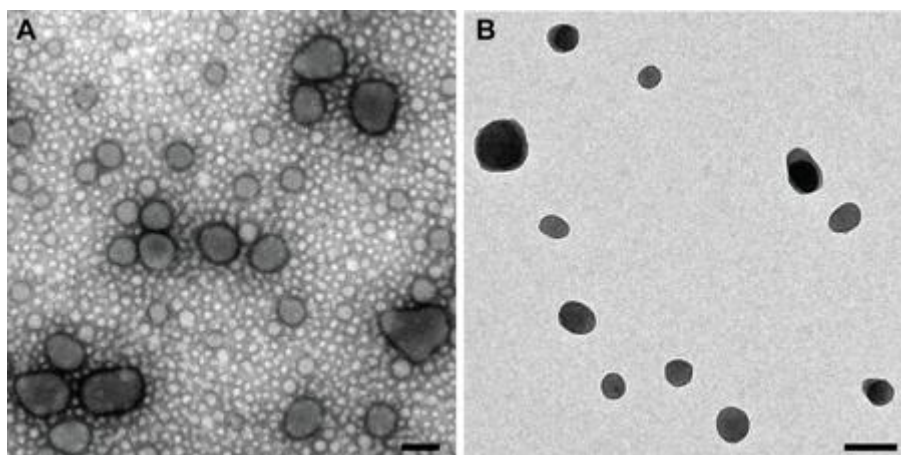


Figure 4. Transmission electron microscopy images of (A) CS/ATP and (B) CS-Fe_{12%}/ATP nanoparticles (scale bars = 100 nm).

3.4. Nanoparticle behavior in physiological media

The effective role of the iron in the stability of CS-Fe nanoparticles in physiological conditions was assessed in media containing increasing sodium chloride concentrations, up to 1% w/v (isotonic conditions correspond to 150 mM or 0.9% w/v). The measurement of the turbidity of the resulting suspensions was first investigated (Figure 5) through the use of UV-Vis spectroscopy [25].

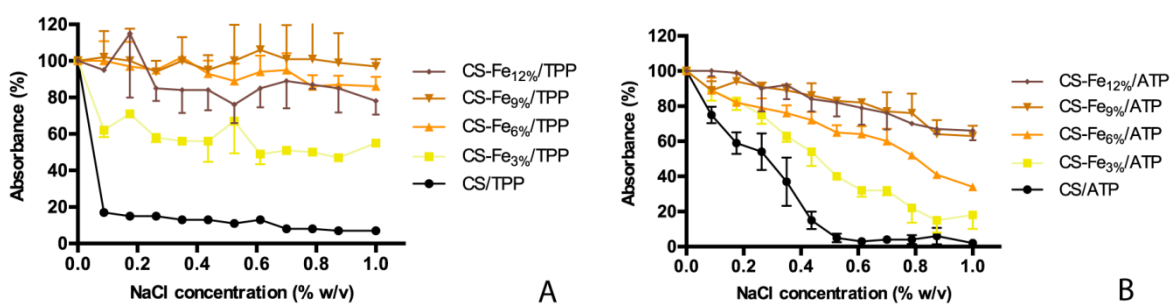


Figure 5. Stability of nanoparticles prepared from CS or CS-Fe complexes and (A) TPP or (B) ATP, assessed in NaCl solutions of increasing concentration by measurement of the turbidity of the resulting suspensions (100% value set in absence of NaCl).

The results confirmed that CS/TPP nanoparticles readily dissociate even at low ionic strength, as shown by the drop in turbidity. This is true also for CS/ATP, although at higher values. However,

nanoparticle stability was found to clearly increase when using CS-Fe complexes with increasing iron content, either in the case of TPP or ATP. For complexes containing the highest amounts of iron, the turbidity was found to retain between 80 and 100% (TPP nanoparticles) and around 70% (ATP nanoparticles) of its initial value, even at 1% w/v NaCl. The ionic bond between CS and phosphate therefore appears displaced by the medium ions in the case of CS nanoparticles, whereas in the case of CS-Fe nanoparticles, more stable interactions result in an increased resistance to ionic strength.

The stability of ATP nanocarriers was also studied from a dynamic point of view. Nanoparticles containing fluorescent ATP were monitored in a small volume by fluorescence fluctuation microscopy before, during and after addition of NaCl, as described in the Materials and methods section. Fluorescence fluctuation was shown to be a relevant method to study siRNA release from nanoparticles [26]; the present setup further allows to follow this dynamics upon dilution with an electrolyte, thus mimicking an injection into the bloodstream.

As shown in Figure 6, in the case of CS/ATP nanoparticles, the addition of NaCl resulted in the decrease of nanoparticle number (disappearance of peaks) together with an increase of released ATP, i.e. free ATP in solution (increase of the baseline fluorescence), which was gradually observed over 60 min. The use of CS-Fe_{3%} significantly slowed down this release by half over the same time interval, while the signal of nanoparticles based on CS-Fe_{6%}, CS-Fe_{9%} and CS-Fe_{12%} remains virtually unchanged over the time of the experiment.

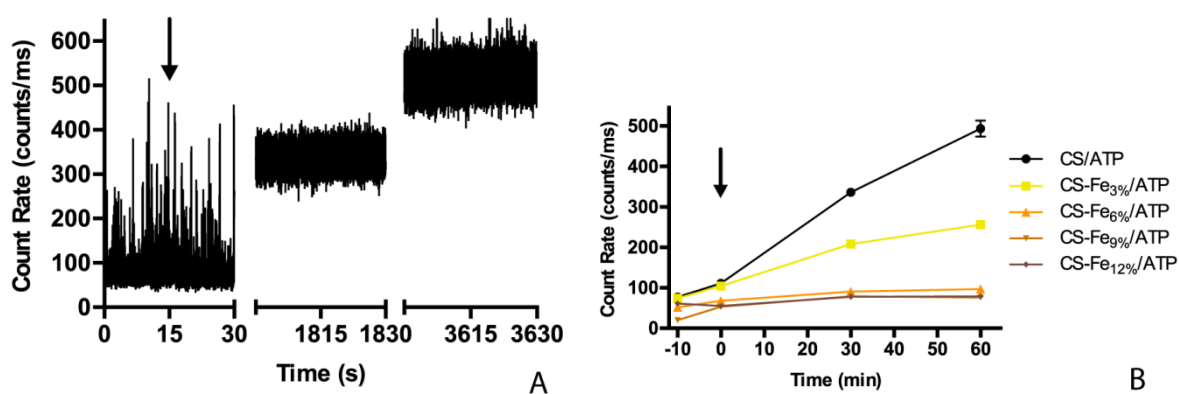


Figure 6. (A) Typical pattern of CS/ATP nanoparticle dissociation (disappearance of fluorescence peaks) and ATP release (increase of fluorescence baseline), followed by fluorescence fluctuation spectroscopy using BODIPY-ATP, upon dilution by NaCl (arrow). Measurements are made during 30 s intervals before NaCl addition, during addition, 30 min and 60 min afterwards. (B) Summary and comparison of various CS-Fe-based nanoparticles (arrow indicates NaCl addition).

3.5. *In vitro* toxicity and uptake

CS-Fe-based nanoparticles' potential as drug carriers was studied using ATP for its relevant pharmacological activity to circumvent hypoxia in ATP-depleted macrophages. In fact, atherosclerotic plaques might become hypoxic, due to the increasing distance for the oxygen to diffuse inside [17]. If ATP is not supplied, this could lead to macrophages death, and could eventually turn out into the formation of a necrotic core [27]. Macrophages are the most present cells in the core of advanced plaques. THP-1 macrophages were used mainly because of the possibility of running nanoparticle uptake kinetics experiments on the long term and also because they come from human monocytes. As a control, J774A.1 macrophages were utilized because they have been used by many groups to investigate the effect of hypoxia on ATP depletion [28], and we wanted to correlate cell interaction on both types of cells.

a. Viability evaluation

Before studying the fate of nanoparticles in contact with cells, it was important to establish the adequate concentrations to work with in order not to create any toxicity effect. Both cell lines were therefore incubated for 24 hours with the different kinds of ATP nanoparticles diluted at different ratios.

On J774A.1 cells, particles do not show any toxicity in terms of mitochondrial activity for concentrations up to 0.6 mg/mL, which correspond to 0.28 mg/ml ATP (0.56 mM) (Figure 7 A). In the case of THP-1 cells, a slight viability decrease can be seen for higher concentrations, which is however not correlated to the iron content (Figure 7 B). On both cell lines, the same general trend for all the nanoparticles can be seen, regardless of their iron content.

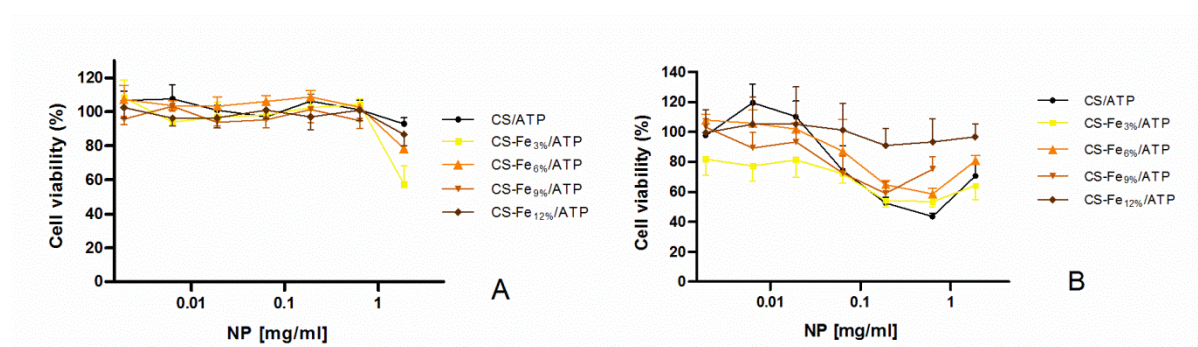


Figure 7. Viability of (A) J774A.1 and (B) THP-1 macrophages after 24 h incubation with nanoparticles prepared from ATP and CS or various CS-Fe complexes. Viability was determined by MTT test as a function of nanoparticle concentration.

Furthermore, the potential of these iron-containing nanoparticles to induce oxidative stress was evaluated on THP-1 cells, using an intracellular probe and hydrogen peroxide as positive control. The nanoparticle concentration used was 0.07 mg/mL, to maintain a good cellular viability. No significant differences were found between nanoparticle-treated cells and non-treated cells, regardless of the iron content (Supplementary data, Figure S3).

b. Uptake quantification

The uptake of ATP delivered by nanoparticles prepared with the different CS-Fe complexes was evaluated over 2 h on J774A.1 cells, and compared to that of free ATP in solution (Figure 8 A). The nanoparticle concentration used was 0.17 mg/ml, as a safe concentration determined through MTT test. While CS/ATP nanoparticles already increase ATP delivery, this increase is much more pronounced with CS-Fe/ATP and directly correlated to the iron content of the CS-Fe. For 3% and 6% iron containing CS, the uptake is around 3-fold higher after 2 hours while for 12% iron containing CS it is around 5-fold higher than free ATP.

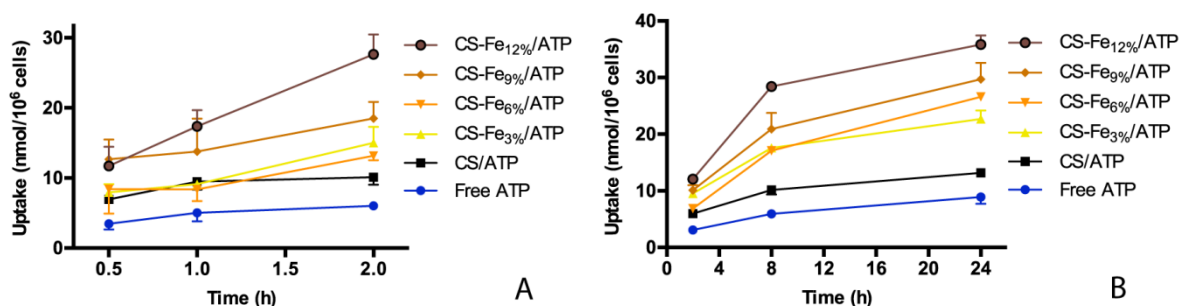


Figure 8. Kinetics of ATP uptake delivered as free molecule, CS/ATP or CS-Fe/ATP nanoparticles to (A) J774A.1 and (B) THP-1 macrophages (nanoparticle concentration = 0.17 mg/mL for A and 0.07 mg/mL for B).

In the case of the non-growing THP-1 macrophages, the kinetics was followed up to 24 hours, allowing a sustained monitoring of ATP uptake (Figure 8 B). The nanoparticle concentration used was 0.07 mg/mL, to maintain a good cellular viability. The uptake of ATP delivered by CS-Fe/ATP nanoparticles is 2 to 3 times higher than with CS/ATP and 3 to 5 times higher than free ATP. Here also, the higher the iron content, the higher the ATP uptake. For both cell lines, the mechanism suggested consists in improved nanoparticle stability, thanks to the presence of iron, allowing a larger number

of nanoparticles to cross cell membranes and reach the cytoplasm, releasing therefore greater amounts of ATP intracellularly.

c. Intracellular distribution

For both cell lines, the intracellular fate of fluorescent ATP following uptake was monitored by confocal laser microscopy (Figure 9). Nanoparticles were prepared using CS-Fe_{12%} at the concentrations determined above and compared to free ATP for up to 2 hours of contact with cells. In all cases, the fluorescence is found intracellularly, mostly in the cytoplasm. On J774A.1 macrophages, this fluorescence is clearly higher for nanoparticle-treated cells compared to ATP-treated cells and increases with incubation time. THP-1 macrophages show lower fluorescence levels, in accordance with the kinetics uptake. While almost no intracellular fluorescence is observed in the case of ATP, the treatment with nanoparticles enables a significant intracellular ATP distribution.

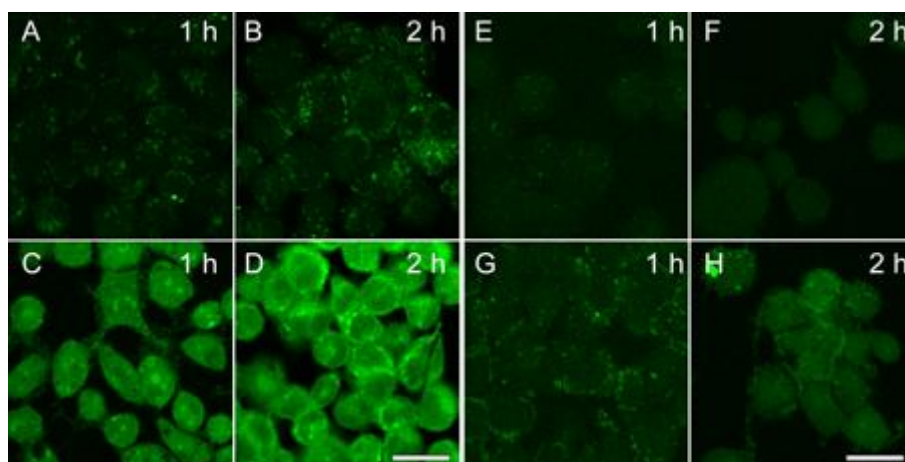


Figure 9. Intracellular distribution of ATP delivered as free molecule (A-B-E-F) or CS-Fe_{12%}/ATP nanoparticles (C-D-G-H) to J774A.1 (A to D) and THP-1 (E to H) macrophages, after 1 h and 2 h incubation, observed on a 0.8 μm thick midpoint optical slice (scale bars valid for all the pictures = 20 μm) (nanoparticle concentration = 0.17 mg/mL for A to D and 0.07 mg/mL for E to H).

4. Conclusions

CS-Fe complexes have been prepared in a way which allows the control of the amount of bound iron. After the CS-Fe obtaining, nanoparticle preparation method is unmodified in comparison to iron-free

nanoparticles. This way, drug payload and association efficiency of ATP are unchanged or even improved, and the process of nanoparticle formation remains very simple and fast, without requiring the use of solvents or chemical cross-linkers. Furthermore, iron proved to have a key role in the stability of nanoparticles, consistently with the amount of iron bound to the CS. Thanks to this improvement, CS-Fe nanoparticles are capable of delivering active drugs across cell membranes, increasing the cellular uptake of ATP up to 5-fold higher than the free molecule. Moreover, the intracellular distribution of this drug was confirmed.

Acknowledgments

The authors wish to thank the Service Central d'Analyse (Solaize, France) for the elemental analysis of CS polymers, IMAGIF (CNRS, Gif-sur-Yvette, France) for the TEM images, Sandrine Lécart at Centre de Photonique BioMédicale imaging facility (Orsay, France) for the fluorescence fluctuation spectroscopy experiments, Valérie Nicolas at IPSIT-Imagerie Cellulaire (Châtenay-Malabry, France) for the confocal laser scanning microscopy. We are also grateful to Magali Noiray (UMR CNRS 8612) for the isothermal titration calorimetry experiences and Marion Quaillet for her help in the experiments.

References

- [1] Calvo, P.; Remuñán-López, C.; Vila-Jato, J. L.; Alonso, M. J., Novel hydrophilic chitosan-polyethylene oxide nanoparticles as protein carriers, *J Appl Polym Sci*, **1997**, *63*, 125-132.
- [2] Garcia-Fuentes, M.; Alonso, M. J., Chitosan-based drug nanocarriers: where do we stand?, *J Control Release*, **2012**, *161*, 496-504.
- [3] Rodrigues, S.; Dionísio, M.; López, C. R.; Grenha, A., Biocompatibility of Chitosan Carriers with Application in Drug Delivery, *J Funct Biomater*, **2012**, *3*, 615-641.
- [4] Zhang, H.; Oh, M.; Allen, C.; Kumacheva, E., Monodisperse chitosan nanoparticles for mucosal drug delivery, *Biomacromolecules*, **2004**, *5*, 2461-8.
- [5] Peng, J.; Xing, X.; Wang, K.; Tan, W.; He, X.; Huang, S., Influence of anions on the formation and properties of chitosan-DNA nanoparticles, *J Nanosci Nanotechnol*, **2005**, *5*, 713-7.
- [6] Katas, H.; Alpar, H. O., Development and characterisation of chitosan nanoparticles for siRNA delivery, *J Control Release*, **2006**, *115*, 216-25.

- [7] Giacalone, G.; Bochot, A.; Fattal, E.; Hillaireau, H., Drug-Induced Nanocarrier Assembly as a Strategy for the Cellular Delivery of Nucleotides and Nucleotide Analogues, *Biomacromolecules*, **2013**, *14*, 737-742.
- [8] López-León, T.; Carvalho, E. L.; Seijo, B.; Ortega-Vinuesa, J. L.; Bastos-González, D., Physicochemical characterization of chitosan nanoparticles: electrokinetic and stability behavior, *J Colloid Interface Sci*, **2005**, *283*, 344-51.
- [9] Leppänen, O.; Björnheden, T.; Ewaldsson, M.; Boren, J.; Wiklund, O.; Levin, M., ATP depletion in macrophages in the core of advanced rabbit atherosclerotic plaques in vivo, *Atherosclerosis*, **2006**, *188*, 323-330.
- [10] Martinet, W.; Schrijvers, D. M.; De Meyer, G. R. Y., Necrotic cell death in atherosclerosis, *Basic Research in Cardiology*, **2011**, *106*, 749-760.
- [11] Lee, G. Y.; Kim, J. H.; Oh, G. T.; Lee, B. H.; Kwon, I. C.; Kim, I. S., Molecular targeting of atherosclerotic plaques by a stabilin-2-specific peptide ligand, *J. Control. Release*, **2011**, *155*, 211-217.
- [12] Borges, O.; Borchard, G.; Verhoef, J. C.; de Sousa, A.; Junginger, H. E., Preparation of coated nanoparticles for a new mucosal vaccine delivery system, *Int J Pharm*, **2005**, *299*, 155-166.
- [13] Nasti, A.; Zaki, N. M.; de Leonardis, P.; Ungphaiboon, S.; Sansongsak, P.; Rimoli, M. G.; Tirelli, N., Chitosan/TPP and chitosan/TPP-hyaluronic acid nanoparticles: systematic optimisation of the preparative process and preliminary biological evaluation, *Pharm Res*, **2009**, *26*, 1918-30.
- [14] Schmitt, F.; Lagopoulos, L.; Kauper, P.; Rossi, N.; Busso, N.; Barge, J.; Wagnieres, G.; Laue, C.; Wandrey, C.; Juillerat-Jeanneret, L., Chitosan-based nanogels for selective delivery of photosensitizers to macrophages and improved retention in and therapy of articular joints, *J Control Release*, **2010**, *144*, 242-50.
- [15] Mi, F. L.; Sung, H. W.; Shyu, S. S.; Su, C. C.; Peng, C. K., Synthesis and characterization of biodegradable TPP/genipin co-crosslinked chitosan gel beads, *Polymer*, **2003**, *44*, 6521-6530.
- [16] Sung, H. W.; Liang, I. L.; Chen, C. N.; Huang, R. N.; Liang, H. F., Stability of a biological tissue fixed with a naturally occurring crosslinking agent (genipin), *J. Biomed. Mater. Res.*, **2001**, *55*, 538-546.
- [17] Bhatia, S. C.; Ravi, N., A magnetic study of an Fe-chitosan complex and its relevance to other biomolecules, *Biomacromolecules*, **2000**, *1*, 413-7.
- [18] Reynaud, F.; Tsapis, N.; Deyme, M.; Vasconcelos, T. G.; Gueutin, C.; Guterres, S. S.; Pohlmann, A. R.; Fattal, E., Spray-dried chitosan-metal microparticles for ciprofloxacin adsorption: Kinetic and equilibrium studies, *Soft Matter*, **2011**, *7*, 7304-7312.
- [19] Lijklema, L., Interaction of orthophosphate with iron(III) and aluminum hydroxides, *Environ Sci Technol*, **1980**, *14*, 537-541.

- [20] Spengler, K.; Follmann, H.; Boos, K. S.; Seidel, D.; Maywald, F., Characterization and extracorporeal application of a new phosphate-binding agent, *Eur J Clin Chem Clin Biochem*, **1994**, *32*, 733-9.
- [21] Fortune, W. B.; Mellon, M. G., Determination of Iron with o-Phenanthroline: A Spectrophotometric Study, *Ind Eng Chem Anal Ed*, **1938**, *10*, 60-64.
- [22] Mosmann, T., Rapid colorimetric assay for cellular growth and survival: application to proliferation and cytotoxicity assays, *J Immunol Methods*, **1983**, *65*, 55-63.
- [23] Fu, D.; Keech, P. G.; Sun, X. L.; Wren, J. C., Iron oxyhydroxide nanoparticles formed by forced hydrolysis: dependence of phase composition on solution concentration, *Phys Chem Chem Phys*, **2011**, *13*, 18523-18529.
- [24] Vinogradov, S. V.; Zeman, A. D.; Batrakova, E. V.; Kabanov, A. V., Polyplex Nanogel formulations for drug delivery of cytotoxic nucleoside analogs, *J Control Release*, **2005**, *107*, 143-157.
- [25] Elsayed, M. M.; Cevc, G., Turbidity spectroscopy for characterization of submicroscopic drug carriers, such as nanoparticles and lipid vesicles: size determination, *Pharm Res*, **2011**, *28*, 2204-22.
- [26] Buyens, K.; Lucas, B.; Raemdonck, K.; Braeckmans, K.; Vercammen, J.; Hendrix, J.; Engelborghs, Y.; De Smedt, S. C.; Sanders, N. N., A fast and sensitive method for measuring the integrity of siRNA-carrier complexes in full human serum, *J Control Release*, **2008**, *126*, 67-76.
- [27] Geiringer, E., Intimal vascularisation and atherosclerosis, *The Journal of Pathology and Bacteriology*, **1951**, *63*, 201-211.
- [28] Parathath, S.; Mick, S. L.; Feig, J. E.; Joaquin, V.; Grauer, L.; Habielski, D. M.; Gassmann, M.; Gardner, L. B.; Fisher, E. A., Hypoxia Is Present in Murine Atherosclerotic Plaques and Has Multiple Adverse Effects on Macrophage Lipid Metabolism, *Circulation Research*, **2011**, *109*, 1141-1152.

Supplementary data

CS-Fe complex	Elemental analysis	UV-Vis
"3%"	3.42	3.51
"6%"	5.86 ± 0.35	6.30 ± 0.13
"9%"	9.95 ± 0.49	9.55 ± 0.95
"12%"	12.24 ± 0.30	11.27 ± 0.49

Table S1. Iron content of selected CS-Fe complexes, as determined by elemental analysis and phenanthroline-based assay (% w/w).

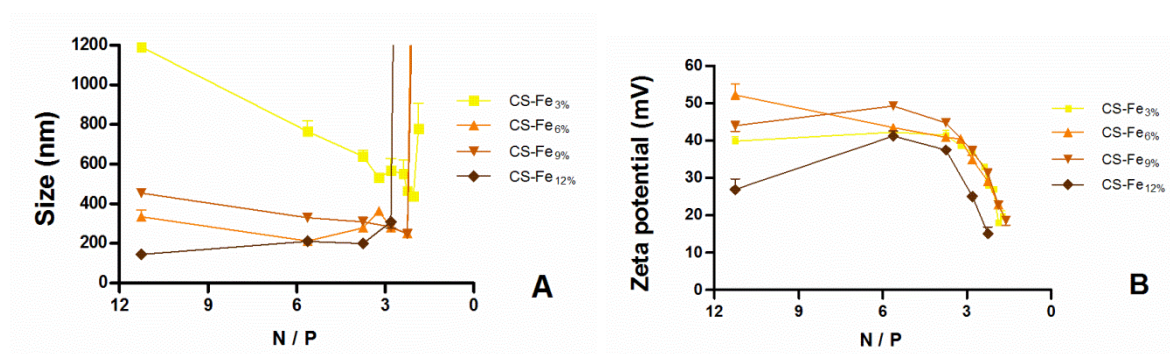


Figure S1. (A) Average hydrodynamic diameter and (B) zeta potential of nanoparticles prepared from various CS-Fe complexes and TPP, using a fixed CS concentration and increasing amounts of TPP.

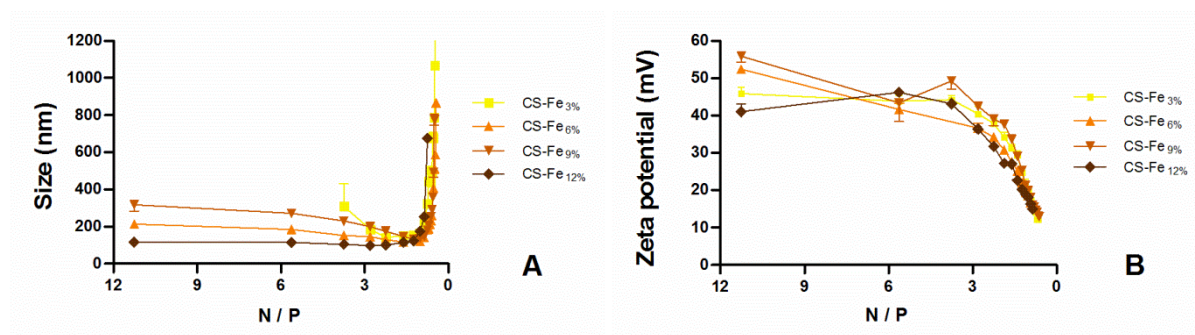


Figure S2. (A) Average hydrodynamic diameter and (B) zeta potential of nanoparticles prepared from various CS-Fe complexes and ATP, using a fixed CS concentration and increasing amounts of ATP.

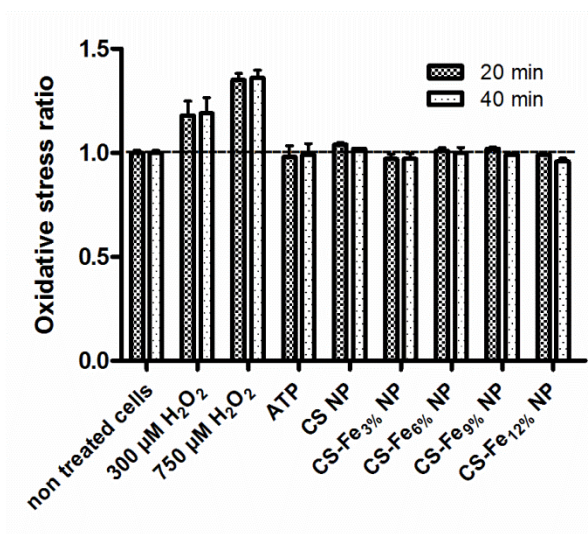


Figure S3. Assessment of oxidative stress in THP-1 macrophages after incubation with ATP, nanoparticles (NP) prepared from ATP and CS or CS-Fe complexes, and H_2O_2 used as positive control (ratio set at 1 for non-treated cells) (nanoparticle concentration = 0.07 mg/mL).

Chapitre 3

**Activité antivirale et ciblage vers les leucocytes et ganglions lymphatiques
de la zidovudine triphosphate associée à des nanoparticules de chitosane-fer**

Chapitre 3

Activité antivirale et ciblage vers les leucocytes et ganglions lymphatiques de la zidovudine triphosphate associée à des nanoparticules de chitosane-fer¹

Résumé

Dans le chapitre précédent, les nanoparticules à base de chitosane (CS) et de TPP ou ATP ont été stabilisées par ajout de fer dans leur formulation, montrant leur efficacité dans la protection et délivrance cellulaire d'ATP. Dans ce chapitre, nous décrivons l'application de ce système à la délivrance d'AZT-TP aux lieux clés de l'infection, au niveau cellulaire (leucocytes) et tissulaire (ganglions lymphatiques). Comme précédemment avec l'ATP, les nanoparticules s'assemblent par interactions ioniques entre CS-Fe et AZT-TP. Ces systèmes sont caractérisés en termes de composition, taille et charge de surface. Des études *in vitro* sur des macrophages murins et humains montrent que les nanoparticules de CS-Fe/AZT-TP n'induisent pas ou peu de toxicité et elles augmentent la capture de l'AZT-TP jusqu'à 6 fois par rapport à la molécule libre. De plus, ces nanoparticules conservent l'activité antivirale de l'AZT-TP sur des lymphocytes T, macrophages et cellules dendritiques infectés par des souches de VIH-1, sans entraîner aucune toxicité pour les cellules utilisées. En particulier, les nanoparticules bloquent *in vitro* la transmission du virus des cellules dendritiques vers les lymphocytes T, un mécanisme clé pour la conservation *in vivo* des réservoirs viraux. De plus, les nanoparticules augmentent significativement la rétention *in vivo* de l'AZT-TP dans les ganglions lymphatiques, qui est doublée 2 heures après administration sous-cutanée chez la souris, par rapport à l'AZT-TP libre. Dans l'ensemble, les nanoparticules de chitosane chargées en molécules antivirales semblent être des nanomédicaments prometteurs pour la destruction des réservoirs du VIH-1.

¹ Les travaux décrits dans ce chapitre ont été conduits par les auteurs suivants :
Institut Galien Paris-Sud : Giovanna Giacalone, Andrey Maksimenko, Hervé Hillaireau, Elias Fattal
Institut Pasteur Paris : Héra Saïdi, Marie-Lise Gougeon

Antiviral activity, leukocyte and lymph node delivery of zidovudine triphosphate loaded in chitosan-iron nanoparticles¹

Abstract

In the previous chapter, chitosan (CS) and TPP or ATP nanoparticles have been stabilized by the incorporation of iron, showing their efficacy in ATP protection and cellular delivery. In this chapter, we describe the application of this system to the delivery of AZT-TP to key sites of the infection at the cellular level (leukocytes) and tissular level (lymph nodes). As previously with ATP, nanoparticles assemble through ionic interactions between CS-Fe and AZT-TP. These systems are characterized in terms of composition, size and surface charge. *In vitro* studies on murine and human macrophages show that CS-Fe/AZT-TP nanoparticles induce no or low toxicity and increase the AZT-TP uptake by up to 6-fold compared to the free molecule. Furthermore, these nanoparticles retained the antiviral activity of AZT-TP, thus inhibiting HIV replication in the main targets of HIV-1 (T cells, macrophages and dendritic cells). Notably, these nanoparticles blocked the transmission of the virus from dendritic cells towards T cells, a key mechanism sustaining *in vivo* the viral persistence. Nanoparticles also significantly increased by 2 fold the *in vivo* retention of AZT-TP in lymph nodes 2 hours after subcutaneous administration to mice. Overall, anti-microbial loaded chitosan nanoparticles appeared to be promising nanomedicines for the destruction of HIV-1 reservoirs.

¹The work described in this chapter was carried out by the following authors:
Institut Galien Paris-Sud: Giovanna Giacalone, Andrey Maksimenko, Hervé Hillaireau, Elias Fattal
Institut Pasteur Paris: H la Saïdi, Marie-Lise Gougeon

1. Introduction

Nucleoside reverse transcriptase inhibitors (NRTIs) are the first drugs discovered and introduced in the treatment of HIV/AIDS. They remain a cornerstone of current highly active antiretroviral therapy (HAART) in association with protease inhibitors (PI) and non-nucleoside reverse transcriptase inhibitor [1]. It is indeed important to include in the therapy a drug that can act at the viral DNA synthesis level by competing with natural nucleosides, in order to target the virus at its different stages. Among the NRTIs, zidovudine (AZT) was the first drug introduced in the anti-HIV therapy, and therefore the one with most clinical data available.

Nevertheless, NRTIs present two main limitations. First, like many drugs, their biodistribution lacks specificity. This can be due to several reasons such as the physicochemical properties of the molecules, protein-binding or metabolization [2]. The concentration of antiretroviral drugs is considerably lower in viral reservoirs like macrophages [3, 4] or viral sanctuaries like lymph nodes [5, 6].

The second drawback of this class of drugs is their limited intracellular activation. Once in the cell cytoplasm, NRTIs need to be triphosphorylated by cellular kinases into their active form. However this conversion can be limited by the poor recognition between the enzymes and the drug, leading to very low portions of the administered drug being in its active form [7, 8]. The administration of the active triphosphate form of NRTIs would bypass this bottleneck, but this approach is made difficult by the chemical instability of the molecule in the physiological environment, and its poor penetration through membranes due to its hydrophilic and charged character. In order to make this strategy possible, there is the need of protecting the molecule and facilitating its membrane crossing.

A solution to this double difficulty was provided by the application of nanotechnology. On the one hand, in order to deliver NRTIs to reservoirs and sanctuaries, polyalkylcyanoacrylate nanoparticles and liposomes have been reported as nanocarriers of AZT [9-11] and ddI [12-14] to the organs of the mononuclear phagocyte system. On the other hand, few studies report the encapsulation of triphosphate forms of NRTIs such as AZT-TP in nanocarriers (PEI nanogels [15], PIBCA nanoparticles [16] or iron carboxylates metal-organic frameworks [17]) in order to protect the triphosphate molecule and enable *in vitro* its uptake by cells. However, few attempts have been made addressing these two challenges, i.e. delivering triphosphate forms of NRTIs *in vivo* to the mononuclear phagocyte system [18, 19].

Recently, we developed a simple strategy to deliver stable ATP nanoparticles taking advantage of its ionic interactions with the iron-modified natural polysaccharide chitosan (CS-Fe) (Chapter 2). The choice of chitosan, a natural polymer, is due to its immunogenicity and its anti-microbial properties [20]. The cationic surface of chitosan is expected to contribute to its superior targeting efficacy to

negatively charged cells. Interestingly, the choice of chitosan-based nanoparticles for the design of a novel drug delivery system is due to their hydrophilic character that facilitates the administration of poorly absorbable drugs across various epithelial barriers. Moreover, the polycationic nature of chitosan is expected to favor deposition of the complement proteins on the nanoparticles, resulting in their better uptake by the macrophages through complement receptors [21]. Since macrophages serve as HIV-1 reservoirs, efficient drug delivery to these cells via chitosan could be an advantage. T cells and dendritic cells (DCs) constitute additional HIV-1 reservoirs. Notably, virus transfer from dendritic cells to T cells was shown to sustain viral persistence [22].

In this study, we investigate the association of AZT-TP to CS-Fe into nanoparticles, the ability of such nanoparticles to deliver AZT-TP to murine and human macrophages, their antiviral activity on HIV-infected primary human T cells, macrophages and DCs, their impact on HIV transfer from DCs to T cells, and finally their *in vivo* effect on AZT-TP accumulation in lymph nodes after subcutaneous administration to mice.

2. Materials and methods

2.1. Nanoparticle preparation

CS-Fe complexes were first prepared as described above [23]. Briefly, iron nitrate (Sigma) was dissolved in water with chitosan (low viscosity, 95% deacetylated, Fluka) (10 mg/mL, pH = 1.5) and the complex was allowed to form overnight under mechanical stirring. The complex was washed from free iron through the precipitation with acetone, until the filtrate was completely free from iron. CS-Fe was then dried paying attention to the formation of films which should be avoided. Different complexation conditions were used in order to achieve different degrees of binding between chitosan and iron (CS-Fe_{3%} 0.5 M iron nitrate, CS-Fe_{6%} 0.1 M iron nitrate, CS-Fe_{9%} 0.1 M iron nitrate stirring 2 days, CS-Fe_{12%} smaller scale).

Nanoparticle formation was then assessed by slow addition of a 27 mM AZT-TP (Chemcyte, Inc., San Diego, USA) solution to a 1 mg/mL CS-Fe solution under magnetic stirring (1000 rpm). For radioactivity studies, AZT-TP nanoparticles were formed from a 27 mM AZT-TP solution prepared using [methyl-³H]-AZT-TP (Perkin Elmer, France) as a tracer, by diluting the commercial 10 mCi/mL (25 mM) with appropriate amount of unlabelled AZT-TP solution.

For *in vitro* studies, nanoparticles were prepared by adding a 27 mM AZT-TP solution to 3 mL of CS-Fe under magnetic stirring. They have been purified from free AZT-TP and CS by centrifugation at 750 × g on a glycerol bed, the supernatant has been discharged and the pellet has been re-suspended. For

storage purposes, nanoparticles have been freeze-dried by adding trehalose at the final 10% w/v concentration. The suspension has been frozen in liquid nitrogen and freeze-dried at -55 °C and 0.01 mbar for 24 hours using a Christ Alpha 1-2 LD Plus.

2.2. Nanoparticle characterization

The mean size of nanoparticles was determined using photon correlation spectroscopy (PCS), with a 173° scattering angle at a temperature of 25°C, and their zeta potential was determined after 1/20 sample dilution in 1 mM NaCl solution, using a Zetasizer MAL 500180 (Malvern Instrument, UK).

In order to determine the amount of AZT-TP associated to the nanoparticles, their composition was studied using [methyl-³H]-AZT-TP (final concentration 1 µCi/mL). Nanoparticles were prepared as described above using 4 different CS-Fe complexes. They were centrifuged at 17000 × g for 1 hour in order to separate them from free AZT-TP. Both pellets and supernatants were then analyzed to determine their radioactivity content using a Beckman Coulter instrument (LS 6500 Multi-Purpose Scintillation Counter). The AZT-TP association efficiency was calculated as the ratio of the pellet radioactivity to the total (pellet + supernatant) radioactivity. The drug loading of nanoparticles was expressed as the ratio of the nanoparticle-associated drug weight to the nanoparticle (drug + CS) weight.

2.3. Cell culture and viability assessment on non-infected cells

J774A.1 mouse macrophages (from ECACC, catalogue number 91051511) and THP-1 human acute monocytic leukemia cells (from ATCC, catalogue number TIB-202) were grown in RPMI 1640 medium (BE 12-702 F, Lonza) supplemented with 10% (v/v) fetal bovine serum (Lonza) (heat-inactivated in the case of J774.A1), penicillin (100 UI/mL) and streptomycin (100 µg/mL). Cells were maintained in a humidified incubator with 95% air/5% CO₂ at 37° C. Cells were used from passage 3 to 20 (J774A.1) or 12 (THP-1) after thawing. THP-1 – derived macrophages were obtained by incubation of THP-1 monocytes with 10⁻⁸ M phorbol 12-myristate 13-acetate (PMA) for 24 hours and subsequent incubation with fresh medium, before running the experiment.

The cytotoxicity of nanoparticles towards both cell lines was determined using an MTT assay [24]. Cells were recovered from flasks, counted with Neubauer chamber and diluted to needed concentration, to be seeded in a 96-well plate at a density of 30,000 cells/well for J774A.1 and 60,000 for THP-1. They were pre-incubated for 24 hours. Nanoparticles were prepared and purified,

diluted at different concentrations in cell culture medium and then incubated with cells for 24 h. Supernatants were then withdrawn and a solution of 0.5 mg/mL MTT in medium was added. After 2 h incubation, supernatant was removed and DMSO was added to dissolve formazan crystals. Plates were stirred a few minutes and absorbance measurement were run at $\lambda = 570$ nm, using a Labsystems Multiskan MS plate reader. The cytotoxicity of CS-Fe solutions at a concentration equivalent to the highest nanoparticle concentration was determined as well for comparison.

2.4. Cellular uptake studies

Nanoparticles containing [methyl-³H]-AZT-TP were prepared and purified as described above then diluted 1:10 in cell culture medium (in order to maintain cell viability above 80% as determined by MTT tests), so to have 70 nCi/well. A control solution of AZT-TP at the same final radioactivity concentration was used for comparison.

Cells were recovered from the culture flasks, counted and seeded in 6-well plates, at a surface density of 800,000 cells/well for J774A.1 and 160,000 for THP-1 using 2 mL medium per well. After 24 h incubation, the medium was withdrawn and 2 mL of AZT-TP nanoparticles or free AZT-TP were added in each well. Nanoparticles and AZT-TP were incubated with cells for 2 and 8 hours, after which the uptake was stopped by removing the cell culture medium. The cells were washed twice with PBS (Lonza) to remove loosely bound compounds and then lysed with 1 mL Solvable (Perkin-Elmer, France). The radioactivity of the supernatant medium, the washing supernatants and the cell lysate were counted. The uptake kinetics of nanoparticle AZT-TP was studied for 2 and 8 hours and compared to that of free AZT-TP.

2.5. Production of HIV viral stock

CCR5-tropic HIV-1Ba-L was amplified in Peripheral Blood Mononuclear Cells (PBMCs) of healthy donors. HIV-1 concentration was quantified in cell culture supernatants by means of the DuPont HIV-p24 antigen ELISA (HIV-1 core profile ELISA; DuPont de Nemours, Les Ulis, France). For screening experiments, a volume of PV stock diluted to a concentration ultimately resulting in a signal of 1×10^5 RLU was used [25].

2.6. *In vitro differentiation of monocyte-derived dendritic cells (DCs) and macrophages*

PBMCs were separated from the blood of healthy adult donors on a Ficoll-Hypaque density gradient. Blood was obtained through the EFS (Etablissement Français du Sang) in the setting of EFS-Institut Pasteur Convention. A written informed consent was obtained for each donor to use the cells for clinical research according to French laws. Our study was approved by IRB, external (EFS Board) as required by French law and internal (Biomedical Research Committee Board, Institut Pasteur). Monocytes were isolated from fresh PBMCs using the Monocyte Negative Isolation Kit (StemCell Technologies) according to the manufacturer's protocol. The enriched cells were assessed for more than 90% purity using the following antibodies: anti-CD14-FITC (Miltenyi Biotec) and anti-CD3-APC (Becton Dickinson-Pharmingen). Monocytes were differentiated to dendritic cells using 10 ng/ml rhGM-CSF (Peprotech) in combination with rhIL-4 (10 ng/ml). Macrophages were differentiated from monocytes using 10 ng/ml of rhM-CSF (Peprotech). After 6 days of culture, flow cytometry analysis demonstrated that CD14^{neg} DC-SIGN⁺ DCs and CD209⁺ macrophages were more than 90% pure.

2.7. *Purification of autologous T lymphocytes*

Peripheral blood lymphocytes (PBL) were subsequently prepared from the monocyte-depleted fraction (>90% CD3⁺ T cells and <1% monocytes, as assessed by flow cytometry). PBL were stimulated for 48 hours in fresh medium supplemented with PHA (2.5 µg/ml) and rhIL-2 (1 µg/ml) and were further cultured with rhIL-2 (1 µg/ml) for 24 hours.

2.8. *HIV-1 entry into primary cells*

In this series of experiments, CS-Fe_{12%}/TPP (Sigma) nanoparticles have been prepared as well as a control ("empty nanoparticles", E-NP). These nanoparticles are similar to CS-Fe_{12%}/AZT-TP in terms of size and composition. They only differ in that AZT-TP is replaced by the inactive triphosphate moiety of AZT-TP (i.e. tripolyphosphate, TPP). CS-Fe_{12%}/TPP nanoparticles are purified and freeze-dried in a similar way as described for AZT-TP nanoparticles. As controls, AZT and AZT-TP solutions at corresponding concentrations have been prepared as well. To assess the entry of HIV-1 into T cells, macrophages and DCs, the cells were washed twice after 6 days of activation/differentiation and seeded into 96-well culture plates (1 × 10⁵ cells/well). HIV-1 (1 ng p24 antigen) and increasing doses of the molecules to be tested were added on indicated cell subsets in triplicate and incubated for 1 h

at 37°C in a 5% CO₂ atmosphere. After 4 washes to remove the unattached virus, cells were lysed by incubation for 45 min at 37°C with 1% Triton X-100. Cell lysates were harvested and centrifuged at 1,800 rpm for 5 min. The amount of cell-associated HIV-1 was evaluated using the p24 antigen capture ELISA.

2.9. Inhibition of HIV-1 infection in T cells, DCs or macrophages

After 6 days of activation or differentiation, cells were washed twice and seeded into 96-well culture plates (25×10^5 cells/well). HIV-1 (1 ng p24 antigen/ml) and increasing concentrations of molecules to be tested were added on indicated cell subsets in triplicate and incubated for 3 h at 37°C in a 5% CO₂ atmosphere. After 4 washes to remove exceeding virus, cells were cultured for 6 days. The level of virus replication was monitored by HIV-1 p24 antigen ELISA. Supernatants were harvested and virus particles were lysed by incubation for 45 min at 37°C with 1% Triton X-100.

2.10. DCs-mediated infection of autologous T cells

To assess the transmission of HIV-1 from DCs to autologous T-cells, DCs were incubated into 96-well culture plates (1×10^5 cells/well) and infected with HIV-1 (1 ng p24 antigen) for 3 h at 37°C in a 5% CO₂ atmosphere. Following four washes, DCs were shortly incubated with increasing concentrations of indicated molecules or AZT (2 μM), and autologous stimulated T cells were added onto HIV-exposed DCs at DC:T-cell ratio of 1:5. Cells were cultured for 6 days. Each sample was performed in triplicate. Culture supernatants were harvested every 3 days and fresh medium with compounds was added. Supernatants were inactivated with 1% Triton X-100 and frozen at -20°C. Viral production by T lymphocytes was evaluated at the sixth day of the co-culture by measurement of p24 antigen in supernatants using capture ELISA.

2.11. Quantification of the frequency of infected cells

Following six days of infection, the frequency of HIV-1-infected cells was determined by flow cytometry to detect intracellular p24 molecule. Cells were surface-stained with antibodies specific for CD3 (BD Biosciences, San Jose, CA) to target T cells or CD206, HLA-DR and CCR5 (BD Biosciences, San

Jose, CA) to target macrophages, and intracellularly stained with p24-specific antibody (Coulter). Stained cells were immediately acquired on a FACScalibur (Becton Dickinson) and analyzed with FlowJo software.

2.12. Apoptosis measurement

Cell survival was determined with the 7-AAD assay, as described previously [26]. Briefly, cultured cells were stained with 20 $\mu\text{g}/\text{mL}$ nuclear dye 7-amino-actinomycin D (7-AAD; Sigma-Aldrich) for 30 minutes at 4°C. Surviving cells were identified as 7-AAD^{neg}.

2.13. Animals

6- to 8-week-old NIH Swiss Outbred female mice were purchased from Harlan Laboratory (UK). All animals were housed in appropriate animal care facilities during the experimental period, with free access to food and water, and were handled according to the principles of laboratory animal care and legislation in practice in France. All *in vivo* studies were performed in accordance with a protocol submitted to the local Ethical Committee (registered with the French Ministry of Research).

2.14. Subcutaneous administration and dosage in lymph nodes

The systemic toxicity of the tested nanoparticles was first investigated and compared to those of free AZT-TP and CS-Fe_{12%} complex after single injection into the hock of healthy mice. Noteworthy, the injected dose of nanoparticles containing AZT-TP was limited by the maximum concentration of nanoparticles possible in suspension and the maximum volume able to be injected, both corresponding to an AZT-TP equivalent dose of 1.3 mg/kg. Whatever the dosing protocol, any toxicity of tested nanoparticles was observed. We therefore used this protocol to evaluate the nanoparticle biodistribution in mice. Practically, 1 mM [methyl-³H]-AZT-TP solution and [methyl-³H]-AZT-TP nanoparticle suspension at the corresponding AZT-TP concentration were prepared as described above. Both formulations were prepared at 20 $\mu\text{Ci}/\text{mL}$ and each mouse received 50 μL , i.e. 1 μCi . For all the injections, a 26-gauge needle was used. 10 minutes before administrations, mice were anesthetized with an intraperitoneal injection of a mixture 10:1 of ketamine/xylazine at 90 mg/kg. The mice were randomly divided into 2 groups of 12 each and all groups received a single injection

into the hock with either (i) [methyl-³H]-AZT-TP solution or (ii) nanoparticles containing [methyl-³H]-AZT-TP. The injected volume was 50 μ L. 2 or 4 hours after injection into the hock, mice (n=6 at each time point) were sacrificed and inguinal and axillary right and left lymph nodes were collected. Samples were then dissolved by addition of 1 ml of Solvable and overnight incubation at 50 °C. Subsequently, they were bleached using hydrogen peroxide (30% w/w, Sigma) and their radioactivity content was determined by scintillation counting. Statistical analyses were performed using T-test and Two-way ANOVA test.

To visualize the lymph nodes, mice were anesthetized with 2.5% isoflurane, and dye (*i.e.*, blue trypan, 0.4%) was injected subcutaneously into the inguinal right lymph node, with the needle pointed in a rostral direction. The injection site should bleb lightly, before the dye is slowly taken up by lymphatic vessels. After 5 to 15 minutes of continuous anesthesia to allow the dye to travel through lymphatics, mice were euthanized with CO₂. The blue-labeled inguinal and axillary lymph nodes were easily located and imaged.

2.15. Statistical analysis

The non-parametric Wilcoxon signed-rank and T-test were used for statistical analysis of *in vitro* studies. A p-value <0.05 was considered significant. The two-way ANOVA and the T-test were used for statistical analysis of *in vivo* studies.

3. Results and discussion

3.1. Nanoparticle formation from CS-Fe and AZT-TP

In the previous chapter, the formulation and application of CS-Fe_{12%}/ATP nanoparticles have been described. These drug delivery systems acted as nucleotide nanocarriers, owning colloidal stability properties in physiological conditions which would allow to administer such a fragile molecule like ATP. *In vitro* uptake studies clearly demonstrated its intracellular delivery to macrophages. Therefore, in this chapter we wanted to investigate the substitution of ATP with the antiretroviral active molecule AZT-TP.

The formation of nanoparticles from CS-Fe complexes and AZT-TP has been investigated at various ratios between the two components, expressed as N/P (N: nitrogen concentration in chitosan solutions; P: phosphorus concentration in AZT-TP solutions). Four CS-Fe complexes have been used,

containing respectively 3, 6, 9 and 12% of iron out of the total mass of the complex, which were synthesized as described previously (Chapter 2). For all formulations, the nanoparticle formation region was determined as occurring above a critical N/P ratio, this ratio corresponding to the N/P value at which visible aggregation occurs. The critical N/P was found to be in the range of 1.4-2.2 depending on the type of CS-Fe complex (Figure 1 A), with the following trend: the more the iron in the CS-Fe complex, the higher the critical N/P. A possible explanation is that the increased presence of iron on the amine sites of chitosan might at some extent limit the access to the phosphate groups for complexation, therefore leading to aggregation at higher N/P. Similar results have been found for CS-Fe/ATP nanoparticle formation (Chapter 2).

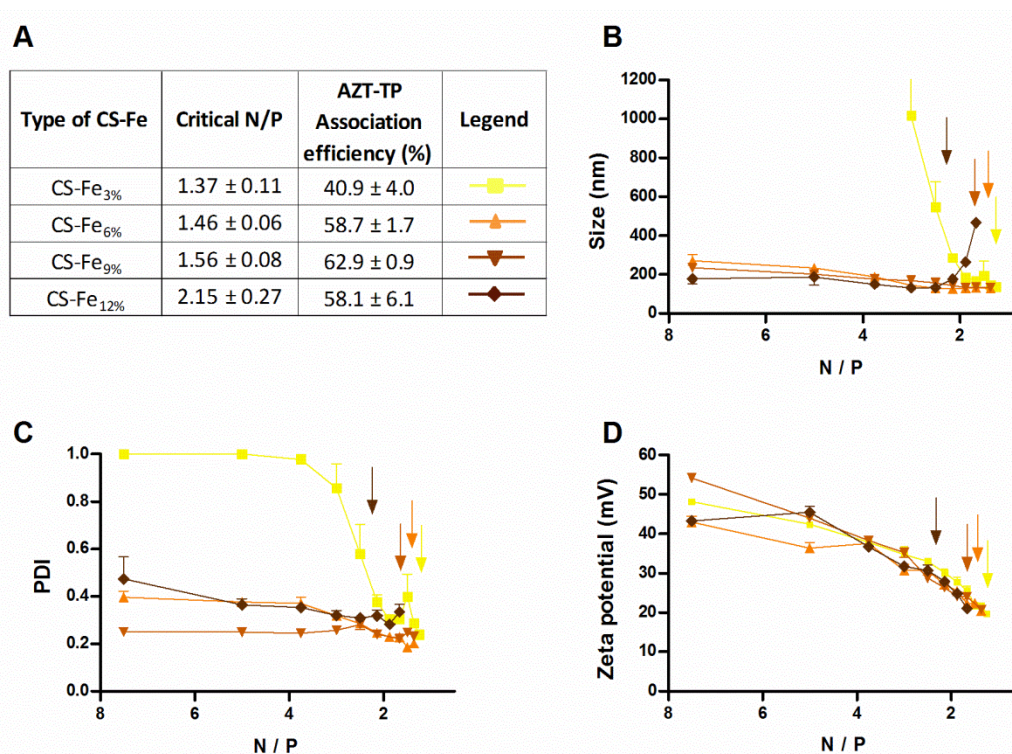


Figure 1. Nanoparticle formation from various CS-Fe complexes and AZT-TP. (a) Critical N/P ratios of nanoparticle aggregation from various CS-Fe complexes, and corresponding AZT-TP association efficiency at the critical N/P. (b) Size, (c) polydispersity index and (d) zeta potential of AZT-TP/CS-Fe formulations as a function of the N/P ratio. Arrows on (b), (c) and (d) indicate the critical N/P ratio for each CS-Fe complex.

All formulations have been further characterized in terms of particle size and polydispersity (PCS) as well as surface charge (zeta potential). The critical N/P ratios were confirmed by PCS measurements, showing a decrease in size until a minimal value around 150 nm is reached, before increasing again due to aggregation (Figure 1 B). The polydispersity index follows the same trend, decreasing down to

around 0.2 at the critical N/P, and increasing again following nanoparticle aggregation (Figure 1 C). Zeta potential is positive as expected because of chitosan charges, and it also decreases consistently with the complexation of the positive charges with the negative ones of the phosphates, down to values around +20 mV below which aggregation occurs (Figure 1 D).

For further experiments, CS-Fe/AZT-TP nanoparticles were used at the critical N/P ratio of each CS-Fe type of complex, corresponding to the smallest and most monodispersed nanoparticles and the higher AZT-TP content (lowest N/P ratio). The AZT-TP amount associated to each type of nanoparticles at this N/P ratio was determined using radioactive drug. AZT-TP encapsulation efficiency was found to increase with the iron content of CS-Fe, up to around 60% for CS-Fe_{9%} and CS-Fe_{12%}. In terms of drug loading, this corresponds to around 45% (calculated as AZT-TP weight on nanoparticle weight).

3.2. Nanoparticle toxicity and uptake by macrophages

AZT-TP nanoparticles have been tested on 2 different macrophage cell lines, murine macrophages J774A.1 and human monocyte-derived THP-1 macrophages which express the CD4 receptor [27]. The toxicity of nanoparticles was first assessed by evaluation of the viability of cells after nanoparticle exposure by an MTT test. Results show that for nanoparticle concentrations up to 0.1 mg/mL, a cell viability of 60-80% is maintained for both cell lines and all the formulations (Figure 2), without any notable trend between the CS-Fe complexes used for nanoparticle formation. Therefore, this concentration has been chosen as safe towards the cells for the next studies. Furthermore, this concentration corresponds to very high amounts of AZT-TP as compared to what is commonly used for *in vitro* studies on HIV-infected cells. The four CS-Fe complexes in solution have been tested as well, revealing a viability around 80% without any notable trend among them (data not shown).

The effect of CS-Fe/AZT-TP nanoparticles on the AZT-TP uptake by macrophages was studied on the two cell lines after up to 8 hour exposure to various formulations prepared with radioactive AZT-TP. For J774A.1 cells, the basal AZT-TP uptake is around 3 nmol per million cells when the free molecule is exposed to cells, whereas nanoparticle-encapsulated AZT-TP is internalized up to 3 times more, the CS-Fe_{12%} – based nanoparticles being the most effective ones (Figure 3 A).

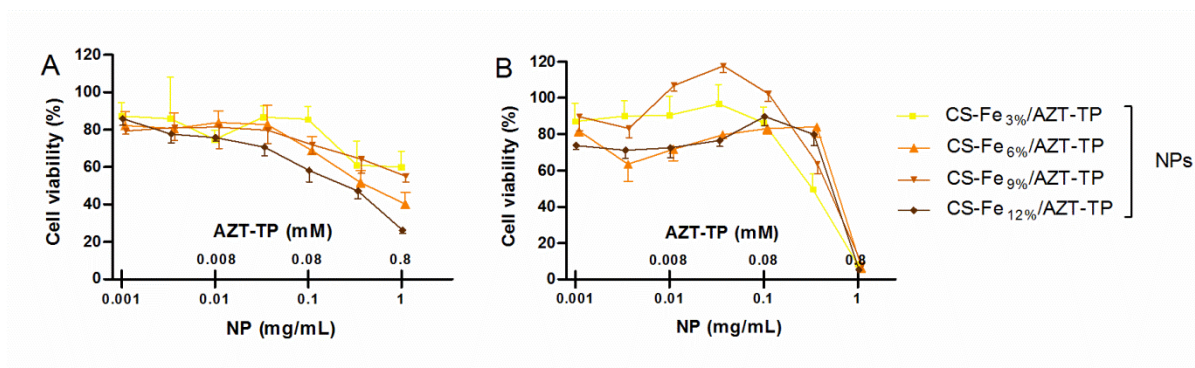


Figure 2. Effect of CS-Fe/AZT-TP nanoparticles on macrophage viability. J774A.1 (a) and THP-1 (b) viability after 24h exposition to nanoparticles (NPs) prepared from AZT-TP and various CS-Fe complexes, assessed by MTT test as a function of nanoparticle concentration (corresponding AZT-TP concentration also indicated).

For THP-1 macrophages, in which basal AZT-TP uptake is even smaller, the effect of nanoparticles is even more pronounced, especially for CS-Fe_{12%} – based nanoparticles which increased AZT-TP uptake by 5- to 6-fold compared to the free drug, reaching 12 nmol per million cells (Figure 3 B). Considering these results, nanoparticles prepared from CS-Fe_{12%} have been selected for further investigations.

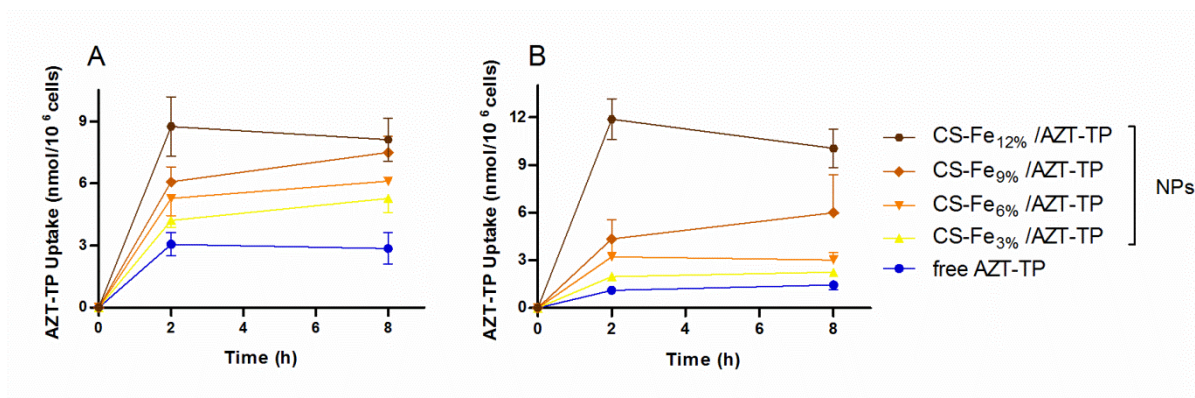


Figure 3. Effect of nanoparticles on AZT-TP uptake by macrophages. [³H]-AZT-TP uptake by (a) J774A.1 and (b) THP-1 macrophages after incubation with various CS-Fe/AZT-TP nanoparticles (NPs) or with free AZT-TP.

3.3. Inhibition of HIV-1 infection of T cells by AZT-TP nanoparticles

In the course of HIV-1 infection, T cells act as the major target for HIV-1 and constitute the primary reservoir for the virus. We therefore tested whether nanoparticles could limit the production of the virus by infected cells.

Because CCR5-tropic viruses are predominantly transmitted *in vivo* [28], T cells were infected for 3 h with the R5 subtype B strain BaL and further cultured either alone (non-treated) or in the presence of free AZT, CS-Fe_{12%}/TPP nanoparticles (E-NP), AZT-TP or CS-Fe_{12%}/AZT-TP nanoparticles (NP). The activity on HIV-infected cells has been investigated for CS-Fe_{12%}/AZT-TP nanoparticles. After six days of culture, the virus production in culture supernatants was monitored with p24 ELISA, and the frequency of infected T cells was determined following the intracellular expression of p24 by flow cytometry. Treatment of HIV-1-infected T cells with nanoparticles resulted in significant inhibition of the viral replication in a dose-dependent manner (Figure 4A). Indeed, increasing concentrations of NP inhibited the release of the virus in the supernatant of infected T cells from 24% to 95% ($p < 0.05$ vs RPMI 1640 control), whereas E-NP had no antiviral activity. Interestingly, NP showed similar inhibitory activity as AZT or AZT-TP. In addition, the treatment of infected T cells with NP reduced significantly the frequency of p24⁺ cells to similar levels to those induced by AZT and AZT-TP ($p < 0.01$ vs non-treated) (Figure 4B).

To further study the mechanism underlying NP-mediated inhibition of viral replication in this model, we assessed the capacity of NP to interfere with the process of virus entry into T cells (Figure 4C). T cells were pre-treated with indicated molecules followed by exposure to HIV-1 for 1h at 37°C. After washing, cell-associated HIV p24 was determined by HIV p24 ELISA. Similarly to AZT, NPs induced a small but significant decrease of virus entry into T cells ($p < 0.05$ for all comparisons by reference to non-treated). However, one may argue that NP-induced decrease of p24 levels was the consequence of T-cell death. To address this hypothesis, we tested the cytotoxicity of the inhibitors using 7-AAD staining to detect apoptotic cells (Figure 4D). Similar frequencies of 7-AAD^{neg} living cells were found in the absence or presence of the highest concentrations of each inhibitor (2 μ M), indicating the lack of toxicity of NP *in vitro*.

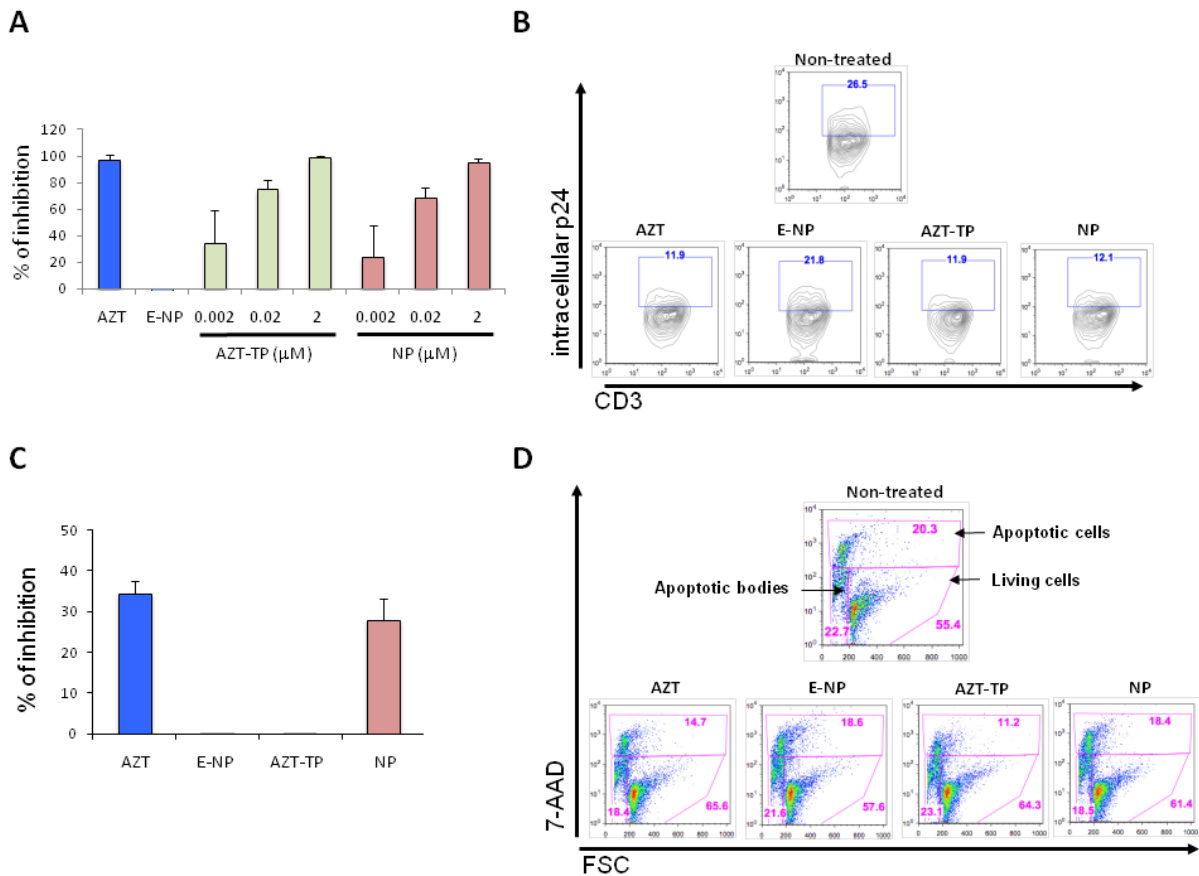


Figure 4. Impact of inhibitors on HIV infection of T cells. T cells were infected with CCR5-tropic HIV-1_{Ba-L} for 3 h and increasing concentrations AZT derivatives were added to infected T cells during 6 days of culture. The level of virus replication was monitored in culture supernatants by the p24 antigen capture ELISA. The infection inhibition is expressed as percentage of the average of three independent experiments (A). The frequency of infected cells was determined by flow cytometry (B). To assess the capacity of AZT derivatives to limit HIV-1 entry to T cells, cells were incubated for 1 h in the presence of each molecule. The amount of cell-associated HIV-1 was evaluated using the p24 antigen capture ELISA (C). To exclude any cytotoxicity of AZT compounds, treated T cells were incubated with the 7-AAD molecule staining specifically dead cells whereas living cells remained unstained (D).

Altogether these data show that nanoparticle encapsulation of AZT-TP preserved its antiviral activity while being non toxic for T cells. Considering that the capacity of NP to interfere with virus entry into T cells was not spectacular (decrease by 1.2 to 1.6 fold), it may indicate that NP act similarly to AZT by interrupting the viral cycle thus preventing new infection rather than acting at early steps of virus entry.

3.4. Inhibition of HIV-1 infection of macrophages by nanoparticles

Macrophages are considered as one of the major targets for HIV *in vivo* and a source of viral reservoir [29, 30]. Macrophages were infected for 3 h with HIV-1BaL and further cultured either alone (non-treated) or in the presence of AZT derivatives. Following six days of culture, virus production was quantified in culture supernatants and the frequency of infected cells determined by flow cytometry. As illustrated in Figure 5A, NP abrogated the production of HIV-1 by macrophages in a dose-dependent manner ($p < 0.05$ for NP at 0.02 and 2 μM , in comparison to RPMI 1640 control). Similarly, treatment of macrophages with AZT and AZT-TP inhibited HIV-1 production, whereas E-NP had no effect. Inhibition by AZT derivatives of viral particle release by infected macrophages was confirmed by the decreased number of p24⁺ cells (Figure 5B). In addition, an efficient capture of nanoparticles by macrophages was suggested by their increased size after treatment, in a dose-dependent manner (Figure 5C). Notably, inhibition of viral production by macrophages, observed in the presence of NP, was not related to a toxic activity of NP *in vitro* (Figure 5D).

Interestingly, E-NP- or NP-treatment of macrophages decreased the expression of HIV-1 coreceptor CCR5 at their surface whereas AZT or AZT-TP treatment did not interfere with the expression of this coreceptor (Figure 5E and 5F), suggesting that besides their AZT-dependent antiviral effect, chitosan-iron nanoparticles may interfere with viral entry by modulating cell surface expression of CCR5.

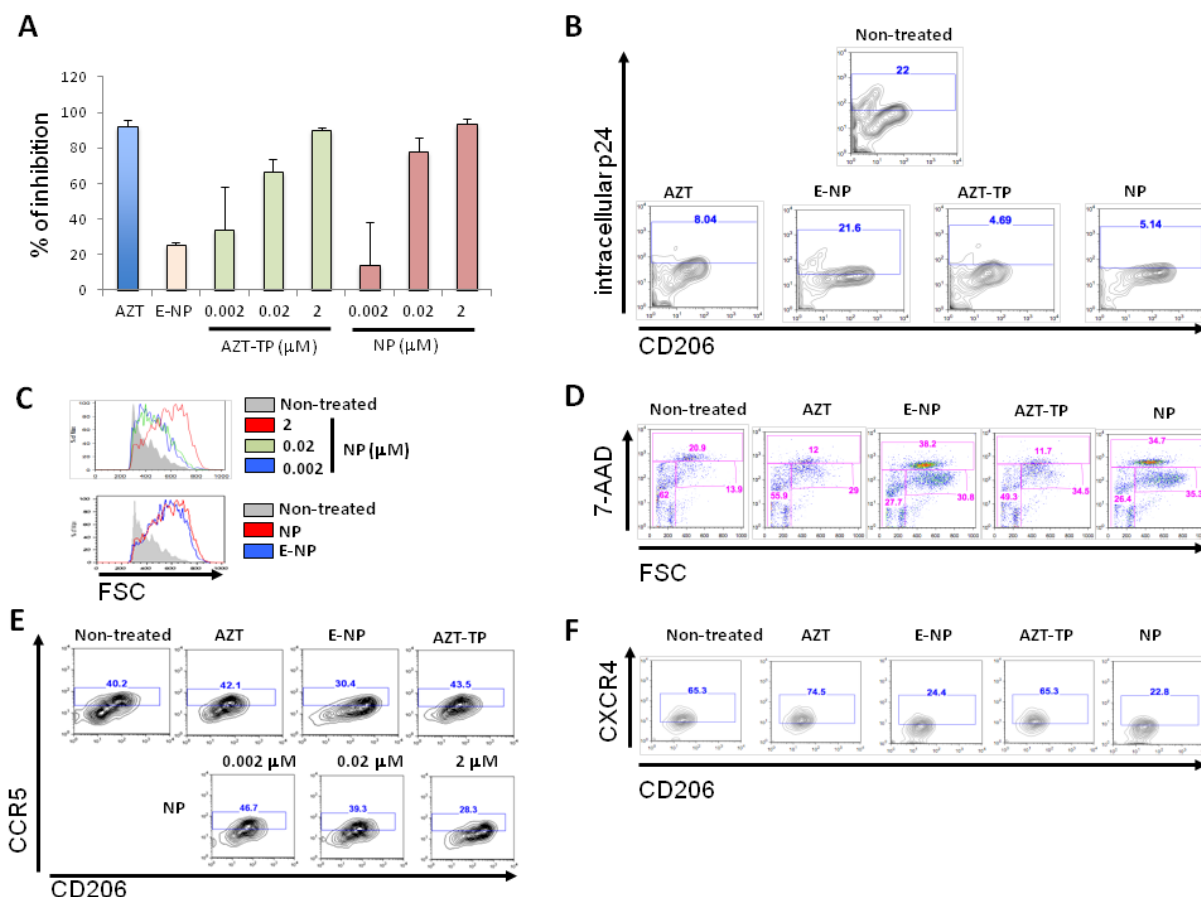


Figure 5. Impact of inhibitors on HIV replication in macrophages. Inhibition of HIV-1 infection of AZT-NP-treated macrophages may be due to the decrease of the expression of the two HIV-1 coreceptors CCR5 and CXCR4. Monocyte-derived macrophages were infected with CCR5-tropic HIV-1_{Ba-L} for 3 h. After several washes, increasing concentrations of AZT derivatives were added to infected macrophages for 6 days of culture. The level of virus replication was monitored in culture supernatants by the p24 antigen capture ELISA. The infection inhibition is expressed as percentage of the average of three independent experiments (A). The frequency of infected cells was determined by flow cytometry (B). Addition of AZT derivatives was followed by the increase of the size of macrophages as assessed by the Forward-Scattered light parameter (FSC) in flow cytometry (C). To exclude any cytotoxicity of AZT compounds, treated macrophages were incubated with the 7-AAD molecule staining specifically dead cells whereas living cells remained unstained (D). Using flow cytometry, the expression of the two HIV-1 coreceptors CCR5 (E) and CXCR4 (F) was determined at the surface of AZT derivatives –treated macrophages.

3.5. NP block HIV-1 infection of DCs and virus transfer from DCs to T cells

The antiviral activity of AZT derivatives was first tested on HIV-1 infected-DCs. NP induced a decrease in viral production that was associated with a lower frequency of p24⁺ T cells (Figure 6B, 6C). We next addressed the question of the impact of NP on HIV-1 transmission from DCs to autologous T cells. In

these experiments, DCs were first infected with HIV-1, then incubated with increasing concentrations of AZT derivatives before T cells were added.

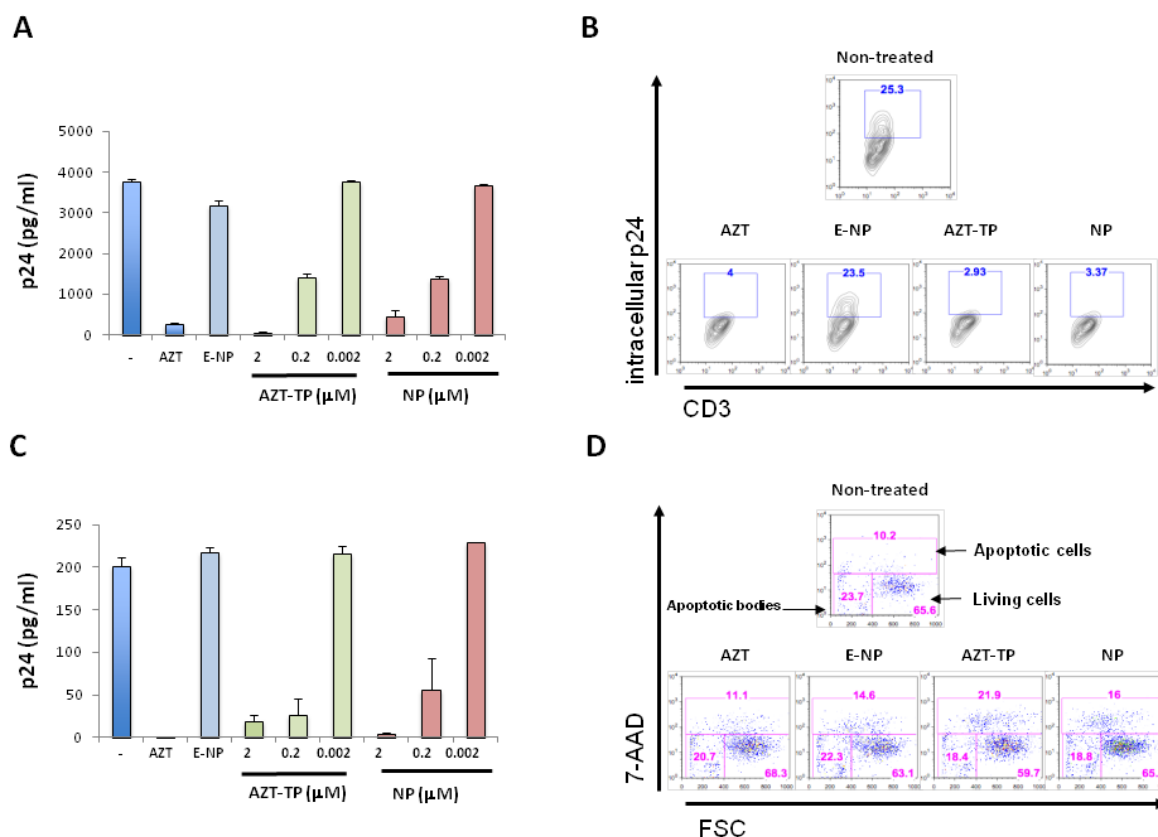


Figure 6. Impact of inhibitors on HIV infection of DCs and transfer of the virus from DCs towards T cells. Non-toxic concentrations of AZT-NP prevent the transfer of HIV-1 from dendritic cells towards T cells by inhibiting the infection of dendritic cells. Monocyte-derived dendritic cells (DCs) were infected with CCR5-tropic HIV-1Ba-L for 3 h. After several washes, T cells and increasing concentrations of AZT derivatives were added to infected DCs for 6 days of culture. The level of virus replication was monitored in culture supernatants by the p24 antigen capture ELISA. The capability of dendritic cells to transfer HIV-1 to T cells is donor-dependent. The picture shows one representative experiment out of three independent experiments (A). The frequency of infected cells was determined by flow cytometry (B). DCs were infected with CCR5-tropic HIV-1Ba-L for 3 h. After several washes, increasing concentrations of AZT derivatives were added to infected DCs for 6 days of culture. The level of virus replication was monitored in culture supernatants by the p24 antigen capture ELISA. The capability of dendritic cells to replicate HIV-1 is donor-dependent. The picture shows one representative experiment out of three independent experiments (C). To exclude any cytotoxicity of AZT compounds, treated DCs were incubated with the 7-AAD molecule staining specifically dead cells whereas living cells remained unstained (D).

Treatment of DCs with NP inhibited the production of HIV-1 in a dose-dependent manner, as observed with AZT and AZT-TP (Figure 6A), thus suggesting that NP were able to interfere with HIV

transmission from DCs to T cells, which constitutes one of the major process of virus dissemination *in vivo*. A possible toxic effect of NPs was ruled out as in Figure 6D with the 7-AAD assay.

3.6. Delivery to lymph nodes

The ability of CS-Fe_{12%}/AZT-TP nanoparticles to improve AZT-TP accumulation in lymph nodes was investigated on mice after subcutaneous administration of nanoparticles or free AZT-TP using radioactive AZT-TP. Mice were administered the treatments by subcutaneous injection into the hock after having been anesthetized. The injection into the hock has already been shown to be a relevant model of subcutaneous administration to target the lymph nodes and reduce animal sufferance [31]. The exposure of lymph nodes to AZT-TP was measured by inguinal and axillary lymph nodes collection 2 and 4 hours after injection. As a control, radioactivity of non-treated mice's lymph nodes has been measured, giving results close to the blank's values. To better illustrate the lymphatic distribution, mice were injected into inguinal lymph node by trypan blue solution as described in Materials and Methods section. This method was developed to identify the hind leg lymphatic drainage of mice and to facilitate our studies of AZT-TP accumulation in the inguinal and axillary lymph nodes. Injection time was not critical, since euthanasia at any time after injection gave visible blue labeling of lymph nodes (Figure 7 A). In fact, dye uptake was detected immediately after euthanasia, indicating that there is some lymphatic drainage post *mortem*. Indeed, the liquid (blue) has diffused through the lymphatic duct (invisible before) and reached the axillary lymph node. Concerning the tissue distribution, two hours after the administration, the detected radioactivity was always higher in the case of nanoparticles as compared to the free molecule (Figure 7 B). These levels then decrease after 4 hours, still remaining higher in the case of nanoparticles in all cases. As expected, higher levels are found in the lymph nodes closest to the injection site, which is in the right hock. These results clearly show the ability of CS-Fe_{12%}/AZT-TP nanoparticles to deliver a triphosphate nucleotide analog to the lymph nodes, one of the most important viral sanctuaries.

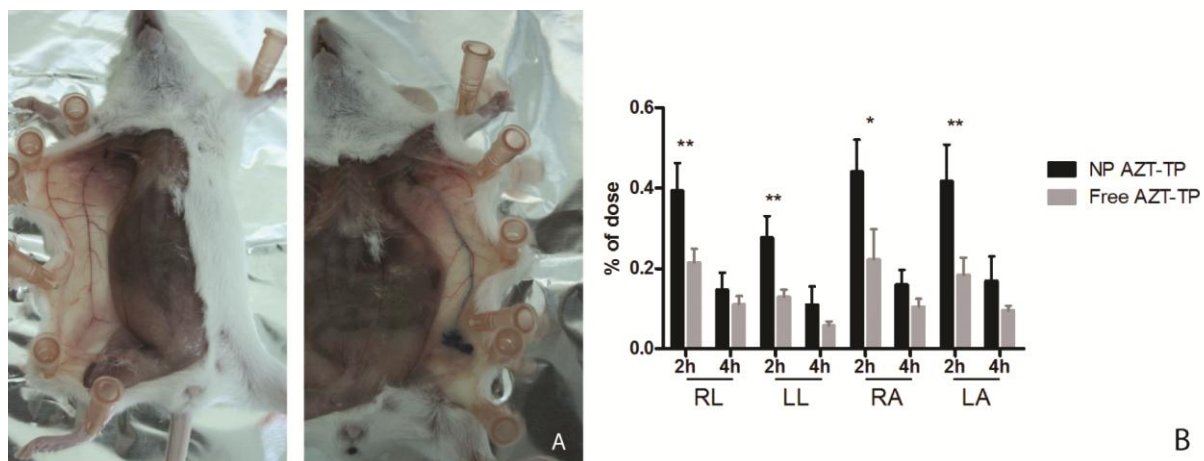


Figure 7. Lymph node retention of [^3H]-AZT-TP nanoparticles after subcutaneous administration to mice. (a) Image of mice before (left panel) and after injection (right panel) of trypan blue, to evidence lymph nodes and lymph ducts. (b) Fraction of injected dose in inguinal and axillary lymph nodes 2 and 4 h post-injection of nanoparticle (NP) AZT-TP or free AZT-TP. RL = right leg, LL = left leg, RA = right arm, LA = left arm. % of dose is calculated as the radioactivity in the lymph node divided by the radioactivity injected. NP AZT-TP values are statistically different from Free AZT-TP values as determined by T test and two-way ANOVA. The symbols * and ** represent significant change to the level of $p < 0.1$ and $p < 0.05$ respectively.

4. Conclusions

Using novel chitosan carriers loaded with AZT-TP (NP), we demonstrate herein a drug encapsulation efficiency greater than 60% and its efficient uptake by the phagocytes. As compared to free AZT, non-toxic concentrations of NP showed similar anti-HIV-1 activity on T cells, macrophages and dendritic cells. Similarly to free AZT, NP blocked the transmission of the virus from DCs to T cells, a mechanism that sustains viral persistence. *In vivo* studies to evaluate their ability to target lymph nodes showed a double AZT-TP accumulation in the case of nanoparticles as compared to the free molecule. The physico-chemistry of the formation process let think that the principle is applicable to other drugs of the same class, based on their chemical structure similarity. Further *in vivo* studies will allow to investigate the potential of these nanocarriers as antiretroviral agents on HIV-infected animal models.

Acknowledgments

The authors wish to thank H el ene Chacun for her support and help during radioactivity experiments.

References

- [1] Department of Health and Human, S.; Available at <http://aidsinfo.nih.gov/ContentFiles/AdultandAdolescentGL.pdf>, **2013**.
- [2] Cory, T. J.; Schacker, T. W.; Stevenson, M.; Fletcher, C. V., Overcoming pharmacologic sanctuaries, *Curr. Opin. HIV AIDS*, **2013**, *8*, 190-195.
- [3] Coleman, C. M.; Wu, L., HIV interactions with monocytes and dendritic cells: viral latency and reservoirs, *Retrovirology*, **2009**, *6*.
- [4] Zalar, A.; Figueroa, M. I.; Ruibal-Ares, B.; Bare, P.; Cahn, P.; de Bracco, M. M. D.; Belmonte, L., Macrophage HIV-1 infection in duodenal tissue of patients on long term HAART, *Antiviral Res.*, **2010**, *87*, 269-271.
- [5] Di Mascio, M.; Srinivasula, S.; Bhattacharjee, A.; Cheng, L.; Martiniova, L.; Herscovitch, P.; Lertora, J.; Kiesewetter, D., Antiretroviral Tissue Kinetics: In Vivo Imaging Using Positron Emission Tomography, *Antimicrob. Agents Chemother.*, **2009**, *53*, 4086-4095.
- [6] North, T. W.; Higgins, J.; Deere, J. D.; Hayes, T. L.; Villalobos, A.; Adamson, L.; Shacklett, B. L.; Schinazi, R. F.; Luciw, P. A., Viral sanctuaries during highly active antiretroviral therapy in a nonhuman primate model for AIDS, *J Virol*, **2010**, *84*, 2913-22.
- [7] Balzarini, J.; Herdewijn, P.; Declercq, E., Differential Patterns of Intracellular Metabolism of 2',3'-Didehydro-2',3'-Dideoxythymidine and 3'-Azido-2',3'-Dideoxythymidine, 2 Potent Anti-Human Immunodeficiency Virus Compounds, *J. Biol. Chem.*, **1989**, *264*, 6127-6133.
- [8] Bourdais, J.; Biondi, R.; Sarfati, S.; Guerreiro, C.; Lascu, I.; Janin, J.; Veron, M., Cellular phosphorylation of Anti-HIV nucleosides - Role of nucleoside diphosphate kinase, *J. Biol. Chem.*, **1996**, *271*, 7887-7890.
- [9] Lobenberg, R.; Araujo, L.; Kreuter, J., Body distribution of azidothymidine bound to nanoparticles after oral administration, *Eur. J. Pharm. Biopharm.*, **1997**, *44*, 127-132.
- [10] Lobenberg, R.; Araujo, L.; von Briesen, H.; Rodgers, E.; Kreuter, J., Body distribution of azidothymidine bound to hexyl-cyanoacrylate nanoparticles after i.v. injection to rats, *J. Control. Release*, **1998**, *50*, 21-30.
- [11] Garg, M.; Jain, N. K., Reduced hematopoietic toxicity, enhanced cellular uptake and altered pharmacokinetics of azidothymidine loaded galactosylated liposomes, *J. Drug Target.*, **2006**, *14*, 1-11.
- [12] Desormeaux, A.; Harvie, P.; Perron, S.; Makabipanzu, B.; Beauchamp, D.; Tremblay, M.; Poulin, L.; Bergeron, M. G., Antiviral Efficacy, Intracellular Uptake and Pharmacokinetics of Free and Liposome-Encapsulated 2',3'-Dideoxyinosine, *Aids*, **1994**, *8*, 1545-1553.

- [13] Harvie, P.; Desormeaux, A.; Gagne, N.; Tremblay, M.; Poulin, L.; Beauchamp, D.; Bergeron, M. G., Lymphoid-Tissues Targeting of Liposome-Encapsulated 2',3'-Dideoxyinosine, *Aids*, **1995**, *9*, 701-707.
- [14] Hillaireau, H.; Dereuddre-Bosquet, N.; Skanji, R.; Bekkara-Aounallah, F.; Caron, J.; Lepetre, S.; Argote, S.; Bauduin, L.; Yousfi, R.; Rogez-Kreuz, C.; Desmaele, D.; Rousseau, B.; Gref, R.; Andrieux, K.; Clayette, P.; Couvreur, P., Anti-HIV efficacy and biodistribution of nucleoside reverse transcriptase inhibitors delivered as squalenoylated prodrug nanoassemblies, *Biomaterials*, **2013**, *34*, 4831-4838.
- [15] Vinogradov, S. V.; Kohli, E.; Zeman, A. D., Cross-linked polymeric nanogel formulations of 5'-triphosphates of nucleoside analogues: Role of the cellular membrane in drug release, *Mol. Pharm.*, **2005**, *2*, 449-461.
- [16] Hillaireau, H.; Le Doan, T.; Appel, M.; Couvreur, P., Hybrid polymer nanocapsules enhance in vitro delivery of azidothymidine-triphosphate to macrophages, *J. Control. Release*, **2006**, *116*, 346-352.
- [17] Agostoni, V.; Chalati, T.; Horcajada, P.; Willaime, H.; Anand, R.; Semiramoth, N.; Baati, T.; Hall, S.; Maurin, G.; Chacun, H.; Bouchemal, K.; Martineau, C.; Taulelle, F.; Couvreur, P.; Rogez-Kreuz, C.; Clayette, P.; Monti, S.; Serre, C.; Gref, R., Towards an Improved anti-HIV Activity of NRTI via Metal-Organic Frameworks Nanoparticles, *Adv. Health. Mater.*, **2013**, *2*, 1630-1637.
- [18] Magnani, M.; Rossi, L.; Brandi, G.; Schiavano, G. F.; Montroni, M.; Piedimonte, G., Targeting Antiretroviral Nucleoside Analogs in Phosphorylated Form to Macrophages - Invitro and In vivo Studies, *Proc. Natl. Acad. Sci. U. S. A.*, **1992**, *89*, 6477-6481.
- [19] Oussoren, C.; Magnani, M.; Fraternali, A.; Casabianca, A.; Chiarantini, L.; Ingebrigsten, R.; Underberg, W. J. M.; Storm, G., Liposomes as carriers of the antiretroviral agent dideoxycytidine-5'-triphosphate, *Int J Pharm*, **1999**, *180*, 261-270.
- [20] Yang, Y.; Chen, J. L.; Li, H.; Wang, Y. Y.; Xie, Z.; Wu, M.; Zhang, H.; Zhao, Z. Z.; Chen, Q.; Fu, M. L.; Wu, K. Y.; Chi, C.; Wang, H. N.; Gao, R., Porcine interleukin-2 gene encapsulated in chitosan nanoparticles enhances immune response of mice to piglet paratyphoid vaccine, *Comp. Immunol. Microbiol. Infect. Dis.*, **2007**, *30*, 19-32.
- [21] Benesch, J.; Tengvall, P., Blood protein adsorption onto chitosan, *Biomaterials*, **2002**, *23*, 2561-2568.
- [22] Gummuluru, S.; KewalRamani, V. N.; Emerman, M., Dendritic cell-mediated viral transfer to T cells is required for human immunodeficiency virus type 1 persistence in the face of rapid cell turnover, *J. Virol.*, **2002**, *76*, 10692-10701.

- [23] Giacalone, G.; Hillaireau, H.; Capiou, P.; Chacun, H.; Reynaud, F.; Fattal, E., Stabilization and cellular delivery of chitosan-polyphosphate nanoparticles by incorporation of iron, *J Control Release*, **2014**, *194*, 211-219.
- [24] Mosmann, T., Rapid colorimetric assay for cellular growth and survival: application to proliferation and cytotoxicity assays, *J Immunol Methods*, **1983**, *65*, 55-63.
- [25] Jenabian, M. A.; Saidi, H.; Charpentier, C.; Van Herrewege, Y.; Son, J. C.; Schols, D.; Balzarini, J.; Vanham, G.; Belec, L., In vitro synergistic activity against CCR5-tropic HIV-1 with combinations of potential candidate microbicide molecules HHA, KRV2110 and enfuvirtide (T20), *J. Antimicrob. Chemother.*, **2009**, *64*, 1192-1195.
- [26] Lecoœur, H.; Melki, M. T.; Saidi, H.; Gougeon, M. L. In *Programmed Cell Death, General Principles for Studying Cell Death, Pt A*; Elsevier Academic Press Inc: San Diego, **2008**; Vol. 442, pp. 51-82.
- [27] Konopka, K.; Duzgunes, N., Expression of CD4 controls the susceptibility of THP-1 cells to infection by R5 and X4 HIV type 1 isolates, *Aids Res. Hum. Retrovir.*, **2002**, *18*, 123-131.
- [28] Margolis, L.; Shattock, R., Selective transmission of CCR5-utilizing HIV-1: the 'gatekeeper' problem resolved?, *Nat. Rev. Microbiol.*, **2006**, *4*, 312-317.
- [29] Koppensteiner, H.; Brack-Werner, R.; Schindler, M., Macrophages and their relevance in Human Immunodeficiency Virus Type I infection, *Retrovirology*, **2012**, *9*.
- [30] Dai, L.; Lidie, K. B.; Chen, Q.; Adelsberger, J. W.; Zheng, X.; Huang, D. W.; Yang, J.; Lempicki, R. A.; Rehman, T.; Dewar, R. L.; Wang, Y. M.; Hornung, R. L.; Canizales, K. A.; Lockett, S. J.; Lane, H. C.; Imamichi, T., IL-27 inhibits HIV-1 infection in human macrophages by down-regulating host factor SPTBN1 during monocyte to macrophage differentiation, *J. Exp. Med.*, **2013**, *210*, 517-534.
- [31] Kamala, T., Hock immunization: A humane alternative to mouse footpad injections, *J. Immunol. Methods*, **2007**, *328*, 204-214.

Chapitre 4

**Implant à formation *in situ* de PLGA pour la libération prolongée
de nanoparticules de nucléotides**

Chapitre 4

Implant à formation *in situ* de PLGA pour la libération prolongée de nanoparticules de nucléotides¹

Résumé

Les approches de vectorisation basées sur des nanovecteurs permettent de protéger les nucléotides et les analogues nucléotidiques de la dégradation due aux enzymes physiologiques, et de les délivrer à l'intérieur des cellules. Cependant, les nanoparticules conçues pour l'administration intraveineuse ne sont pas toujours adaptées au traitement de certaines maladies chroniques. C'est pour cela qu'un implant sous-cutané avec des caractéristiques de libération prolongée peut représenter une alternative valable, tout en étant peu invasif et capable d'atteindre les tissus lymphatiques, cible importante de plusieurs thérapies (notamment contre le VIH). Dans ce chapitre, nous présentons le développement d'un implant injectable pour la rétention de nanoparticules d'ATP au niveau du site de l'injection et leur libération progressive. Ce système est basé sur un polymère biodégradable et biocompatible, le PLGA, solubilisé dans un solvant miscible à l'eau, le N-méthyl-2-pyrrolidone, dans lequel les nanoparticules sont dispersées avant l'injection. Une fois en contact avec les fluides physiologiques, la suspension prend la forme d'un dépôt solide. Ces systèmes ont été caractérisés en termes de propriétés rhéologiques et ont été visualisés en microscopies confocale et STED. Des études de libération *in vitro* montrent leur capacité de retenir les nanoparticules à l'intérieur de la matrice et de les libérer de façon progressive pendant 5 jours. Après administration sous-cutanée chez la souris, les implants de PLGA contenant les nanoparticules ont retenu l'ATP au lieu de l'injection jusqu'à 50 heures, comparé à quelques heures pour l'ATP libre et les nanoparticules libres, montrant ainsi leur pertinence comme systèmes pour la libération prolongée de nucléotides.

¹ Les travaux décrits dans ce chapitre ont été conduits par les auteurs suivants : Giovanna Giacalone, Nicolas Huang, Amélie Bochot, Hervé Hillaireau, Elias Fattal.

***In situ* forming implant of PLGA for sustained release of nucleotide nanoparticles¹**

Abstract

In order to protect nucleotides and nucleotide analogs from degradation due to physiological enzymes, and to deliver them intracellularly, nanoparticle-based drug delivery approaches offer such a double advantage. Nanoparticles designed for intravenous injections though are not always convenient, e.g. in the case of chronic diseases. Therefore, a subcutaneous implant with sustained release features might represent a valid alternative, which is less invasive and can reach lymphatic tissues (important targets of many therapies, especially HIV). In this chapter, we present the development of an *in situ* forming implant for the retention of ATP nanoparticles at the injection site and their progressive release. This system is based on a biodegradable and safe polymer, PLGA, solubilized in a water-miscible solvent, NMP, in which nanoparticles are dispersed before injection. Once in contact with physiological fluids, the suspension turns into a solid depot. These systems are characterized in terms of rheological properties and are visualized by confocal and STED microscopy. *In vitro* release studies show their ability to retain nanoparticles inside the matrix and to gradually release them over 5 days. After subcutaneous administration to mice, PLGA implants containing nanoparticles were able to retain ATP at the injection site for up to 50 hours, as compared to few hours of free ATP or free nanoparticles, showing therefore their relevance as sustained release systems of nucleotides.

¹ The work described in this chapter was carried out by the following authors: Giovanna Giacalone, Nicolas Huang, Amélie Bochot, Hervé Hillaireau, Elias Fattal.

1. Introduction

Administration of nucleotides and nucleotide analogues is a main challenge in the drug delivery field because of their fragile triphosphate moiety, which is easily hydrolyzed in physiological conditions. Furthermore, their hydrophilicity and negative charge limits their passage through cellular membranes. In order to circumvent these drawbacks, nanoparticle-based drug delivery approaches offer such a double advantage of protecting the molecule from rapid degradation and enhancing its intracellular penetration. Several nanoparticle formulations have been designed for intravenous injection [1], but in the case of repeated and/or prolonged treatments, a daily intravenous administration is not suitable in terms of patient comfort and acceptability. The subcutaneous route of administration is an interesting alternative, less invasive and offering the possibility to target the lymph nodes (cf. chap. 3), which could be highly beneficial in the context of HIV/AIDS treatments. Therefore, a subcutaneous implant, combining these targeting potential and sustained release properties, is a promising candidate to turn the challenging administration of nucleotide/nucleotide analogue nanoparticles into a realistic therapeutic approach.

In situ forming implants were introduced in the late 90s [2]. Compared to microparticles or pre-formed implants, they present the advantages of easy preparation and better compliance for the patients [3]. Furthermore, no surgery is needed, as a simple subcutaneous injection is required and can be performed by the patient without any sanitary assistance. Such implants generally consist of a hydrophobic, biodegradable polymer and the drug dispersed in a water-miscible solvent. After injection, a depot is formed thanks to the precipitation of the polymer once in contact with aqueous body fluids [4], allowing drug release by diffusion and/or polymer degradation.

Poly(lactic-co-glycolic acid) (PLGA) and N-methyl-2-pyrrolidone (NMP) have been used for the preparation of *in situ* forming implants. PLGA is a biodegradable and biocompatible polymer largely used for purposes of controlled release [5], while NMP is a water-miscible solvent which has been chosen for its physiological safety [6]. Several examples of such systems have been reported, containing aspirin [7], bovine serum albumin [8] or human growth hormone [9]. The first example on the market is Eligard™ (Sanofi-Aventis), containing the peptide leuprolide acetate for the treatment of advanced prostate cancer [10]. Among the PLGA/NMP systems, one of them has been developed for the dispersion of nanoparticles [11], in the context of solid tumor treatment by local hyperthermia using superparamagnetic iron oxide nanoparticles, without any drug encapsulated.

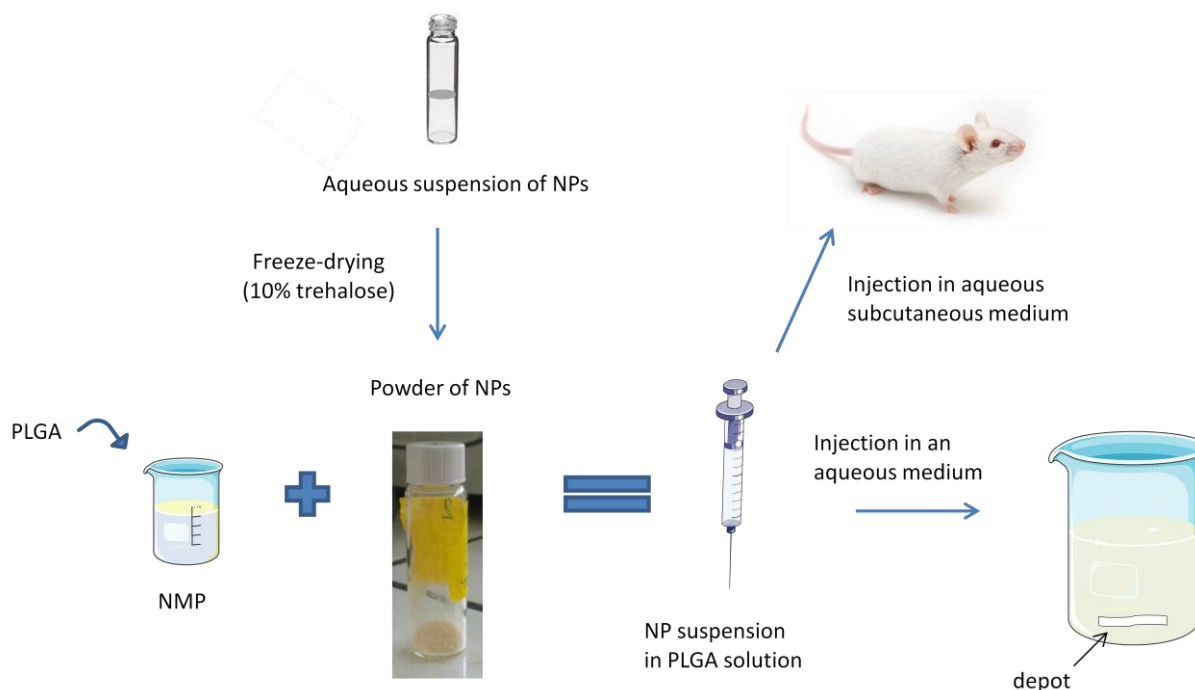
In this study, we investigate the potential of PLGA and NMP to form an injectable *in situ* forming implant system able to entrap and release nucleotide-chitosan nanoparticles sustainably from the injection site following subcutaneous administration. ATP has been chosen as nucleotide drug because of its own pharmacological properties, and also for its structural similarity to triphosphate

nucleotide analogues, which can be used as antiretroviral drugs, in order to investigate the potential of these systems to deliver active molecules to the HIV sanctuaries.

2. Materials and methods

2.1. Materials

Nanoparticles have been prepared using a chitosan-iron complex (referred to in the following as CS-Fe) containing 12% iron, synthesized as previously described (chap. 2) from chitosan low viscosity (DD 95%, Fluka) and Iron (III) nitrate nonahydrate (Sigma). Adenosine 5'-triphosphate (ATP) was from Sigma and BODIPY-FL ATP (fluorescently-labeled ATP) from Invitrogen, France. $[\gamma\text{-}^{33}\text{P}]\text{-ATP}$, the scintillation liquid Ultima Gold and the strong base Solvable were from Perkin Elmer (France). PLGA polymers of medical grade quality (Resomer) are from Evonik Industries (Germany) and 1-methyl-2-pyrrolidone from Sigma.



Scheme 1. Formulation process of *in situ* forming implant based on PLGA and nanoparticles.

2.2. Nanoparticle formulation

Nanoparticles are prepared from a 1 mg/mL CS-Fe solution and a 15 mg/mL ATP solution, under magnetic stirring at 1000 rpm, as described in chapter 2. A solution of trehalose as cryoprotectant is then added in order to have a final 10% w/v concentration. The obtained nanoparticle suspension is freeze-dried by rapid freezing in liquid nitrogen followed by drying in a Christ Alpha 1-2 LD Plus at -55 °C and 0.01 mbar for 24 hours.

For fluorescence studies, nanoparticles are prepared starting from a 1 mg/mL CS-Fe solution and a 15 mg/mL ATP solution containing the fluorescent dye ATP-BODIPY. Subsequently, they are formed and freeze-dried in the same conditions as previously described, protecting the vial from light with aluminum foil.

For release studies, nanoparticles are prepared starting from a radioactive solution of ATP containing [γ -³³P]-ATP as a tracer. Subsequently, they are formed as described above and freeze-dried at -25 °C and 0.007 mbar for 24 hours, with a Christ Alpha 2-4 freeze-drier (Laboratoire de Radiotoxicologie expérimentale at IRSN, Fontenay-aux-Roses).

2.3. Implant formulation

PLGA used are Resomer RG 502 H (Mn = 7000 - 17,000 g/mol, acid termination, in the following called PLGA50/50a), RG 502 (Mn = 7000 - 17,000 g/mol, ester termination, PLGA50/50e) and RG 752 S (Mn = 7000 - 17,000 g/mol, ester termination, PLGA75/25). They were solubilized with different ratios (34-45% w/w) in 1-methyl-2-pyrrolidone (Atrigel Delivery System from *Tolmar Therapeutics*, Inc.). Subsequently, different amounts of freeze-dried nanoparticles (4-11% w/w) are added and dispersed in the solution, in order to obtain a homogeneous suspension. For the implant formation, the suspensions are injected in an aqueous medium (PBS) where they turn into a solid depot (Scheme 1).

2.4. Rheological studies

For the viscosity studies, all rheological measurements were carried out on a rotational rheometer RheoStress 600 (Thermo Scientific). The geometry was a titanium cone/plate (diameter 4 cm, angle 1° and cone truncation 28 μ m) which was equipped with a solvent trap to avoid evaporation. TRIOS

software was used for data analysis. Flow properties of the three PLGA solutions with and without nanoparticles were determined at 37°C by a stress sweep. After a 5-minute equilibration time, the shear rate was increased gradually from 0 to 5000 (1/s). Measurements were performed in triplicate at room temperature.

The syringeability of the PLGA solutions with and without nanoparticles was studied using a home-made device described previously by Burckbuchler *et al.* [12]. This device was coupled to a texture analyzer TAXT2i (Stable MicroSystems, Godalming, UK) in compression mode which was equipped with a force transducer calibrated with a 30 kg sensor. The principle consists of applying a given displacement rate to the plunger of the syringe filled with the solution or suspension and in measuring the resulting force. The systems were introduced into 1 mL Terumo Syringes, equipped with 25G (diameter, $d = 0.5$ mm and length, $l = 16$ mm, Terumo) needles. The displacement rate of the plunger was 0.5 mm/s corresponding to a flow rate of 0.4 mL/min, which is similar to a manual injection rate. All measurements were performed in triplicate at room temperature.

2.5. Confocal and STED microscopy observations

For the confocal laser scanning and STED microscopy experiments, nanoparticles have been prepared as described above, but adding ATP-BODIPY to the ATP solution prior to nanoparticle formation. Nanoparticles were then suspended in a PLGA RG 502 H solution. The systems were observed using an inverted confocal laser scanning microscope LSM 510-Meta (Carl Zeiss, Germany) using a Plan-Apochromat 63X/1.4 NA oil immersion objective lens. $\lambda_{\text{ex}} = 488$ nm / $\lambda_{\text{em}} = \text{LP} > 505$ nm. The pinhole was set at 1.0 Airy unit. 12 bit numerical images were acquired with LSM 510 software version 3.2.

For the visualisation by Time-gated Stimulated Emission Depletion (STED) Nanoscopy, nanoparticles were observed with an inverted Leica TCS SP8 gated-STED super-resolution microscope (Leica, Germany) using a HCX PL APO 100x/1.4 STED oil immersion objective lens. The samples were observed using $\lambda_{\text{ex}} = 485$ nm (WLL Laser; average power) / $\lambda_{\text{em}} = 592$ nm (depletion laser STED; 200 mW). The gated detection of $T_g = 5$ ns. The sample acquisition was done with the Leica SP8 LAS AF software version 3.6.

2.6. *In vitro release study*

For the release studies, nanoparticles have been prepared using [γ - ^{33}P]-ATP added as a tracer to the ATP solution. After addition of nanoparticles to the PLGA solution, aliquots of 50 μL of the suspension are injected with 1 ml syringes and 25G needles into 1 ml of PBS in an Eppendorf. Samples are placed at 37 °C on agitation for different times up to 45 days. At scheduled time, the release medium is separated from the depot. This release medium is centrifuged at 17000 \times g for 1 hour, then supernatant is separated from pelleted nanoparticles. Depots and nanoparticles are dissolved by adding 1 ml of Solvable and kept 2 hours at 50 °C. All samples are subsequently treated with 10 mL Ultima Gold and then analyzed to determine their radioactivity content using a Beckman Coulter (LS 6500 Multi-Purpose Scintillation Counter) instrument. Free ATP is calculated as supernatant radioactivity/ (depot + pellet + supernatant radioactivity). Nanoparticle ATP is calculated as the ratio between pellet radioactivity and the total radioactivity. Total ATP present in the medium is the addition of these two above. Total ATP left in the depot is the difference between the total radioactivity and the total ATP present in the medium.

2.7. *Animals*

Three- to 5-week-old NIH Swiss Outbred female mice were purchased from Harlan Laboratories, UK. All animals were housed in appropriate animal care facilities during the experimental period, with free access to food and water, and were handled according to the principles of laboratory animal care and legislation in practice in France. All *in vivo* studies were performed in accordance with a protocol submitted to the local Ethical Committee (registered with the French Ministry of Research).

2.8. *Subcutaneous injection and fluorescence retention at injection site*

For *in vivo* studies, suspensions are prepared in the same way as described for confocal laser scanning microscopy, using fluorescent nanoparticles. Moreover, other formulations are prepared as control, namely: the same suspension with free ATP instead of nanoparticles; the nanoparticles suspension in water; the free ATP in solution. All the formulations have the same ATP-BODIPY content. Animals were divided into 4 groups of 6 mice, namely group 1 received an ATP solution, group 2 the nanoparticle suspension in water, group 3 received the ATP dispersed in the organic

solution, group 4 the nanoparticles dispersed in the PLGA solution. Animals had free access to food and water. They were anesthetized under 2.5% isoflurane and 50 μL of relative solution or suspension were injected subcutaneously in the hock. Mice were subsequently imaged at scheduled times (after fur removal) for fluorescence detection with the Xenogen IVIS Lumina (Caliper Life Sciences). Two excitation filters and two emission filters were chosen, namely 400-445 and 445-490 nm for excitation; 515-575 and 575-650 nm for the emission. Binning and duration settings varied at every acquisition depending on ATP amount detected. For images treatment, the spectral unmixing technique is applied with Living Image Software in order to subtract the fluorescence due to the tissue and to the food. The fluorescence due to the region of interest (ROI) is calculated in radiant efficiency (fluorescence emission radiance per incident excitation power) in order to be independent from experiment features.

3. Results and discussion

3.1. Implant formation

Viscous solutions could be obtained from 3 different kinds of PLGA polymers and NMP. All of them were soluble in NMP at high concentration, namely 34 % w/w. Freeze-dried nanoparticles have been added to the PLGA solutions and after the necessary time for the clusters to disperse, a homogeneous suspension was obtained. The nanoparticles used are the ones presented in chapter 2, having an average size of 134 ± 2 nm and a zeta potential of 20.2 ± 0.5 mV. After injection of the organic solution into aqueous medium (PBS), the resulting suspension showed the typical behavior of an *in situ* forming implant, turning into a solid due to a phase inversion phenomenon. The whole formulation process is summarized in Scheme 1. Since this process takes place relatively fast, this could lead to a matrix with large pores.

The amount of NMP has been chosen in order to be as low as possible to avoid toxicity. Ratios and amounts have been selected based on magnitude orders typically found for this kind of systems.

3.2. Rheological studies

The viscosity and shear stress of the three PLGA solutions has been investigated, in absence or presence of nanoparticles in suspension.

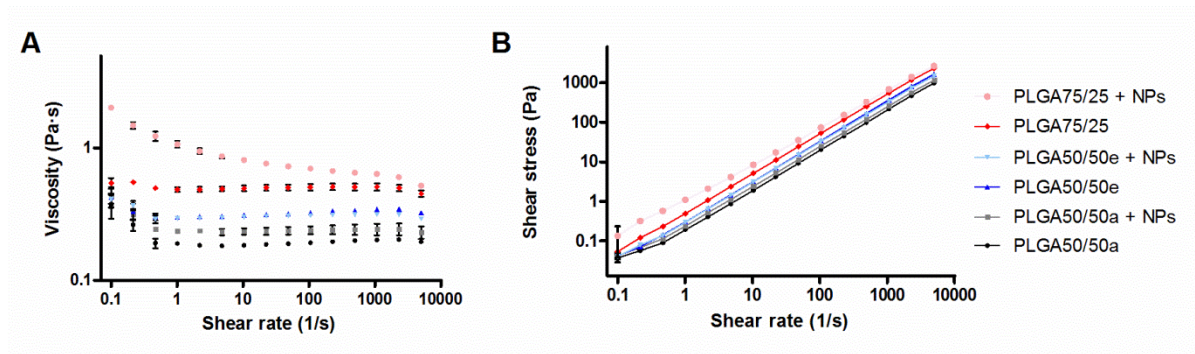


Figure 1. Viscosity (A) and shear stress (B) as a function of shear rate, for different PLGA solutions with and without nanoparticles.

As it can be seen in Figure 1, viscosity (A) and shear stress (B) increase in the three cases with the addition of nanoparticles, as expected. Furthermore, the viscosity increases with the amount of nanoparticles added (data not shown). The most viscous behavior is presented by the PLGA having a lactic-to-glycolic ratio of 72:25. This behavior is expected since viscosity is supposed to increase with increasing molecular weight of the polymer [13]. For the two 50:50 polymers, a higher viscosity is found for the ester-terminating polymer compared to the acidic one. All the formulations seem to be slightly shear thinning, which could be helpful in terms of injection.

The ability of these PLGA solutions to be injected was quantified in presence or absence of nanoparticles in suspension by measuring the syringeability. Syringeability relates to the force (expressed in Newton) necessary for the injection of a formulation at a given injection rate with a needle of specific gauge and length. It is difficult to establish a general syringeability limit since it can vary depending on the population involved [14]. Nevertheless 20 Newton can be considered as an acceptable limit for parenteral injections. It is important to investigate this parameter before considering any *in vivo* applications of the systems.

Injection force (N)		
	no NPs	NPs
PLGA50/50a	1.9 ± 0.6	2.7 ± 0.3
PLGA50/50e	2.1 ± 0.4	3.7 ± 0.3
PLGA75/25	2.8 ± 0.1	8 ± 0.2

Table 1. Injection force necessary (in Newton) for the different PLGA solutions with and without nanoparticles.

As it can be seen in Table 1, the force is quite low for all PLGA solutions and increases in presence of nanoparticles, but remains below 10 N. Even when the nanoparticle concentration is doubled, the injection force remains below 20 N (data not shown). Among the different types of PLGA, the injection force is found to increase consistently with the rheology measurements.

The first polymer (PLGA50/50a) is the one proportionally less influenced by the presence of nanoparticles and it has therefore been retained for further experiments.

3.3. Microscopy observations

The formation of the implant was investigated by confocal laser scanning microscopy (CLSM). For this purpose, nanoparticles were prepared using the fluorescent ATP-BODIPY, dispersed in the PLGA organic solution, and the implant was formed by injection of PBS under microscopic observation.

Figure 2A is a representative image of freeze-dried nanoparticles suspended in the PLGA solution. Nanoparticles appear as micron-scale clusters dispersed in the organic solution. During the first few minutes after PBS addition, it is possible to see the formation of the solid depot. Nanoparticles are moving and diffusing from the clusters to the aqueous droplets, probably thanks to their higher affinity for PBS (Figure 2B). At the same time, the presence of PBS induces PLGA precipitation and implant formation. After the formation is completed, the fluorescence is quite homogeneous, even though slightly more on the edges of the implant, which is consistent with a homogeneous dispersion of nanoparticles (Figure 2C). However the resolution of this type of optical CLSM observation does not allow to distinguish nanoparticles from ATP in solution.

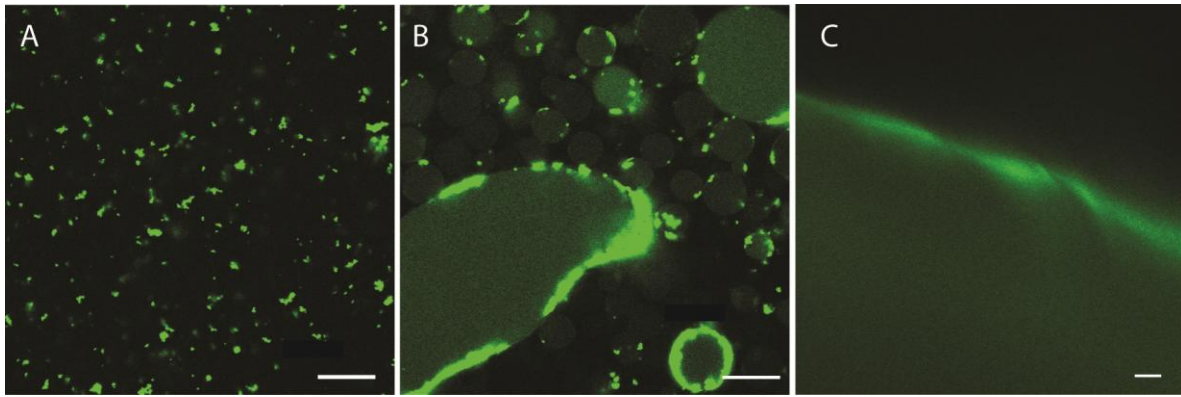


Figure 2. Confocal laser scanning microscopy images. A) PLGA solution with ATP-BODIPY NPs in suspension. B) Formation of solid depot. C) depot formed. Scale bars = 20 μm (A and B), 50 μm (C).

To ensure that nanoparticles are still intact in the implant, observations were conducted using the STED technique, which allows a higher resolution, in parallel to classical CLSM (Figure 3).

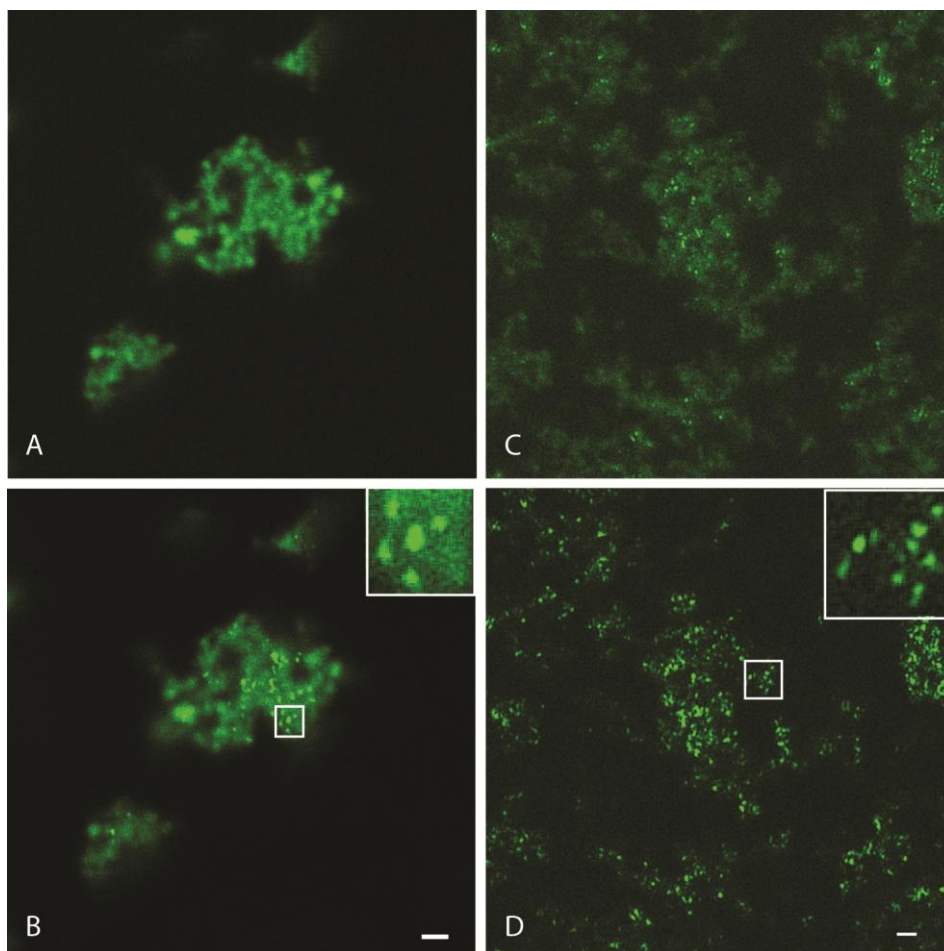


Figure 3. Confocal (A and C) and corresponding STED (B and D) microscope images of nanoparticles dispersed in the PLGA depot. The insets in B and D show magnified views of the section highlighted in white squares. Scale bars = 1 μm .

Figure 3 shows the images of nanoparticles suspended in the depot. Nanoparticles can clearly be seen with a size around 100-300 nm, confirming their dispersion in the system and the conservation of their size.

3.4. Release behavior

Release from a PLGA *in situ* forming implant typically follows 3 phases: burst during implant formation, migration of nanoparticles out of the matrix by diffusion, and degradation of the matrix [15].

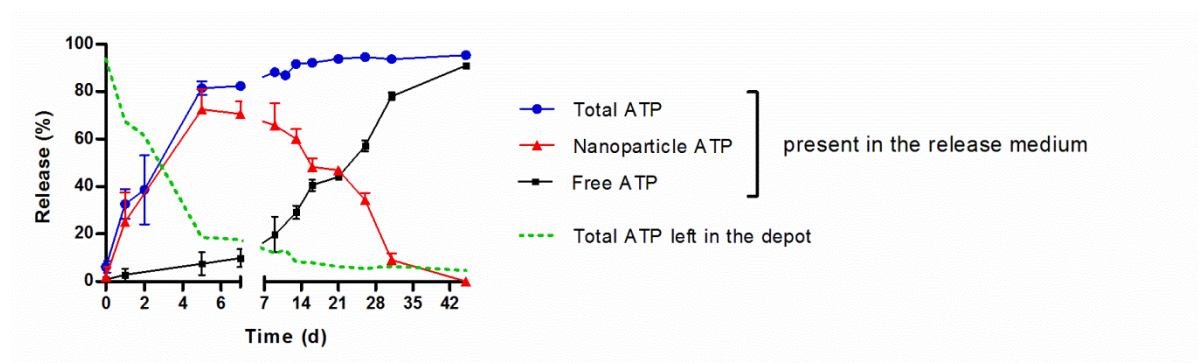


Figure 4. *In vitro* release of nanoparticles and ATP from the PLGA depot after injection in PBS.

After nanoparticles have been suspended in the PLGA solution, the systems have been injected into PBS, where they formed an *in situ* forming implant. ATP and nanoparticle release from the depots have been monitored thanks to radioactivity labeling for up to 45 days.

The first phase of the release from the implant is rather constant, from day 0 to day 5 (Figure 4). This release is taking place almost only in form of nanoparticles, having less than 10% of free ATP. Afterwards, starting from day 5, a slow release of the rest of nanoparticles can be found, but especially a progressive release of ATP from nanoparticles. The faster initial release as compared to the second phase might be explained by the rapidity of the implant formation, which can lead to large pores in the matrix. Nanoparticle release is complete after around 45 days. In conclusion, this implant enables a progressive release of intact nanoparticles over 5 days, which allows us to apply these systems for *in vivo* evaluation.

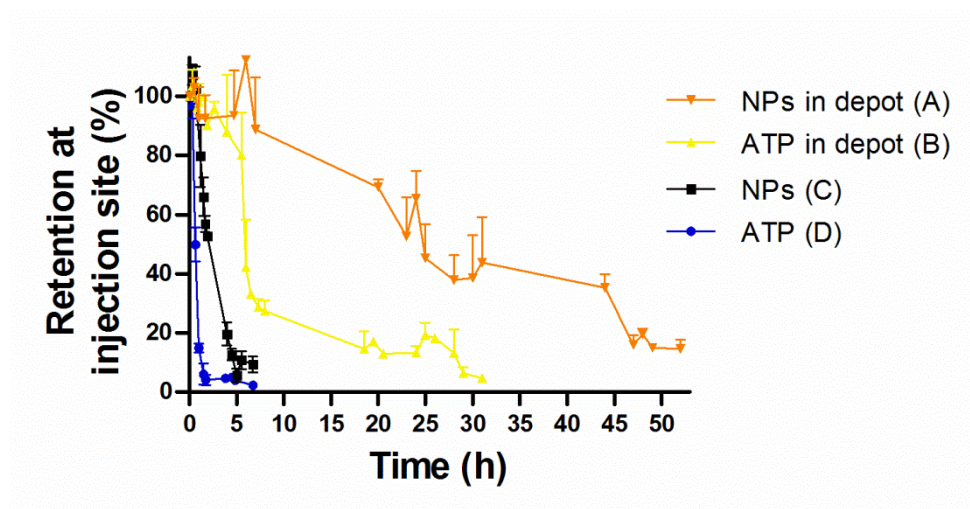
3.5. In vivo studies

One of the issues concerning the use of *in situ* forming implants is the solvent removal phase. Among them though, PLGA/NMP systems are considered safe and biocompatible [16]. Indeed, PLGA is a safe polymer approved by FDA, for which then we possess a long clinical history. No evident toxicity effects were observed on mice throughout the whole experiment.

A disadvantage related to this kind of systems is the important variability in the depot shape depending on the injection speed. If injected slowly, they are more likely to form a rod, whereas for slow injections the form will be rather spherical [17]. This feature renders the *in vivo* behavior of this system often not predictable based on the *in vitro* studies.

Nevertheless, the *in vivo* studies performed on mice showed a clear trend (Figure 5). Free ATP in solution disappeared from the injection site within few hours. The nanoparticle suspension had a slightly better retention behavior, but still reaching only 20% of injected dose after 5 hours. When ATP was dispersed in the PLGA solution, a significant improvement has been achieved in the resident time at the site of injection. The ATP signal was still detectable 24 hours post-injection (around 20%). Eventually, when nanoparticles are dispersed in the PLGA implant, the fluorescence signal present in the mice hock was optimally detectable after 48 hours, being around 20% at 52 hours.

Eventually, the final release phase due to the matrix erosion might be underestimated, because of the degradation of the BODIPY dye, which was previously observed *in vitro*. Therefore, retention time at injection site might be even longer than what described here above.



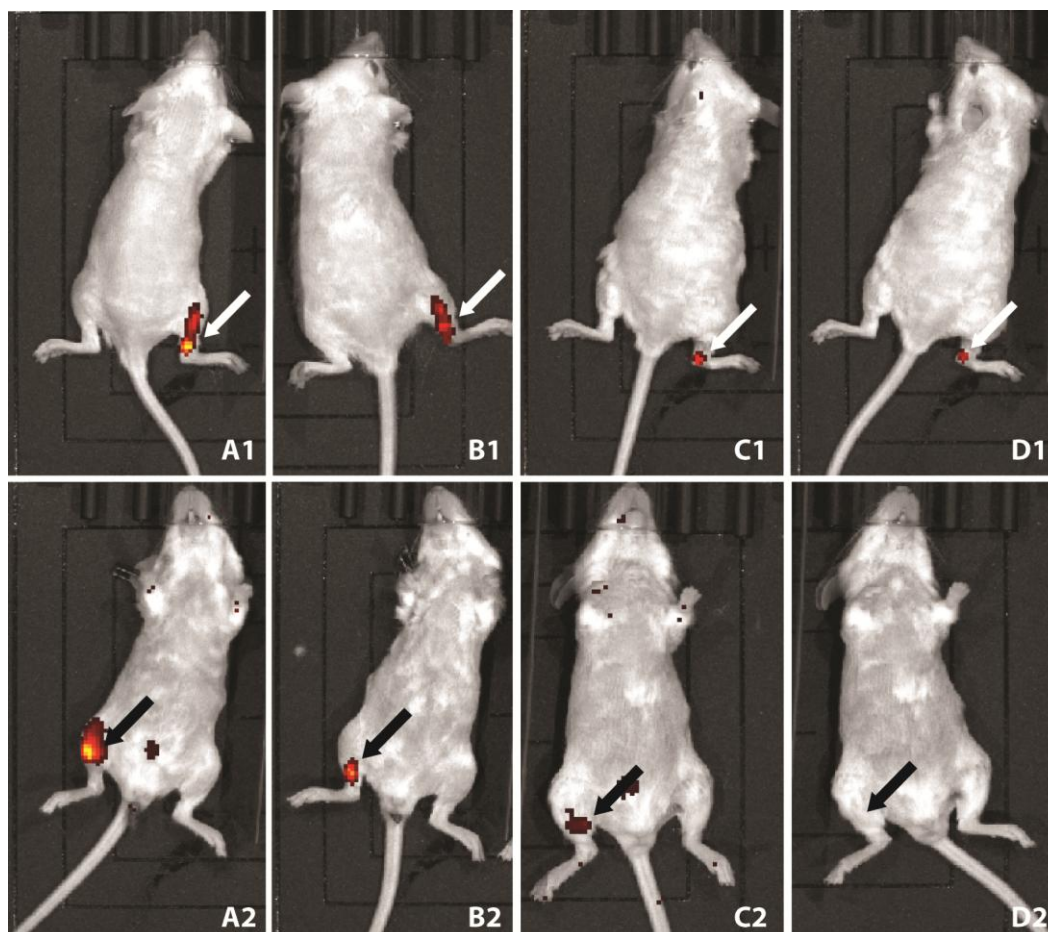


Figure 5. Top: retention of ATP-BODIPY from different formulations at the injection site (mice hock, n = 6). Bottom: representative examples of mice dorsal (A1 to D1) and ventral (A2 to D2) images at 7 hours after injection (sites indicated by the arrows) for the 4 different formulations.

4. Conclusions

CS-Fe/ATP nanoparticles have been efficiently and homogeneously dispersed in a PLGA solution. This system, during *in vitro* studies mimicking subcutaneous injection, allowed the formation of a solid depot, from which the nanoparticles have been released in a sustained and controlled manner over at least 5 days. When tested *in vivo* on mice, the *in situ* forming implant showed an improved retention at injection site compared to free solution, free nanoparticles and free ATP dispersed in the PLGA solution. The substitution of ATP with nucleotide analogs could open the way to effective treatments of infections like HIV.

Acknowledgments

The authors wish to thank Guillaume Phan from IRSN (Fontenay-aux-Roses, France) for freeze-drying of radioactive nanoparticles, Sarah Villebrun for the rheological experiments, Valérie Nicolas (IFR IPSIT, Université Paris-Sud) for the confocal and STED experiments, Andrey Maksimenko for the subcutaneous injections, and Simona Mura for Lumina expertise.

References

- [1] Wacker, M., Nanocarriers for intravenous injection - The long hard road to the market, *Int. J. Pharm.*, **2013**, *457*, 50-62.
- [2] R.L. Dunn, J. P. E., D.R. Cowsar, D.P. Vanderbilt: US, **1990**.
- [3] Parent, M.; Nouvel, C.; Koerber, M.; Sapin, A.; Maincent, P.; Boudier, A., PLGA in situ implants formed by phase inversion: Critical physicochemical parameters to modulate drug release, *J. Control. Release*, **2013**, *172*, 292-304.
- [4] Graham, P. D.; Brodbeck, K. J.; McHugh, A. J., Phase inversion dynamics of PLGA solutions related to drug delivery, *J. Control. Release*, **1999**, *58*, 233-245.
- [5] Anderson, J. M.; Shive, M. S., Biodegradation and biocompatibility of PLA and PLGA microspheres, *Adv. Drug Deliv. Rev.*, **1997**, *28*, 5-24.
- [6] Lee, K. P.; Chromey, N. C.; Culik, R.; Barnes, J. R.; Schneider, P. W., Toxicity of N-Methyl-2-Pyrrolidone (Nmp) - Teratogenic, Subchronic, and 2-Year Inhalation Studies, *Fundam. Appl. Toxicol.*, **1987**, *9*, 222-235.
- [7] Tang, Y.; Singh, J., Controlled delivery of aspirin: Effect of aspirin on polymer degradation and in vitro release from PLGA based phase sensitive systems, *Int. J. Pharm.*, **2008**, *357*, 119-125.
- [8] Lambert, W. J.; Peck, K. D., Development of an in-Situ Forming Biodegradable Poly-Lactide-Co-Glycolide System for the Controlled-Release of Proteins, *J. Control. Release*, **1995**, *33*, 189-195.
- [9] Brodbeck, K. J.; Pushpala, S.; McHugh, A. J., Sustained release of human growth hormone from PLGA solution depots, *Pharm. Res.*, **1999**, *16*, 1825-1829.
- [10] Sartor, O., Eligard: Leuprolide acetate in a novel sustained-release delivery system, *Urology*, **2003**, *61*, 25-31.

- [11] Le Renard, P. E.; Buchegger, F.; Petri-Fink, A.; Bosman, F.; Rufenacht, D.; Hofmann, H.; Doelker, E.; Jordan, O., Local moderate magnetically induced hyperthermia using an implant formed in situ in a mouse tumor model, *Int. J. Hyperthermia*, **2009**, *25*, 229-239.
- [12] Burckbuchler, V.; Mekhloufi, G.; Giteau, A. P.; Grossiord, J. L.; Huille, S.; Agnely, F., Rheological and syringeability properties of highly concentrated human polyclonal immunoglobulin solutions, *Eur. J. Pharm. Biopharm.*, **2010**, *76*, 351-356.
- [13] McHugh, A. J., The role of polymer membrane formation in sustained release drug delivery systems, *J. Control. Release*, **2005**, *109*, 211-221.
- [14] Adler, M., Challenges in the Development of Pre-filled Syringes for Biologics from a Formulation Scientist's Point of View, *Am. Pharm. Rev.*, **2012**, *15*, <http://www.americanpharmaceuticalreview.com/Featured-Articles/38372-Challenges-in-the-Development-of-Pre-filled-Syringes-for-Biologics-from-a-Formulation-Scientist-s-Point-of-View/>.
- [15] Brodbeck, K. J.; DesNoyer, J. R.; McHugh, A. J., Phase inversion dynamics of PLGA solutions related to drug delivery - Part II. The role of solution thermodynamics and bath-side mass transfer, *J. Control. Release*, **1999**, *62*, 333-344.
- [16] Royals, M. A.; Fujita, S. M.; Yewey, G. L.; Rodriguez, J.; Schultheiss, P. C.; Dunn, R. L., Biocompatibility of a biodegradable in situ forming implant system in rhesus monkeys, *J. Biomed. Mater. Res.*, **1999**, *45*, 231-239.
- [17] Kempe, S.; Mäder, K., In situ forming implants - an attractive formulation principle for parenteral depot formulations, *J. Control. Release*, **2012**, *161*, 668-679.

Discussion générale

General discussion

Context and objectives

In the context of HIV treatment, important progresses have been achieved with the introduction of the first nucleoside analogues. After the establishment of the Highly Active Anti Retroviral Therapy, the life expectancy and quality of patients improved sensibly. Nevertheless, no cure from the disease is still available today. The current therapy is able to reduce the viremia under detectable limits, but is not able to remove completely the virus from the body. There are some body compartments and cells, called respectively sanctuaries and reservoirs, where the virus stays in its latent form and is therefore able to escape the pharmacological treatment. This condition allows it to start to replicate once the therapy is suspended. Therefore, a complete virus eradication has not been possible yet. As a consequence, no suspension of the therapy is allowed in order to avoid viral rebound and development of resistances. This implies a 'pill burden' for the patient, because of the multiple daily drug intake for the entire life.

From this viewpoint, there was a need to develop a system that can target the reservoirs, in order to purge the virus, and a formulation which allows sustained release in order to better match the patient compliance. Therefore, the work of this thesis can be divided into two main objectives:

- a) To develop a system which is able to protect, carry and deliver the antiretroviral drug into the viral reservoirs.

Among the reservoirs, important ones are the macrophages located in the lymph nodes. Nanoparticles are typically taken up by macrophages, so in this case the strategy adopted consisted of using this feature as an advantage to deliver molecules inside this type of cells. Therefore, the encapsulation of a drug in a nanoparticle system would result in the double advantage of protecting and delivering active molecules. The protective role of nanoparticles is particularly needed in the case of nucleotide analogs. Among the drugs active against HIV, nucleoside analogs are the first class introduced and an important one to target the virus at its replication stage. Because of their poor intracellular activation, the use of active nucleotide analogs would be a strategy to bypass this limitation. The triphosphate moiety of the active form though renders these molecules even more challenging to be administered and therefore requiring for a carrier system. For this work, zidovudine (AZT) has been chosen

since it is the first nucleoside analog approved and therefore the one with more clinical history available. Even though it is now not often used in the HAART, we consider that it can be taken as a model for the entire class of nucleoside analogs.

- b) To develop an administration strategy able to deliver the drug in the lymph nodes, one of the main HIV sanctuaries.

For this purpose as well, the nanoparticles appear like a suitable tool, as they are typically drained by the lymph after subcutaneous injection and delivered to the lymph nodes. Nevertheless, an additional system is required, since frequent subcutaneous injections would represent a serious discomfort for the patient. In order to reduce the nanoparticle administration frequency, a sustained release system has been considered.

Among the sustained release systems available in literature, *in situ* forming implants present the advantage of being relatively easy to prepare and also easy to be administered. Microparticle formulations are usually delicate and complex to prepare, whereas preformed implants require surgery for their application and, if not biodegradable, also for their removal after treatment. Since they are designed to be injected subcutaneously, they are less invasive for the patient compared to an intravenous injection and also auto-administrable. Furthermore, the subcutaneous route allows for the targeting of the lymph nodes through lymphatic uptake. Among the existing *in situ* forming implants, PLGA based systems have the advantage of being biocompatible and safe (PLGA is approved by FDA), with convenient possibilities of tuning release time depending on its composition. Nanoparticles can then be suspended in the PLGA solution and be released in a sustained way after the implant formation.

During my thesis, in most cases experiments have been done with ATP as model molecule, because of the better practical availability of this molecule compared to AZT-TP. When it was possible, ATP and AZT-TP have been tested, showing always a similar behavior from a physico-chemical point of view. This led us to believe that their substitution is a reliable technique for experiments not involving any biological effect. Nevertheless, ATP has also its importance as a pharmacological active molecule, even though no experiment has been carried out in this direction.

1. Design of AZT-TP nanoparticles

The first objective of this work was to encapsulate AZT-TP in a nanocarrier system which would allow the protection of the molecule and could deliver it intracellularly or to specific regions or compartments of the body. The main feature of these two molecules from a chemical point of view is the presence of the triphosphate group. Among the nanoparticle formulations involving a triphosphate group, an interesting approach using chitosan is found in literature [1]. Chitosan (CS) is a natural hydrophilic polymer, which can be easily protonated on the amino groups. Therefore, the nanoparticle can be formed thanks to the interaction between the positive charges of chitosan and the negative charges of the phosphate groups of tripolyphosphate (TPP). Since their introduction, CS/TPP nanoparticles have seen large use and application, especially for the encapsulation and delivery of proteins [2] and nucleic acids [3, 4]. An initial strategy was to substitute the TPP with the active molecule, since it contains the triphosphate group necessary for nanoparticle formation. This allows to simplify the process and to take advantage of a feature of the molecule. Nevertheless, throughout the whole study, the three types of nanoparticles have been compared, namely made of TPP, ATP or AZT-TP.

Particles could be obtained thanks to a process called ionotropic gelation, which gives also the name of nanogels to the nanoparticles obtained. The nanoparticles are formed thanks to ionic interactions between the positive charges on the amino groups of the chitosan and the negative charges on the phosphate groups of the triphosphate molecule. The first aim was to identify the optimal concentration ranges of chitosan and triphosphate molecule in which nanoparticle formation takes place. These can be expressed using the ratio between amino groups of chitosan (N) and phosphate group of complexing molecule (P), namely N/P. Interestingly, it was found out that these regions are similar irrespectively of the molecule used. For N/P values between 2 and 1 aggregation occurs, which possibly means that all the available amino groups on chitosan have been occupied by a negative charge of the phosphate group. Since this first result has been obtained visually, the nanoparticles have then been characterized in terms of size, polydispersity index (PDI) and surface charge using DLS and zeta potential respectively. These particles present a size around 200 nm, regardless of the molecule used to form them. PDI is slightly high, around 0.2, but this value is considered acceptable for nanoparticles prepared with natural polymers, in contrast to chemically synthesized ones. Concerning zeta potential, their surface charge is positive, due to the presence of terminating chains of chitosan. For ATP and AZT-TP nanoparticles, encapsulation efficiency has been evaluated thanks to the use of radioactive labeled ATP and AZT-TP. Depending on the formulation chosen, rates could reach up to 70%. Since no other reagent is involved in the particle formation, drug loading could reach values as high as 44% w/w, higher than other results found in literature so

far [5, 6]. After these evaluations, we selected a so-called N/P critical ratio (slightly above the aggregation point) at which the nanoparticles possess the best features in terms of size and triphosphate molecule content. Before further investigating about these nanoparticles, it was important to purify them in order to remove unbound chitosan and triphosphate molecule. The dialysis technique has not been taken into account since it was thought that the process might disrupt the nanoparticles and trigger the release. Several centrifugation parameters have been tested in order to find the ideal conditions (see annex, Table 1), which allow to remove unwanted compounds but at the same time to be able to restore nanoparticles. The final purification technique retained involves nanoparticle centrifugation at reduced speed on a layer of glycerol, to dampen their impact with the tube bottom. The force of centrifugation varies between TPP or ATP ($1500 \times g$) and AZT-TP ($750 \times g$).

Using these purified formulations, the release behavior of ATP and AZT-TP nanoparticles has been investigated on 24 hours. In a first time, the release medium chosen was PBS as classically used one. The nanoparticle dissociation in this medium occurred very quickly, releasing 70% or 90% of ATP or AZT-TP respectively after one hour. Nevertheless, it has been supposed that the technique used was not necessarily appropriated as the long and strong centrifugation step might induce a release, thus leading to an overestimation. Therefore, this study was compared with another technique, taking advantage of the intensity size distribution obtained from DLS measurements. Fixing the attenuation value and the measurement position, the changes in intensity size distributions are therefore only due to a change in nanoparticle number. With this second method, a slightly slower release kinetics was found as compared to the previous technique. The mechanism suggested for the nanoparticle disaggregation is the ionic competition from the salts present in PBS. To validate this hypothesis, the release kinetics was investigated in another isotonic medium but non ionic, that is 5% glucose. As expected, the release occurs more slowly without any burst release as compared to release in PBS. In a second time, the behavior of CS nanoparticles has been investigated *in vitro* on a murine macrophages cell line (J774A.1). Macrophages have been chosen since they represent one of the most important HIV reservoirs [7]. The three kinds of nanoparticles did not display any toxicity effect up to concentrations around 0.6 mg/mL, as assessed by MTT test, resulting in cellular viability between 80 and 100%. When incubated 2 hours with the cells, they increased the ATP and AZT-TP uptake 2-fold as compared to the free molecule. Nanoparticles have been prepared with a fluorescent dye as well (ATP-BODIPY) and their internalization has been followed by confocal laser scanning microscopy, confirming the previously found results. In conclusion, the innovation brought by this part of the work consists in the use of the molecule as cross-linker. This strategy is simple and fast, allows reducing the carrier weight and limits the toxicity concerns.

2. Stabilization of nanoparticles by the use of iron

The systems developed in the first part presented a drawback which is quite known in literature for CS/TPP nanoparticles [8]. When diluted into physiological media, they have the tendency to disassemble, resulting in TPP and CS back free in solution. This was also true in the case of ATP or AZT-TP nanoparticles as assessed by the release experiments in the first chapter. In order to strengthen the bond, a complex has been synthesized between chitosan and iron. As found in literature, iron is able to bind strongly to chitosan [9, 10] as well as to phosphate groups [11, 12]. Therefore, the iron could be used as a 'bridge' between amino groups of chitosan and phosphate groups of triphosphate molecules. Subsequently, this chitosan derivative is used as in the previous chapter for the formation of nanoparticles. Different percentages of iron have been bound to chitosan, depending on the preparation parameters. Among them, 4 have been selected for further studies, namely containing 3, 6, 9 and 12% w/w of iron. Nanoparticles were successfully obtained with 4 different types of CS-Fe and TPP or ATP. They have been characterized in terms of size, polydispersity index and zeta potential. For these three features, they are not particularly different from previous ones, not containing iron. The size is slightly smaller, which can be attributed to the denser condensation due to the iron. Transmission electron microscopy (TEM) pictures of both kinds of nanoparticles confirmed this supposition. The association efficiency of ATP to the different CS-Fe complexes has been investigated, revealing values similar or even improved as compared to the previous nanoparticles (60 to 80%). In order to prove the actual role of iron in nanoparticle formation, the strength of the bonds has been further characterized by isothermal titration calorimetry, where it can be seen that the free energy and the binding constant increase as the amount of iron does. In order to test the effective improved stability in physiological media, nanoparticles have been diluted in increasing concentrations of NaCl and PBS. Here again, thanks to the use of spectrophotometry, it was demonstrated that their stability increases as the amount of included iron does. To investigate nanoparticles release kinetics, a new technique was adopted which involves the use of fluorescence fluctuation spectroscopy [13]. Nanoparticles prepared with fluorescent ATP can be followed during time, and ATP release can be quantified since for this kind of nanoparticles the release coincides with nanoparticle disassembly. For nanoparticles containing 6, 9 and 12% iron, virtually no release has been observed over one hour, whereas CS-Fe_{3%} and CS nanoparticles showed an important ATP release from the first minutes. In a second time, the ATP-containing systems have been tested *in vitro* on two macrophages cell lines. J774A.1 are murine macrophages which have been used also in the previous part of the work, whereas THP-1 are human derived monocytes which can be activated into macrophages. This second cell line allows us to better

match physiological conditions because of their human origin, and to follow longer uptake kinetics since they stop to grow once activated into macrophages. On both cell lines, cytotoxicity has been investigated through the MTT test, revealing a good cell viability up to 0.1 mg/mL of nanoparticles for all the CS-Fe complexes and both cell lines. Furthermore, on THP-1 the oxidative stress has been investigated, which could be induced by the presence of iron in the formulation. No difference has been found between non treated cells and ATP or nanoparticles treated ones, showing nanoparticle safety in terms of oxidative stress induction. At these safe concentrations, nanoparticles have been tested on cells to study their internalization, which in the case of THP-1 was possible on a longer time. Here again, it could be seen that the amount of ATP taken up is directly correlated to the amount of iron present in the complex. This result has been confirmed on both cell lines by confocal laser scanning microscopy, where higher fluorescence levels could be detected in cells treated with nanoparticles, as compared to free ATP-treated cells, after 1 or 2 hours incubation. This new strategy of associating iron to the chitosan to strengthen the bond with phosphate groups showed its actual role in making the particles more resistant in physiological conditions, and in allowing a greater amount of ATP to cross cell membranes.

3. Application of AZT-TP nanoparticles to HIV-infected cells

After having demonstrating the ability of CS nanoparticles to deliver nucleotides intracellularly and having stabilized their formulation through the use of iron, it was relevant to study if stable nanoparticles could be formulated also with AZT-TP. Furthermore, it was pivotal for the objective of the project to investigate their antiviral activity on HIV-infected cells, their possible toxicity towards infected cells and their role in preventing the transfer of the virus from dendritic cells towards T lymphocytes. Nanoparticles could be formed between all the types of CS-Fe and AZT-TP. After their formation domains and critical N/P ratios have been identified, they have been characterized in terms of size, PDI, zeta potential and association efficiency. The results obtained here are similar to those found for ATP, confirming again the possible similar behavior of the nanoparticles independently of the molecule associated. These nanoparticles have been tested on murine and human macrophages, because of their main role as virus reservoirs. On non-infected cells, they showed an increased AZT-TP uptake as compared to free AZT-TP but also to CS nanoparticles. After these promising results, nanoparticles have been tested also on HIV-infected cells. These cells are derived from human donors and they include T lymphocytes, and macrophages and dendritic cells generated from monocytes. No toxicity has been observed on the cells at any concentration tested. Interestingly, the nanoparticles are able to maintain the antiviral effect of AZT-TP in a dose-

dependent manner in the three cell lines. On macrophages, the nanoparticle uptake was confirmed by the increased cell size after nanoparticle exposure. Furthermore, nanoparticles blocked the viral transmission from dendritic cells to T lymphocytes. This latter result is particularly important as this is a crucial mechanism responsible for the virus diffusion after the infection and for the development of reservoirs. After the confirmation of nanoparticle potential on HIV-infected cells, the next step was to investigate the nanoparticle ability as drug carrier in targeting the lymph nodes, in order to reach the macrophages reservoir. Therefore, nanoparticles have been administered subcutaneously in the hock to the mice, and compared to free AZT-TP. The subcutaneous route has been chosen since it brings the injected material into the hypoderm, where lymphatic vessels drain substances from tissues to lymph nodes. An interesting study revealed how nanoparticles injected subcutaneously in the hind leg are drained from the lymph and distributed into lymph nodes [14]. The administration site in the hock has been chosen since it has been reported [15] that it can target the lymph nodes and bring less suffering to the animals as compared to the footpad injection. At 2 and 4 hours post-injection, right and left inguinal and axillary lymph nodes have been collected and the presence of AZT-TP has been determined through radioactivity. In all the cases, but more clearly after 2 hours, AZT-TP is more present when it has been administered in form of nanoparticles. This result shows the actual role of nanoparticles as carriers for antiretroviral drugs to be targeted to the viral sanctuary of the lymph nodes.

4. Towards an implantable system for the sustained release of nanoparticles

Antiretroviral drugs not only have to be targeted to the viral sanctuaries, but in order to be more patient-friendly, they also have to be administered ideally in a sustained release form. Therefore, it was important to formulate nanoparticles in a microreservoir system which could be injected subcutaneously and release nanoparticles in a sustained way. For this purpose, microparticles could represent a strategy, even though their formulation might be costly, difficult to scale-up and often leading to low encapsulation rates [16]. Another possibility is the use of preformed implants, but they have to be implanted in the patient through a small surgery, and also removed at the end of the treatment if they are not biodegradable. In this case, the patient compliance would be reduced. A more interesting approach is represented by *in situ* forming implants. These systems are liquid during their formulation, not too viscous to be injected, but they precipitate when they enter in contact with body fluids, forming therefore a solid implant. The most extensively used are based on the copolymer PLGA, two examples of which are already on the market (Eligard© and Atridox©). They

consist in PLGA solubilized in *N*-Methyl-2-pyrrolidone (NMP), a physiologically compatible solvent which is mixable with water. After the injection, the aqueous body fluids mix with NMP which is displaced out of the injection site. This brings to inversion phase and polymer precipitation, since it is not soluble in aqueous media. The drug or the nanoparticles remain entrapped in the polymer matrix, and are released by diffusion or following matrix degradation. This system though is not free from drawbacks; the main issue for *in situ* forming implants is their frequent burst release, which increases as the depot formation rate does.

Following this approach, three different types of PLGA have been chosen to be tested with NMP, in order to find the most suitable for our purposes. The three polymers differ in lactic-to-glycolic ratio and termination as follows: (i) 50:50 acid termination, (ii) 50:50 ester termination and (iii) 75:25 ester termination. Since subcutaneous administration of the implant is foreseen, it is important as first thing to investigate the viscosity and syringeability of the system in order for the injection to be realistic. Syringeability studies have been carried out to verify that the force required for injection is within standard levels. Rheological experiments revealed that the viscosity increases with the addition of nanoparticles, and with their amount. The viscosity is also found to increase with the lactic content and with the ester termination. Nevertheless, all values were still within a range that allows normal injections, among which the less viscous has been retained for further experiments (PLGA50/50a). In order to visualize nanoparticle suspension and distribution in the PLGA solution and after the depot formation, the systems have been observed with confocal and STED microscopies. The application of these techniques was possible because nanoparticles were successfully prepared using a fluorescent conjugate of ATP, i.e. ATP-BODIPY. The observations at microscope enabled us to follow the depot formation, confirming the previous hypothesis of mechanism. Before the formation of the depot, the nanoparticles are dispersed in form of clusters, whereas after the addition of PBS they migrate and distribute resulting in a more homogeneous fluorescence. When the implant is formed, fluorescence is homogeneous but slightly more present on the borders of the system.

In order to identify the single nanoparticles suspended in the implant, the high-resolution microscope STED allowed us to confirm the size of nanoparticles and their distribution in the implant. In a second time, the efforts have been shifted on the investigation of the release kinetics of this system, as the sustained release is the main feature expected from the depot. Nanoparticles have been suspended in the PLGA solution and the suspension has been injected *in vitro* into PBS, where the depot formed. The systems were incubated at 37 °C for multiple days, up to 45. The release showed two different behaviors, being rather constant at the beginning (0 to 5 days) and then continuing very slowly up to day 45. This faster initial behavior matches with the presence of more fluorescence at the borders as determined by microscopy techniques. Noteworthy, in the first phase

almost only nanoparticles are released from the implant, showing therefore the relevance for the application *in vivo* of the PLGA implant.

For the *in vivo* evaluation of PLGA systems as sustained release implants, the same administration setup as for the experiments in the third chapter was applied. This time, the nanoparticles contain ATP, since the detection technique was suitable for fluorescent molecules, and no fluorescent dye of AZT-TP is available. The *In Vivo* Image System (IVIS) is an instrument which allows to follow the fluorescence in living animals. This feature brings the important advantage of sensibly reducing the number of animals and of following the behavior on the same individual at any time point. Images of the animals are collected, from which the fluorescence of the region of interest can be measured in terms of radiance efficiency. To improve the fluorescence signal and reduce background noise, mice have been shaved, as hair can give fluorescence signal. The effect of nanoparticles in the implant was clearly demonstrated as compared to the 3 controls. As expected, free ATP and nanoparticles are drained from the injection site within few hours (respectively 2 and 6 hours). ATP dispersed in the depot was still detectable in the hock up to 30 hours, whereas nanoparticles in the depot were visible at injection site after 50 hours. Nevertheless, these results might be underestimated since the fluorescence in the visible wavelength overlaps with the tissue and food fluorescence, which reduces significantly the instrument sensitivity. Therefore, the retention time at injection site might be even longer during the phase of the matrix degradation. The use of a fluorescent dye absorbing and emitting in the near-IR region would help in improving the signal sensitivity and quality. The use of another PLGA with higher lactic monomer content could result in an even better profile as it might reduce the degradation rate of the implant and therefore slow down the nanoparticle release. Nevertheless, these systems demonstrated their ability of retaining nanoparticles at injection site on a few days time frame, being therefore relevant candidates for a sustained release therapy.

Conclusions

In conclusion, an efficient system has been developed and validated for the protection and cellular delivery of nucleotides and nucleotide analogs. These nanoparticles are easy and fast to prepare and can achieve high drug loadings. Thanks to the introduction of iron in the formulation, they have been stabilized which improved their intracellular delivery as well. When formulated with AZT-TP, CS-Fe nanoparticles are efficient in inhibiting the HIV replication in T lymphocytes, macrophages and dendritic cells. Moreover, they prevent the viral transmission from dendritic cells to T lymphocytes. In this first part, the objective of protecting and delivering active molecules to the viral reservoirs has been achieved.

When tested subcutaneously on mice, nanoparticles were also able to target the molecule to the lymph nodes, one of the main sanctuaries of HIV, accumulating the double of AZT-TP in the lymph nodes as compared to the free molecule. Furthermore, these systems have been formulated as a suspension in a PLGA solution for an injectable *in situ* forming implant. This system is able to control the release of nanoparticles on days, as demonstrated after subcutaneous injections on mice. These last results fulfill the objective of sanctuary targeting and sustained release established for the second part of the work. This approach could therefore represent a strategy to improve the life of HIV-infected patients.

Perspectives

In order to continue the project, *in vivo* experiments on HIV-infected animals should be carried out, on mice in a first time (MAIDS) and if positive results are found, on macaques. Since AZT is less and less used in the anti-HIV therapy today [17], it would be worth it to investigate its substitution with a newer nucleoside analog, for example emtricitabine or lamivudine. Since the virus in the reservoirs is in its latent stage, the nanoparticle administration should be supported by an agent able to reactivate virus replication, in order for nucleoside analogs to be active and effective. This can be achieved for example through the use of histone deacetylase inhibitors, which are responsible for folding and unfolding of DNA and can therefore play an important role in controlling HIV reservoirs [18].

Even though the recommendations in the anti-HIV therapy are susceptible to change suddenly, the association of different drug classes seems to remain a necessary feature. Therefore, these drug delivery systems could be tested on animals treated at the same time with another class' antiviral

drug. Alternatively, another kind of nanocarrier could be developed for the delivery of another class of drugs, and both kinds of nanoparticles could be then suspended in the PLGA *in situ* forming implant.

Because of their iron content, these nanoparticles might have an application as contrast agents in Magnetic Resonance Image techniques. Similar application to chitosan nanoparticles has been achieved through the use of gadolinium [19]. Preliminary studies have been carried out on nanoparticles suspensions of CS and the different CS-Fe complexes. When observed at 3T, the intensity of the signal is found to increase with the iron content in T_1 , whereas the opposite effect is observed in T_2 (Figure 1). No difference with water could be detected in the case of CS nanoparticles.

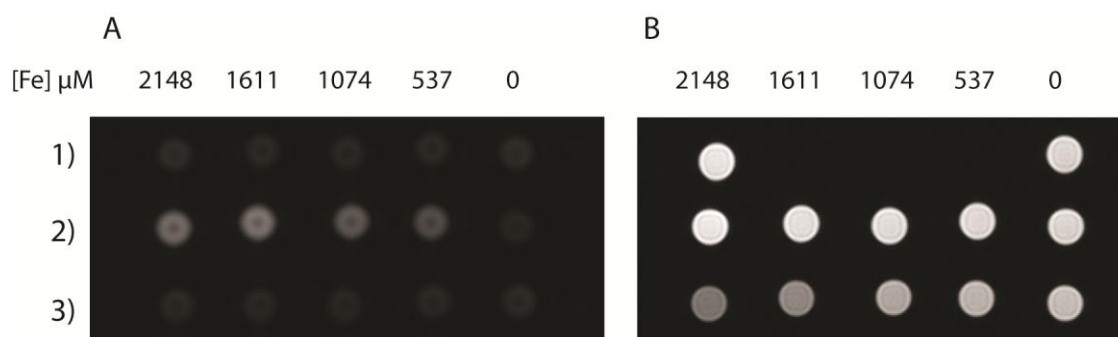


Figure 1. A) T_1 -weighted images of 2) iron-containing nanoparticles at different concentrations, 1) and 3) water as control. B) T_2 -weighted images of 3) iron-containing nanoparticles at different concentrations, 1) and 2) water as control. All samples are imaged at 3 T, 37°C.

These promising results open the way to further investigations concerning their role as diagnostic tools. Relaxivity studies can be carried out to determine the exact role of the iron in the production of the signal. Concerning the cellular uptake, this technique could confirm us the actual presence of the chitosan inside the cell, whereas previous experiments run only revealed us the position of ATP or AZT-TP. Along the same line, these nanoparticles can be tested *in vivo* on mice or rats, in order to track their distribution in the body. If coupled with fluorescence or radioactivity on ATP or AZT-TP, this technique can also reveal us the possible integrity or not of the particle at any moment and position. If the signals are co-located, an integrity of the nanoparticles can be supposed.

Multiple perspectives are possible in different directions, which could make the system developed during this thesis work an important tool in order to reach a step closer to a cure for HIV.

References

- [1] Calvo, P.; Remuñán-López, C.; Vila-Jato, J. L.; Alonso, M. J., Novel hydrophilic chitosan-polyethylene oxide nanoparticles as protein carriers, *J Appl Polym Sci*, **1997**, *63*, 125-132.
- [2] Zhang, H.; Oh, M.; Allen, C.; Kumacheva, E., Monodisperse chitosan nanoparticles for mucosal drug delivery, *Biomacromolecules*, **2004**, *5*, 2461-8.
- [3] Peng, J.; Xing, X.; Wang, K.; Tan, W.; He, X.; Huang, S., Influence of anions on the formation and properties of chitosan-DNA nanoparticles, *J Nanosci Nanotechnol*, **2005**, *5*, 713-7.
- [4] Katas, H.; Alpar, H. O., Development and characterisation of chitosan nanoparticles for siRNA delivery, *J Control Release*, **2006**, *115*, 216-25.
- [5] Vinogradov, S. V.; Kohli, E.; Zeman, A. D., Cross-linked polymeric nanogel formulations of 5'-triphosphates of nucleoside analogues: Role of the cellular membrane in drug release, *Mol. Pharm.*, **2005**, *2*, 449-461.
- [6] Kohli, E.; Han, H.-Y.; Zeman, A. D.; Vinogradov, S. V., Formulations of biodegradable Nanogel carriers with 5'-triphosphates of nucleoside analogs that display a reduced cytotoxicity and enhanced drug activity, *J Control Release*, **2007**, *121*, 19-27.
- [7] Koppensteiner, H.; Brack-Werner, R.; Schindler, M., Macrophages and their relevance in Human Immunodeficiency Virus Type I infection, *Retrovirology*, **2012**, *9*.
- [8] López-León, T.; Carvalho, E. L.; Seijo, B.; Ortega-Vinuesa, J. L.; Bastos-González, D., Physicochemical characterization of chitosan nanoparticles: electrokinetic and stability behavior, *J Colloid Interface Sci*, **2005**, *283*, 344-51.
- [9] Bhatia, S. C.; Ravi, N., A magnetic study of an Fe-chitosan complex and its relevance to other biomolecules, *Biomacromolecules*, **2000**, *1*, 413-7.
- [10] Reynaud, F.; Tsapis, N.; Deyme, M.; Vasconcelos, T. G.; Gueutin, C.; Guterres, S. S.; Pohlmann, A. R.; Fattal, E., Spray-dried chitosan-metal microparticles for ciprofloxacin adsorption: Kinetic and equilibrium studies, *Soft Matter*, **2011**, *7*, 7304-7312.
- [11] Lijklema, L., Interaction of orthophosphate with iron(III) and aluminum hydroxides, *Environ Sci Technol*, **1980**, *14*, 537-541.
- [12] Spengler, K.; Follmann, H.; Boos, K. S.; Seidel, D.; Maywald, F., Characterization and extracorporeal application of a new phosphate-binding agent, *Eur J Clin Chem Clin Biochem*, **1994**, *32*, 733-9.
- [13] Buyens, K.; Lucas, B.; Raemdonck, K.; Braeckmans, K.; Vercammen, J.; Hendrix, J.; Engelborghs, Y.; De Smedt, S. C.; Sanders, N. N., A fast and sensitive method for measuring the integrity of siRNA-carrier complexes in full human serum, *J Control Release*, **2008**, *126*, 67-76.

- [14] Rao, D. A.; Forrest, M. L.; Alani, A. W. G.; Kwon, G. S.; Robinson, J. R., Biodegradable PLGA Based Nanoparticles for Sustained Regional Lymphatic Drug Delivery, *J. Pharm. Sci.*, **2009**, *99*, 2018-2031.
- [15] Kamala, T., Hock immunization: A humane alternative to mouse footpad injections, *J. Immunol. Methods*, **2007**, *328*, 204-214.
- [16] Packhaeuser, C. B.; Schnieders, J.; Oster, C. G.; Kissel, T., In situ forming parenteral drug delivery systems: an overview, *Eur. J. Pharm. Biopharm.*, **2004**, *58*, 445-455.
- [17] Department of Health and Human, S.; Available at <http://aidsinfo.nih.gov/ContentFiles/AdultandAdolescentGL.pdf>, **2013**.
- [18] Margolis, D. M., Histone deacetylase inhibitors and HIV latency, *Curr. Opin. HIV AIDS*, **2011**, *6*, 25-29.
- [19] Courant, T.; Roullin, V. G.; Cadiou, C.; Callewaert, M.; Andry, M. C.; Portefaix, C.; Hoeffel, C.; de Goltstein, M. C.; Port, M.; Laurent, S.; Vander Elst, L.; Muller, R.; Molinari, M.; Chuburu, F., Hydrogels Incorporating GdDOTA: Towards Highly Efficient Dual T1/T2 MRI Contrast Agents, *Angew. Chem.-Int. Edit.*, **2012**, *51*, 9119-9122.

Annex

Technique	Observation
High speed centrifugation	Pellet cannot be resuspended
High speed centrifugation + ultrasounds on pellet	Pellet cannot be resuspended
Centrifuge filters (Amicon 3000, 10000, Microcon 3000)	Clogging (NPs create a pellet on the filter)
Ultrafiltration cell	Clogging (NPs create a plug on the membrane)
Centrifugation on silicon oil layer	Pellet cannot be resuspended
Centrifugation in presence of poloxamer	Pellet cannot be resuspended
Centrifugation in presence of glycerol	Pellet is softer
Centrifugation at lower speed	Pellet is softer
Centrifugation at lower speed + presence of glycerol + resuspension after 30' in a small volume	Pellet can be resuspended Homogeneous NP suspension

Table 1. Nanoparticle purification techniques approached and resulting achievements.

Acknowledgments

First, I would like to thank my thesis director Prof. Elias Fattal, for allowing me to pursue this thesis in his laboratory and for supervising my doctoral studies. I am very grateful to Dr Hervé Hillaireau for all what he taught me during my thesis period, for his patience and motivation. This thesis could not have been realized without their valuable guidance and supervision.

I would like to express my gratitude to Dr Giuseppe De Rosa and Dr Catherine Le Visage for accepting to act as the reviewers of this manuscript. Prof. Amélie Bochot, Dr Marie-Lise Gougeon and Prof. Thierry Delair are also acknowledged for participating in the jury as examiners.

I am thankful to the team 5 and the entire group “Institut Galien Paris-Sud” for the informal scientific exchanges and helps during my stay here, and for all the nice moments we spent together in the last four years.

I express my warm thanks to Dr Héra Saïdi and Prof. Marie-Lise Gougeon from Institut Pasteur for the valuable collaboration and the important experiments with HIV.

Dr Sandrine Lécart and the CLUPS are acknowledged for introducing me to the fluorescence fluctuation spectroscopy.

I would like to thank Prof. Françoise Chuburu, Dr Maïté Callewaert and Dr Cyril Cadiou for their nice welcome in Reims and the magnetic resonance experiments.

I would like to acknowledge Valérie Nicolas for confocal, STED and videomicroscopy observations.

I also want to thank Magali Noiray for the supervision during ITC experiments and Hélène Chacun for her assistance with the radioactivity experiments. Florence Agnely, Nicolas Huang and Sarah Villebrun are acknowledged for rheological studies. I also thank Stéphanie Denis for her supervision in cell culture room, and Andrey Maksimenko and Simona Mura for their precious advices and helps with *in vivo* experiments.

My sincere thanks also go to Marion Quaillet and Pauline Capiou for their enthusiasm and precision during their internships and their help with the experiments.

Abstract

In order to improve anti-HIV treatments, chitosan nanoparticles are prepared and evaluated for the intracellular delivery of nucleotides and nucleotide analogs. These nanoparticles are stabilized by the addition of iron in the formulation, and they are tested for their antiviral activity on HIV-infected cells. *In vivo* studies investigate their ability to carry the drug to the lymph nodes, a sanctuary of the infection. Once formulated as an *in situ* forming implant, these systems are injected subcutaneously to mice to evaluate their sustained release of nanoparticles.

Keywords: nanoparticles, HIV, ATP, chitosan, sustained release, drug delivery

Résumé

Dans le but d'améliorer le traitement contre le VIH, des nanoparticules de chitosane sont préparées et évaluées pour la délivrance intracellulaire de nucléotides et d'analogues nucléotidiques. L'ajout de fer dans leur formulation permet la stabilisation des nanoparticules, qui sont ensuite testées pour leur activité antivirale sur des cellules infectées par le VIH. Des études *in vivo* examinent leur capacité à délivrer la molécule vers les ganglions lymphatiques, un sanctuaire de l'infection. Une fois formulées comme un implant à formation *in situ*, ces systèmes sont injectés par voie sous-cutanée chez la souris, pour évaluer la libération prolongée des nanoparticules.

Mots-Clés : nanoparticules, VIH, ATP, chitosane, libération prolongée, vectorisation

PÔLE : PHARMACOTECHNIE ET PHYSICO-CHIMIE PHARMACEUTIQUE

LABORATOIRE DE RATTACHEMENT :

Institut Galien Paris-Sud

UMR CNRS 8612 – UNIVERSITÉ PARIS-SUD

UFR «FACULTÉ DE PHARMACIE DE CHATENAY-MALABRY »

5, rue Jean Baptiste Clément

92296 CHÂTENAY-MALABRY Cedex